University of Naples Federico II

School of Engineering

Department of Chemical Engineering, Materials and Industrial Production

Ph.D in Engineering of Materials and Structures

XXV Cycle

3D COMPLEX ENDOGENOUS TISSUE EQUIVALENT *IN VITRO*: PROCESSING AND BIOTECHNOLOGICAL APPLICATION

Ph.D Thesis

Costantino Casale

TUTOR
Prof. Dr Paolo A. Netti

COORDINATOR
Prof. Dr Giuseppe Mensitieri

ADVISOR
Dr. Giorgia Imparato

April 2013

Table of Contents

…TO MY WIFE

SUMMARY

Most living tissues are composed of repeating units on the scale of hundreds of microns, which are ensembles of different cell types with well defined three-dimensional (3-D) micro-architectures and tissue-specific, functional properties. To generate thick and functional engineered tissues, the recreation of these structural features is of great importance in enabling the resulting function [1]. To address this need recent efforts [2–4] have been concentrated on bottom-up approaches aimed at generating a larger tissue construct by the assembly of smaller building blocks, which mimics the *in vivo* tissue structure of repeating functional units.

In this PhD thesis a novel bottom-up approach, recently published [4], has been improved and used to produce thick functional tissues. First of all the chapter 1 deals with a critical analysis of the literature which highlights how the morphological, mechanical e functional properties of tissue *in vivo* are strictly regulated by extra cellular matrix and cell cross talking has been [5,6]. Then in chapter 2 the realization of 3D dermis equivalent *in vitro* tissue completely made up of endogenous extracellular matrix by assembling functional microtissues precursor is reported. In particular it is highlighted how the microscaffold degradation rate affects the assembly and maturation of de novo synthesized ECM in a 3D dermis equivalent *in vitro* by means of morphological analysis that highlights the composition and of ECM's main components.

In the chapter 3 the processing of a millimetric thick 3D dermis equivalent model is described underlining the capability of the process to overcome the classical diffusion limits of traditional top-down tissue engineering [7]. A comparative survey between 3D dermis realized and native human dermis has been reported by means of immunofluorescence analyses. Moreover multiphoton microscopy, a non invasive microscopic techniques that guarantee high resolution capability, has been used to

assess the capability of our model of responding to external stimuli such as the UVA, stating that: the 3D dermis model is able to recapitulate the intricate pathway that in vivo plays a fundamental role in phenomena in which the structural proteins of ECM are involved [6].

In chapter 4 is reported the bio-fabrication of a skin full thickness in vitro model by testing different co-coltures condition in order to adjust the keratinocytes differentiation properties that are strongly affected by the growth factor present in the medium and by the interaction with an endogenous ECM such as the dermis equivalent tissue realized [8]. Since the human skin model realized, is made up of endogenous ECM it could be used *in vitro* both as screening tool and as model for the study of healthy and disease skin, and *in vivo* as skin substitute in clinical application [9,10]. At last in chapter 5 an industrial application of the tissue engineering strategy developed has been explored. Dermis equivalent of animal origin having different shape such as fiber, disk, sheet and “doll shoes” has been produced demonstrating the versatility of the bottom-up that guarantee control of the final tissues shape [1,2]. Moreover, the realized tissues equivalent have been subjected to chrome tanning to demonstrate its possible application as an useful alternative to animal skin in the textile fields.

REFERENCES

1. Hugo Fernandes,Lorenzo Moroni,Extracellular matrix and tissue engineering applications. Journal of Material Chemistry.

2. V. Mironov, R. P. Visconti, V. Kasyanov, G. Forgacs, C. J. Drake and R. R. Markwald, Organ printing: tissue spheroids as building blocks, Biomaterials, 2009, 30(12), 2164–2174.

3. H. Onoe, R. Gojo, Y. Tsuda, D. Kiriya, M. Kato-Negishi and S. Takeuchi, Cell fibers: construction of centimeter-scale 3D tissues by weaving, 14th International

Conference on Miniaturized Systems for Chemistry and Life Sciences, 2010, pp. 629–631.

4. Palmiero C, Imparato G, Urciuolo F, Netti PA. Engineered dermal equivalent tissue *in vitro* by assembly of microtissue precursors. Acta Biomat 2010;62:548–2553.

5. Lydia Sorokin**.**The impact of the Extraacellular matrix on inflammation. Nature review Immunol. 2010 Vol. 10

6. Serini, G. & Gabbiani, G. Mechanisms of myofibroblast activity and phenotypic modulation. *Exp. Cell Res.* **250**, 273–283 (1999

7. McGuigan AP, Sefton MV. Vascularized organoid engineered by modular assembly enables blood perfusion. Proc Natl Acad Sci U S A 2006;103(31):11461–6

8. Yuan Liu a, Fumihiko Suwa. Reconstruction of a tissue-engineered skin containing melanocytes. Cell Biology International 31 (2007) 985e990

9.Rostislav V. Shevchenko, Stuart L. James and S. Elizabeth James. A review of tissue-engineered skin bioconstructs available for skin reconstruction. *J. R. Soc. Interface* 2010 **7**, 229-258

10. Lee DY, Ahn HT, Cho KH. A new skin equivalent model: use of a dermal substrate which combines de-epidermized dermis with fibroblast-populated collagen matrix. J Dermatol Sci 2000;23:132—7.

Chapter 1

Extra cellular matrix and skin tissue engineering applications: an overview

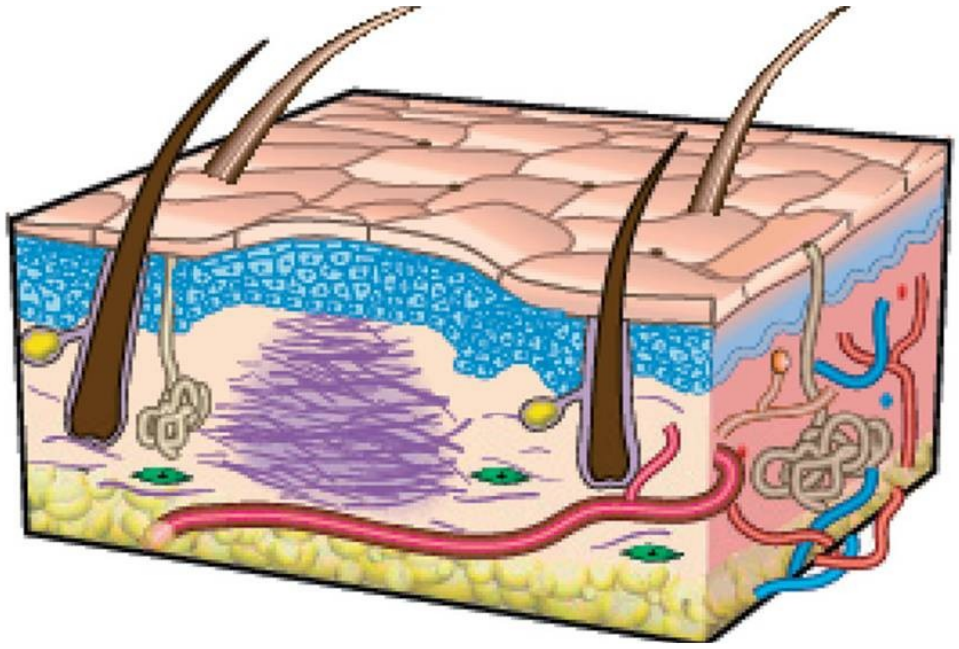

Extracellular matrix and its properties

The ECM exists in several biochemical and structural forms and is secreted and assembled by cooperative activity of numerous cell types [1]. The individual components of the ECM and its three-dimensional ultra-structure and biophysical properties can signal specific information to cells and modulate essential immune-function, such as cell migration into and within inflamed tissue, cell activation and proliferation, and cell differentiation processes. In our body, the cell's direct environment is composed of an intricate 3D network of fibrillar proteins, proteoglycans and glycosaminoglycans (GAGs), collectively termed the extracellular matrix (fig.1). Each single component and three-dimensional ultrastructure impart specific signal to cell that modulate basic function that are important for regeneration and maintenance of tissues and organs, and it therefore plays a critical role in successful tissue engineering as well [2]. The first mission is to identify to know the components of ECM. An obvious choice is to start with the most abundant protein: collagen. More than 20 genetically different types of collagen have been identified so far. Collagen molecules consist of three polypeptide a chains, each of them containing at least one repeating Gly-X-Y sequence, where X and Y are usually proline and hydroxyproline, respectively [3,4]. The three chains are supercoiled around a central axis in a right-handed manner to form a triple helix. Collagen molecules self-assemble into collagen fibrils, which form the collagen fibers after crosslinking. During the biosynthesis of collagen, the molecule undergoes several post-translational modifications, i.e. hydroxylation and glycosylation of particular residues. Depending on their structure and supra-molecular organization, collagens can be classified into fibrillar (accounting for 90% of all collagens) and non-fibrillar

collagens. For example, fibrillar collagens provide torsional stability and tensile strength and can be found in tissues such as bone, cartilage or ski

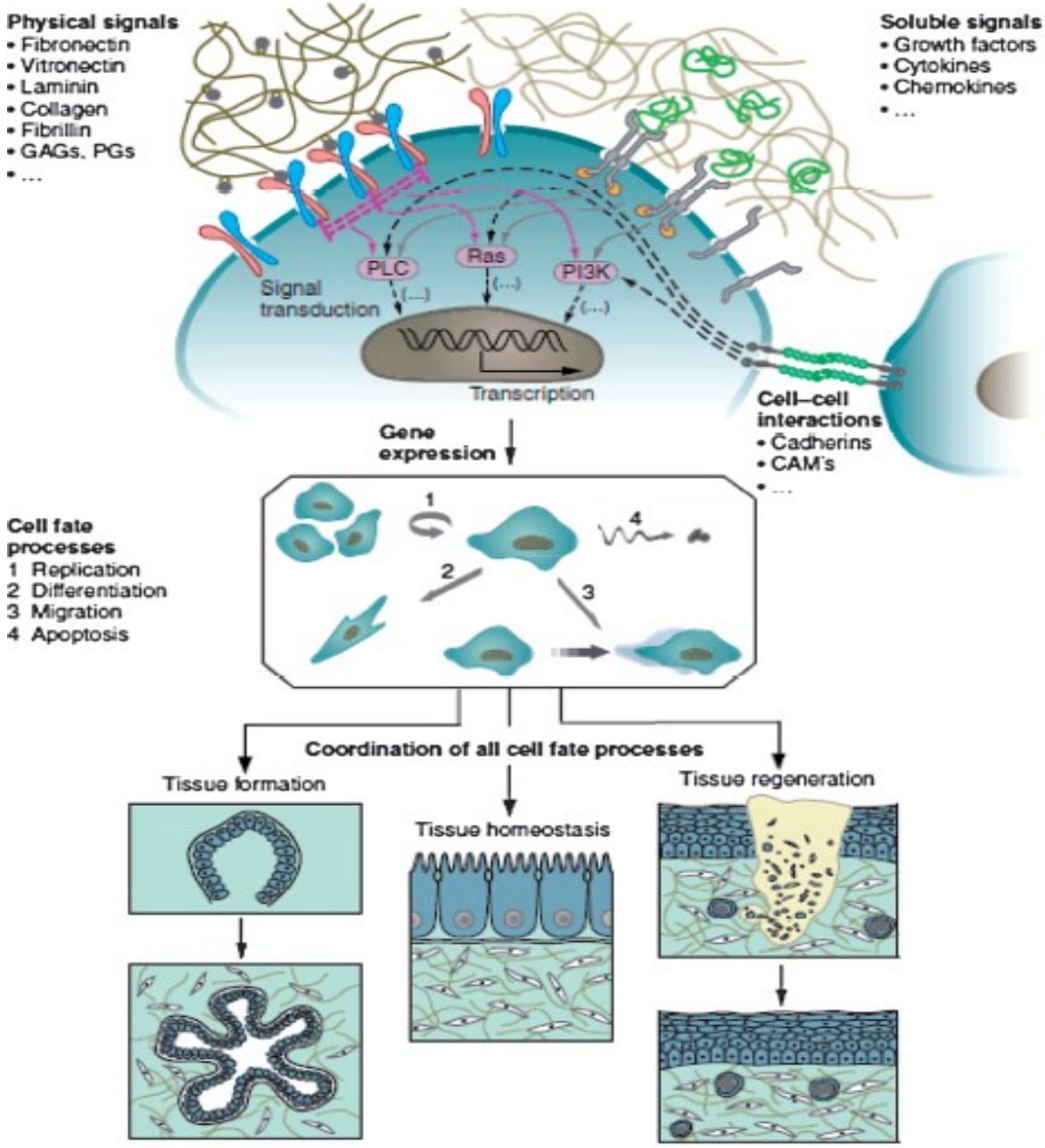

Figure 1.: Overview of the cell microenvironment. The cell's surrounding is composed of a highly hydrated environment containing physical and soluble signals, which can control signaling and activation of certain target genes. The activation of these genes will control the phenotype of the cell.[2]

In contrast, basement membrane collagens such as collagen type IV are more flexible, giving the basement membrane its typical characteristics [3,5]. In general, collagens are mainly seen as structural proteins although they contain small

sequences responsible for binding to cellular receptors. Elastin is a protein which can be found in ECM of tissues that have the ability of transiently stretching such as skin, oesophagus, lungs or blood vessels. Tropoelastin is the soluble precursor of elastin which, upon secretion to the extracellular space, can be stabilized by covalent crosslinking between the side chains of lysine, resulting in massive macro-arrays of mature elastin. Due to the extensive crosslinking there is a decrease in the solubility. The elastic properties of elastin have been attributed to the conformational entropy between the non-polar peptide sequences and lysine sequences which are extensively crosslinked. [6,7]. In short, collagen and elastin may be considered as the bricks of ECM due to their contribution to the mechanical properties of ECM. Another mode of action can be seen with the GAGs, which contribute to the gel-like characteristics of ECM. GAGs are long unbranched carbohydrated polymers consisting of repeating disaccharide units. These units are composed of one of two modified sugars-N-acetylgalactosamine or N-acetylglucosamine. They are responsible for growth factor sequestration and, due to their ability to retain water, they contribute to the characteristic appearance of ECM. When hydrated, GAGs are responsible for increase in tissue stiffness as they act as water pumps under mechanical loads. The reason for this can be due to water molecules binding to GAGs anionic groups as previously proposed[8]. Two of the most common proteins responsible for cell adhesion are fibronectin and laminin. Fibronectin is the second most abundant protein in ECM, where it is organized into a fibrillar network. It is a large glycoprotein dimer and each monomer contains three types of repeating units designated type I, II and III. In these units we can find functional domains responsible for interaction with cell surface receptors and with fibronectin itself. Laminin is a complex adhesion molecule especially found in the basement membrane of almost every tissue.

The role of ECM-cells cross talking in pathological events: wound healing and photoaging

The role of myofibroblast in ECM production and reorganization (fig. 2) in wound contraction is an example showing the crosstalk between ECM and cells [9]. In simple way it has been shown that during skin wound healing, a fibrin matrix is formed in the wound bed serving as a scaffold, allowing migration and proliferation of dermal fibroblasts [10] The development of mechanical stress stimulates fibroblasts to develop stress fibres and to produce collagen, so they acquire the proto-myofibroblast phenotype that secrete transforming growth factor β1 (TGF-β1) and in a feedback loop, proto-myofibroblasts become differentiated myofibroblasts by synthesizing α-smooth muscle actin and generating increased contractile force in a process of remodelling results in shortening of the collagen matrix with wound closure. The other example is the photoaged skin that is characterized by alteratios to the dermal connective tissue. The extracellular matrix in the dermis mainly consists of type I and type III collagen, elastin, proteoglycans, and fibronectin. In particular, collagen fibrils are important for the strength and resilience of skin, and alterations in their number and structure are thought to be responsible for wrinkle formation. In photoaged skin, collagen fibrils are disorganized and abnormal elastin-containing material accumulates and collagen and elastin may be considered as the bricks of ECM due to their contribution to the mechanical properties of ECM [11]. Biochemical studies have revealed that in photoaged skin levels of type I and III collagen precursors and crosslinks are reduced, whereas elastin levels are increased, and an imbalance between activation of matrix metalloproteinases MMPs and their respective tissue inhibitors of metalloproteinases TIMPs could lead to excessive proteolysis [12,13]. So, In this introduction we will highlight the role of the

extracellular matrix and discuss the latest technological possibilities to exploit the extracellular matrix in tissue engineering.

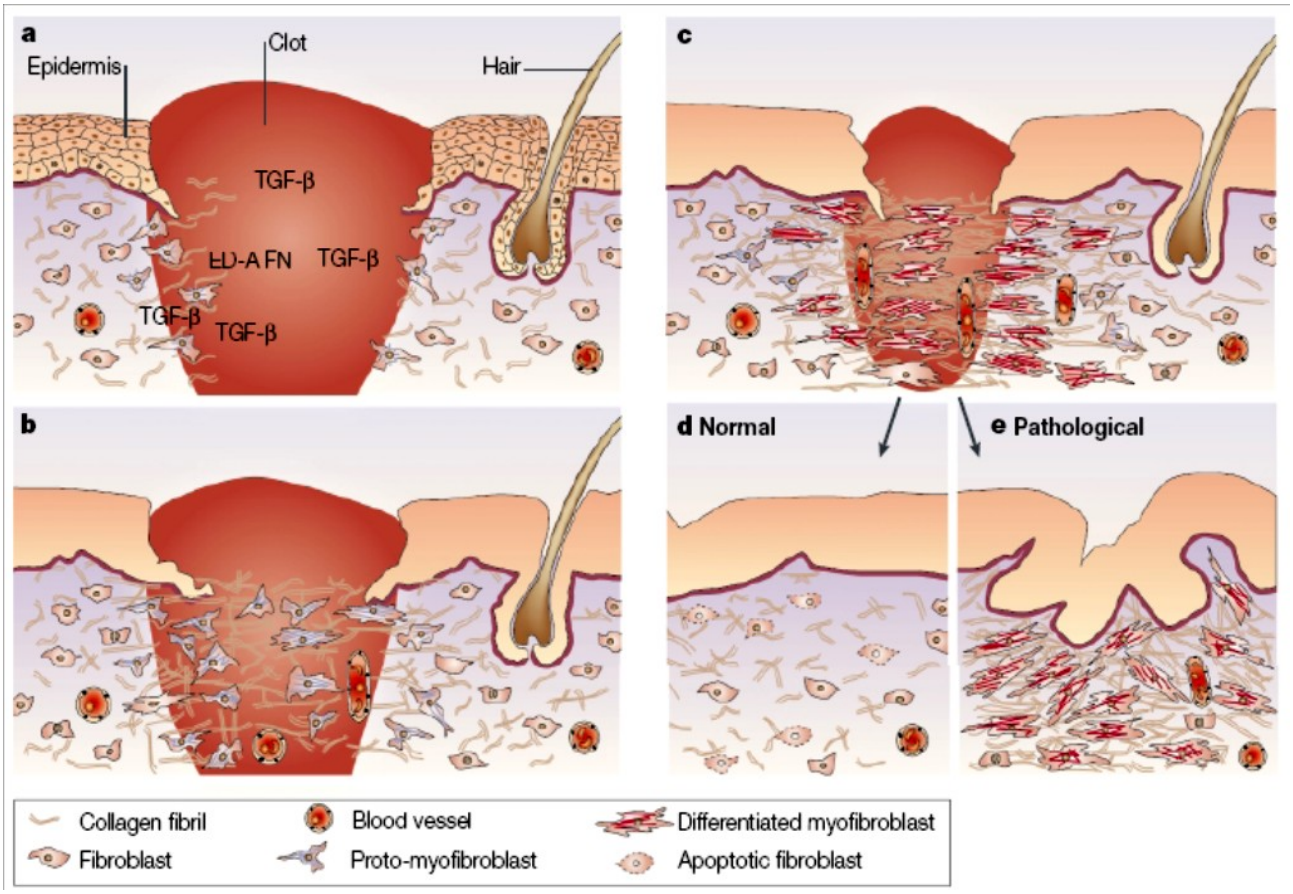

Figure 2.: model of the role of myofibroblasts during the healing of an open wound. a | In normal tissues, fibroblasts experience a relatively low amount of tension owing to stress-shielding by the surrounding collagen matrix, When a full-thickness dermal wound is filled by a fibrin clot, local growth factors stimulate fibroblasts from the adjacent intact dermis to invade this provisional matrix. b | The development of mechanical stress stimulates fibroblasts to develop stress fibres and to produce collagen, so they acquire the proto-myofibroblast phenotype. Tensional forces and growth factors stimulate proto-myofibroblasts to secrete transforming growth factor β1 (TGF-β1).c | In a feedback loop, proto-myofibroblasts become differentiated myofibroblasts by synthesizing α-smooth muscle actin and generating increased contractile force. At the same time, differentiated myofibroblasts lay down collagen and other extracellular-matrix (ECM) components, and produce proteases. This complex process of remodelling results in shortening of the collagen matrix with corresponding wound closure. d | When a normal healing wound closes, myofibroblasts disappear by apoptosis and a scar is formed. e | However, in many pathological situations, such as hypertrophic scar formation, myofibroblasts persist and continue to remodel the ECM, which results in connective-tissue contracture. In conclusion, myofibroblasts, far from being a 'bad' cell type, are functionally essential cells. It is their dysregulation that is the cause of tissue dysfunction.[13]

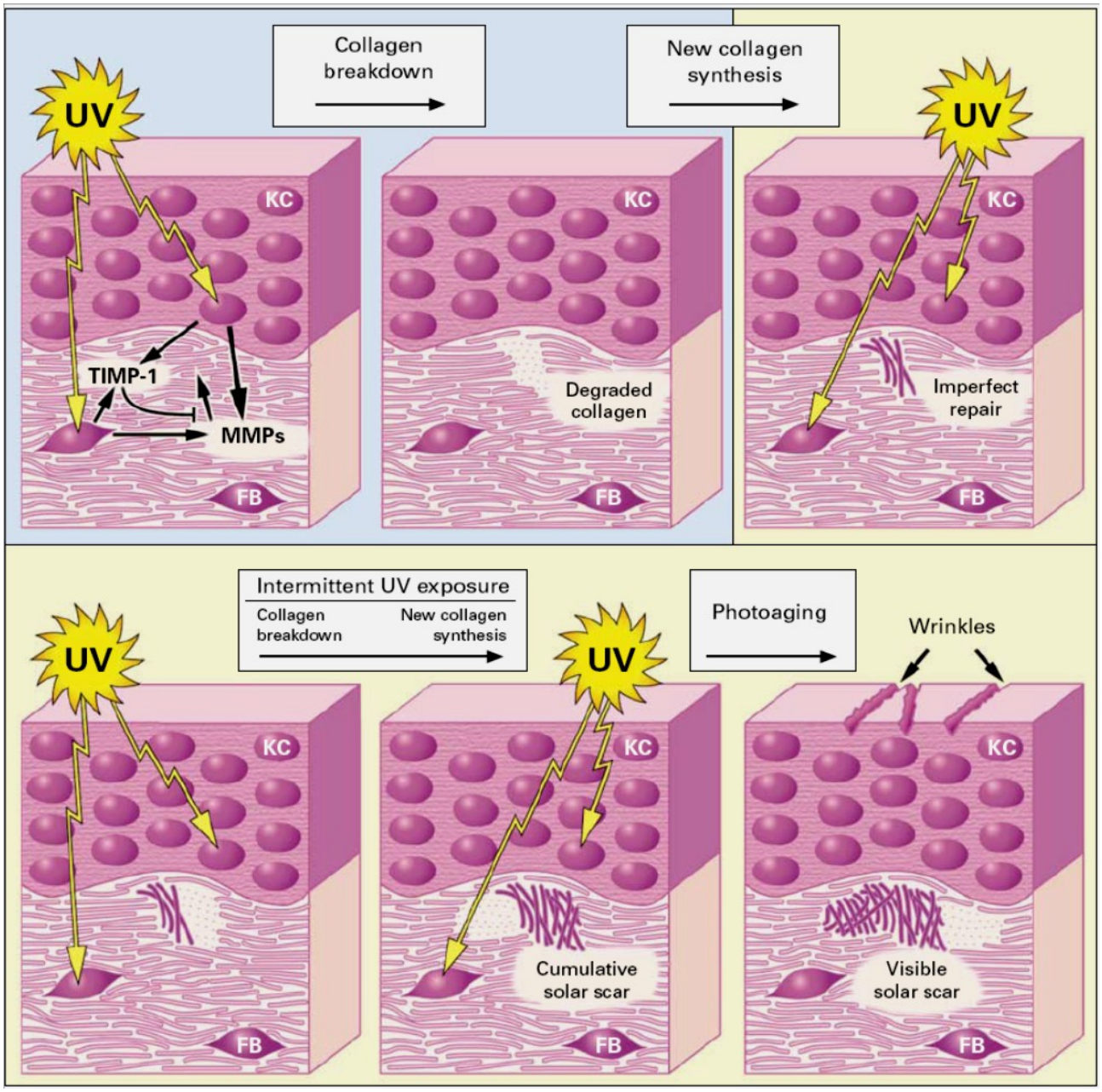

Figure 3.: Hypothetical Model of the Pathophysiology of Dermal Damage and Photoaging Induced by Ultraviolet Irradiation. Exposure to levels of ultraviolet (UV) light that cause no detectable sunburn induces the expression of matrix metalloproteinases (MMPs) in keratinocytes (KC) in the outer layers of skin, as well as fibroblasts (FB) in connective tissue; these metalloproteinases degrade collagen in the extracellular matrix of the dermis. The extent of matrix destruction is limited by the simultaneous induction of tissue inhibitor of matrix metalloproteinases-1 (TIMP-1), which partially inhibits the activity of matrix metalloproteinases. The breakdown of collagen is followed by synthesis and repair, which, as with all types of wound healing, is imperfect and leaves subtle, clinically undetectable deficits in the organization or composition of the extracellular matrix, or both. Matrix damage, followed by imperfect repair, occurs with each ensuing exposure to the sun, leading to the accumulation of altered matrix (solar scar) and, eventually, observable photoaging (wrinkles). The upper panels with the blue background depict the processes examined in our study, and the upper and lower panels with the yellow background depict hypothetical processes that are consistent with our results.[11]

How build-up a tissue equivalent *in vitro*: bottom-up approach.

Tissue engineering is an interdisciplinary field that applies the principles of engineering and life sciences toward the development of biological substitutes that restore, maintain, or improve tissue function [14].

Traditional tissue engineering strategies typically employ a “top-down” approach, in which cells are seeded on a biodegradable polymeric scaffold (fig. 4). In top-down approaches, the cells are expected to populate the scaffold and create the appropriate extracellular matrix (ECM) and microarchitecture often with the aid of perfusion [15], growth factors [16] and/or mechanical stimulation.

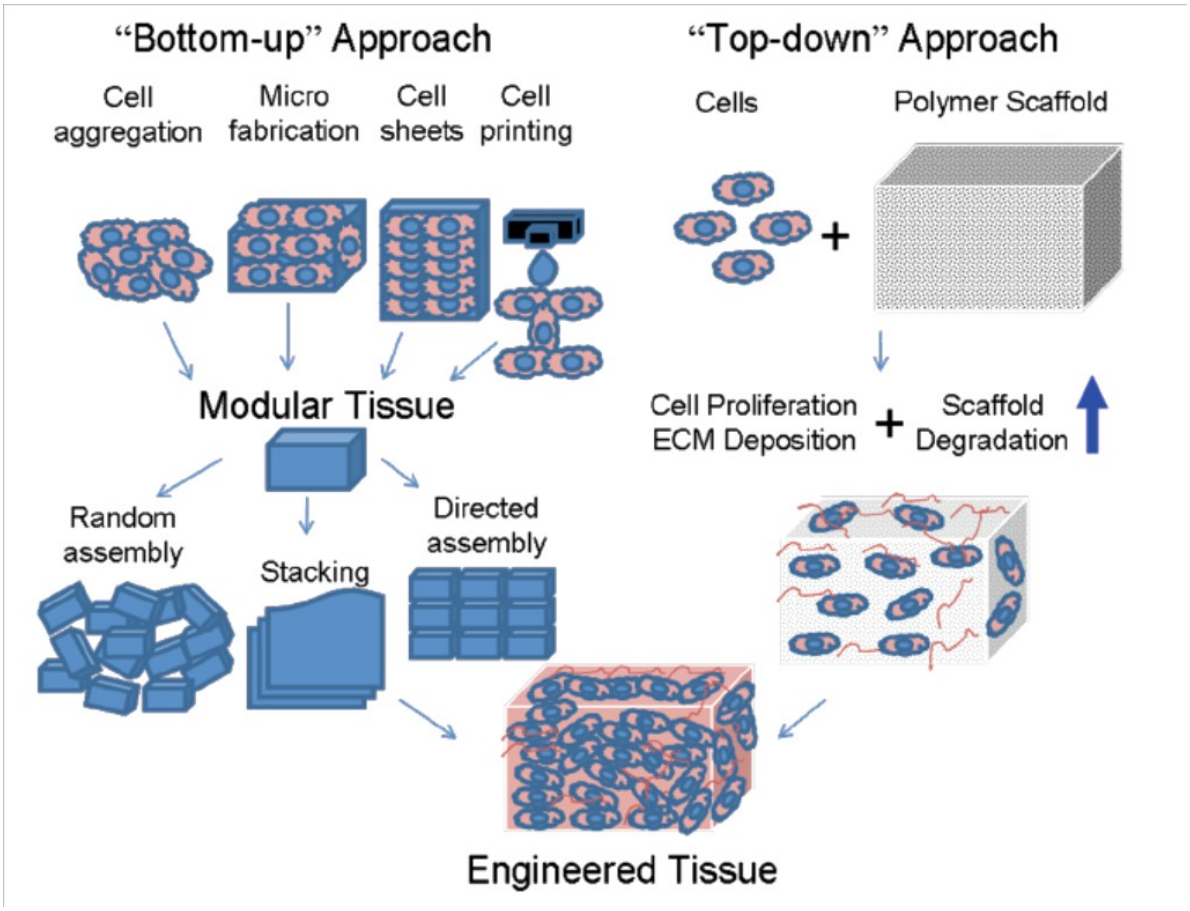

Figure 4.:Bottom-up & Top-down approaches to tissue engineering. In the bottom-up approach there are multiple methods for creating modular tissues, which are then assembled into engineered tissues with specific microarchitectural features. In the top-down approach, cells and biomaterial scaffolds are combined and cultured until the cells fill the support structure to create an engineered tissue.[14]

Top-down approaches often have difficulty recreating the intricate microstructural features of tissues. Subsequently, from an engineering point of view, (fig.4) it was proposed to build tissues by assembling blocks mimicking those units in a bottom-up or modular approach [17,18]. This approach brings versatility and scalability to the fabrication of *in vitro* tissue models or implants. The fabrication of those tissue models necessitates tools to create an initial architecture and to systematically manipulate their microenvironments in space and time [19]. One of the major challenges of bottom-up tissue engineering is to assemble modular tissues with specific micro architectures into macroscale biomimetic engineered tissues. Other challenge is to retain the microarchitecture and cellular behavior of modular tissues, while creating engineered tissues with robust mechanical properties. Technologies developed within the bottom-up strategy are numerous and include: method favors fabrication of Microscale Building Blocks (MBBs) as show in figure 4, that can be assembled into larger constructs. MBBs are gel encapsulated cells [20] or spontaneously aggregated cells [21]. It gained versatility and precision with microfabricated templates using photolithography [22], micromachining [23], soft lithography [24], membrane technology [25], centrifugal casting [26] or the combination of multiple processes [27]. Templates are rather cheap and allow rapid production of big quantities of MBBs of defined shape and size. Their assembly into ordered constructs requires further development (Fig. 5)

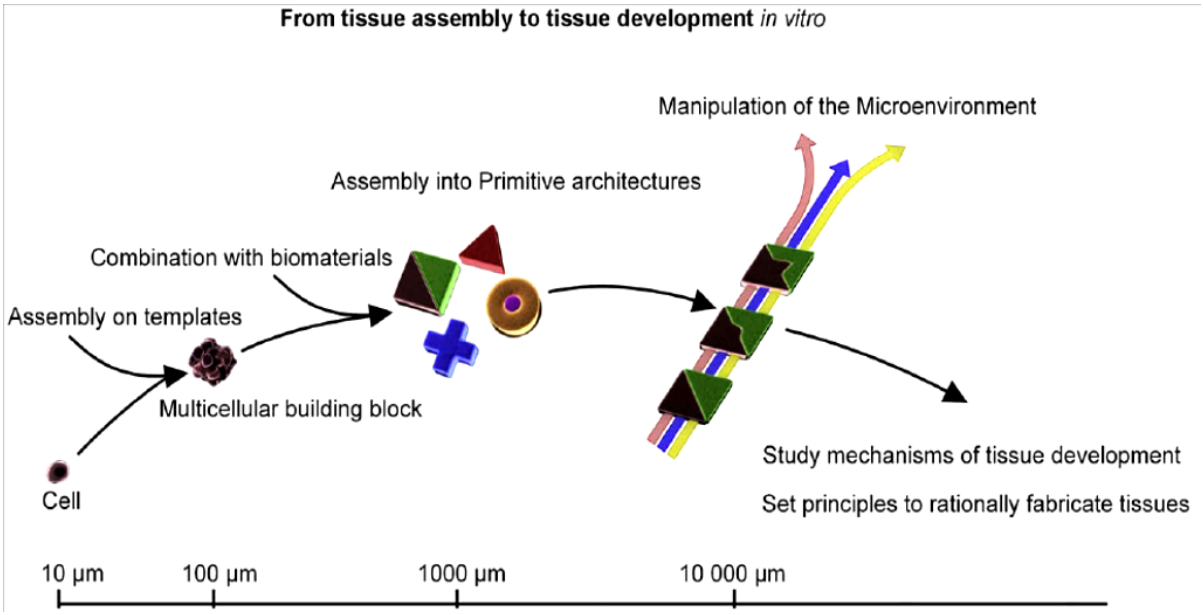

Figure 5.: from tissue assembly to tissue development *in vitro*. Tissue fabrication methods allow the assembly of cells into primitive tissue compartments, which are prone to remodeling. The tissue geometry along with the manipulation of the environment at a microscale further promote the self-organization of cells into more complex tissues *in vitro*. [14]

Examples of constructs resulting from a bottom-up approach include structures from various single cell types and from mixtures of different cell types by pouring different types of cell beads into a single PDMS mold (fig 6A). Although approximately 100000 monodisperse cell beads are required to fabricate millimetrescale 3D tissue.The primary advantages of this method are rapid production of millimetre-thick 3D cell structures, homogeneous cell density, and tissue formation without necrosis in a period of less than a week because of the supply of the cell culture medium through cavities between cell beads. In addition, when the millimetre-thick 3D cell structure was composed of HepG2 cells and NIH 3T3 cells, albumin secretion increased daily from the HepG2 cells in the 3D tissue, but not in the 2D culture system. However, the construction of the vessel network in the 3D cell structures is required to maintain cell viability over a long period. Adaptations of this method will allow the formation of capillary networks in the structure because methods using the mold can integrate cell-laden fibers as capillaries into bead-based cell structures[28]. As another method

of a bead-based assembly, the printing of cellular spheroids or cell-laden hydrogel beads can be used to sequentially stack these materials layer-by-layer.[29-32] Combined with computer-aided printing systems, the printing approach enables the rapid construction of complex 3D structures with different types of cells.

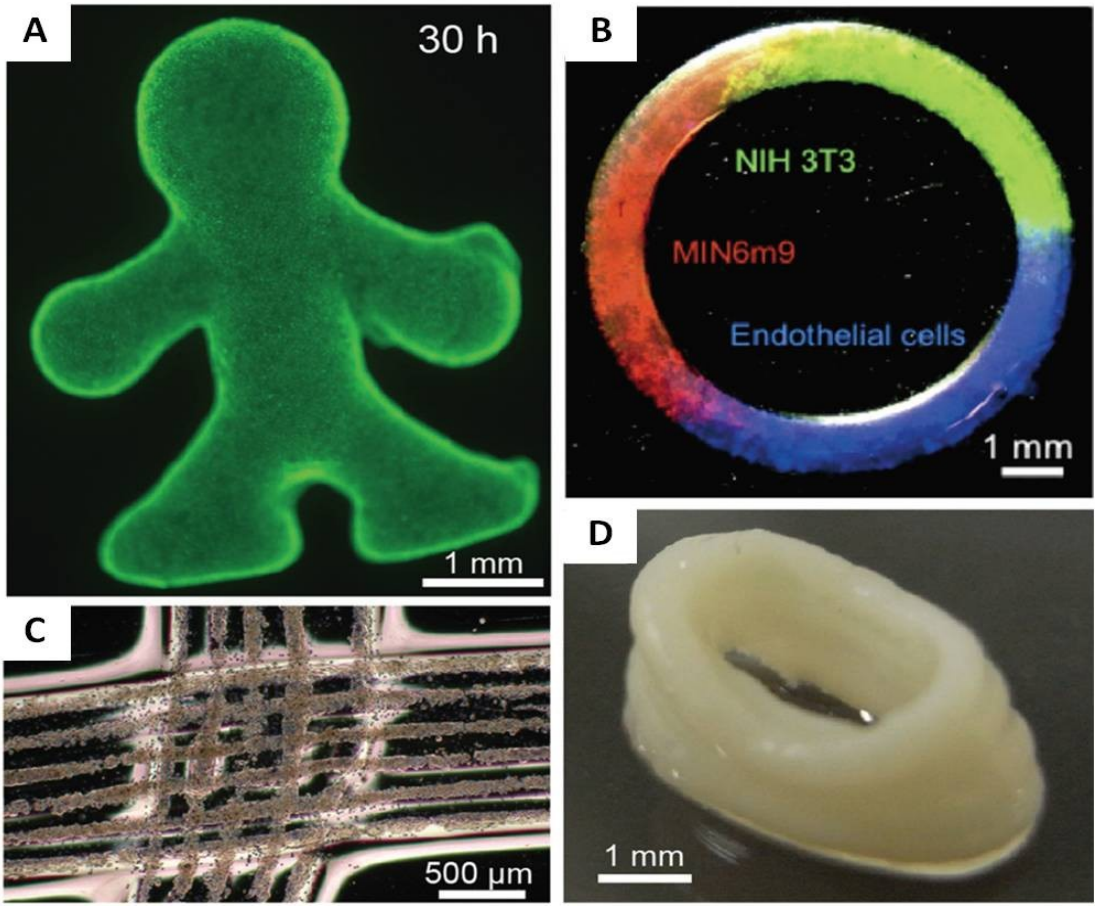

Figure 6.: 3D organotypic construct (i) Fluorescent image of a macroscopic structure with a complex shape. Live cell staining indicates that almost all cells within the structure are alive.(j) 3D cell structures formed by knitting cell-laden hydrogel fibers. The fibers are composed of collagen and alginate gel encapsulating HeLa cells.34 (k) Ring-shaped cell structure fabricated by printing cell beads. Various cell types are spatially coded within the structure.30 (l) Tube-shaped structure prepared by printing cell beads.30.[28]

For example, the printing of cellular spheroids or cell-laden collagen beads has been used to reproducibly construct ring-shaped structures containing multiple cell-laden beads in specific designed locations (Fig.6B) and hollow tubes (Fig. 6D) [29,31,32]. A fiber-based assembly method was recently proposed for the construction of 3D cell

structures with complex shapes. Assemblies of cell-laden hydrogel fibers can be formed by weaving these fibers together, much as threads are woven to form cloth [33]. These approaches produce a metastable multicellular construct that will remodel over time according to biological and physical principles (i.e. migration of the cells, shrinkage of the hydrogel). Shapes and patterns are not inevitably translated to the final tissue. Designs must thus focus on promoting proper remodeling into the final architecture. Clearly, understanding and promoting tissue self organization would tremendously improve tissue microfabrication

The study of the emergence of forms and functions *in vitro* tissue models is still in its infancy. It is likely that those strategies of auto assembly can only reach a limited complexity and should be followed by more complex manipulations of the microenvironment. The rapid development of complex microfluidic systems, microbioreactors and detecting tools allows the long term culture of microscale tissues in precisely defined microenvironment. Microbioreactors permit the long term culture in controllable and continuous environment using minute amounts of biological factors [34] and to include parameters like shear stress, interstitial flow [35,36] or gradients of soluble factors [37,38]. They present great possibilities to culture microtissues in controlled, heterogeneous environments.

Mechanisms underlying tissue organization and the development and maintenance of tissues architecture and function are highly conserved through organisms and are better understood now than two decades ago [39] It appears clearer that, beyond genetic regulation, the tissue architecture and microenvironment feeds back to promote its development, maintain its integrity and function [40,41]. Thus, to promote *in vitro* tissue developments, of special interest are (i) the creation of multicellular architectures prone to remodeling and (ii) strategies and tools to manipulate the microenvironment and promote *in vitro* organization.

Tissue Engineering of skin

The skin is the largest organ in mammals and serves as a protective barrier at the interface between the human body and the surrounding environment. It guards the underlying organs and protects the body against pathogens and microorganisms. Accordingly, it is directly exposed to potentially harmful microbial, thermal, mechanical and chemical influences. In the past 25 years, great efforts have been made to create substitutes that mimic human skin [43]. These skin substitutes were made possible by employing advanced tissue engineering approaches and have been used for clinical applications, promoting the healing of acute and chronic wounds, or utilized as complex human-based organ-like test systems for basic or pharmaceutical research [44]. In skin TE, various biological and synthetic materials are combined with *in vitro*-cultured cells to generate functional tissues (Fig. 7)

However, besides their use as *in vivo* grafts, recently, other applications have emerged for skin substitutes as *in vitro* test systems [2] (Fig. 7). In this context, they enable not only the investigation of fundamental processes in the skin, but also the hazard assessment of various chemical compounds that are topically applied on the skin without the need to use animal models. Results gained from experiments conducted in animal models are often of limited value due to differences in the metabolism and the anatomical architecture compared to human skin. *In vitro* experiments in two-dimensional (2D) monolayer cultures of human cells are also of low relevance due to the lack of complex cell–cell and cell–ECM interactions [48]. However, tissue-engineered skin substitutes can overcome these problems by using human-derived cells that are arranged

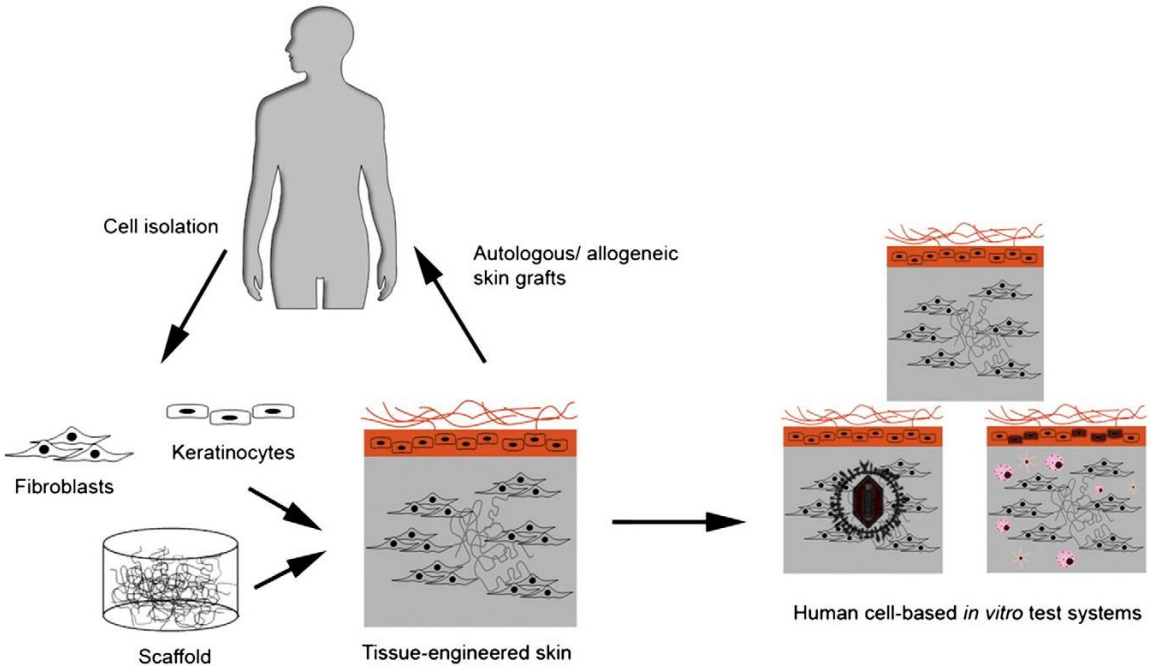

Fig. 7.:schematic illustration of principles of skin tissue engineering. Primary keratinocytes and fibroblasts are isolated from human donor tissues, which are then *in vitro* expanded prior seeding onto suitable scaffold materials/matrices. For a full-thickness skin equivalent, the fibroblasts and the matrix are initially used to establish the dermal part. The keratinocytes are seeded afterwards on the top of the dermis to ultimately form the epidermal part of the skin substitute. The *in vitro*-engineered skin can serve as skin graft or can be used as human-cell based *in vitro* test system.[2]

in a 3D physiological environment, allowing the interaction of the different cell types with one another and the surrounding matrix. In basic research, skin substitutes can help to elucidate fundamental processes in the skin such as the stimuli that lead to the formation of the epidermis [49,50], the molecular cross-talk between different cell types [51,52], the maintenance of the stem cells [51], the process of wound healing [53], and the infection with different kinds of pathogens [55,56]. One great advantage of skin substitutes is that the cellular composition is completely controllable by the researcher. Thus, a certain cell type can be specifically integrated or omitted to determine the relevance of the cell type in the biological process under investigation. To date, many types of skin substitutes have been developed by different groups [51,53,54,56–60]. Some of these are commercially available such as Skinethic™ RHE, Episkin™ (SkinEthic/ L'Oreal, France), Epiderm™, Epiderm FT™(MatTek

Corporation, USA), EST1000, and AST2000 (CellSytems, Germany) (Table 1). These skin substitutes can be classified in two types. The first type consists of keratinocytes seeded on a synthetic or collagen carrier simulating only the human epidermis (epidermal substitutes). The second type consists additionally of a dermal layer of human fibroblasts embedded in various kinds of scaffolds (full-thickness skin substitutes) (Fig. 8).

Brand name/manufacturer	Scaffold material	Cell source	Dermis
Episkin™/L'Oreal Nice, France	Collagen	Keratinocytes (mammary/abdominal samples obtained from healthy consenting donors during plastic surgery)	No
Skinethic™ RHE/L'Oreal, Nice, France	Polycarbonate membrane	Keratinocytes (neonatal foreskin tissue or adult breast tissue)	No
Epiderm™/MatTek Corporation, Ashland MA, USA	Collagen-coated, polycarbonate membrane	Human keratinocytes (neonatal foreskin, adult breast skin)	No
EpiDermFT™/MatTek Corporation, Ashland MA, USA	Collagen	Human keratinocytes (neonatal foreskin, adult breast skin), human fibroblasts (neonatal skin, adult skin)	Yes
EST-1000/CellSystems, Troisdorf, Germany	Polycarbonate membrane	Keratinocytes (neonatal foreskin)	No
AST-2000/CellSystems, Troisdorf, Germany	Collagen	Human keratinocytes Human fibroblasts	Yes
Phenion® FT Model/Henkel AG&Co.KGaA Duesseldorf, Germany	Bovine, cross linked, lyophilized collagen	Primary human keratinocytes (neonatal foreskin), human fibroblasts (neonatal foreskin)	Yes
StrataTest®/Stratatech Corporation Madison WI, USA	Collagen I	immortalized, human NIKS® keratinocytes dermal fibroblasts	Yes

Table 1.: commercially available *in vitro* epidermal and full-thickness skin substitutes.[2]

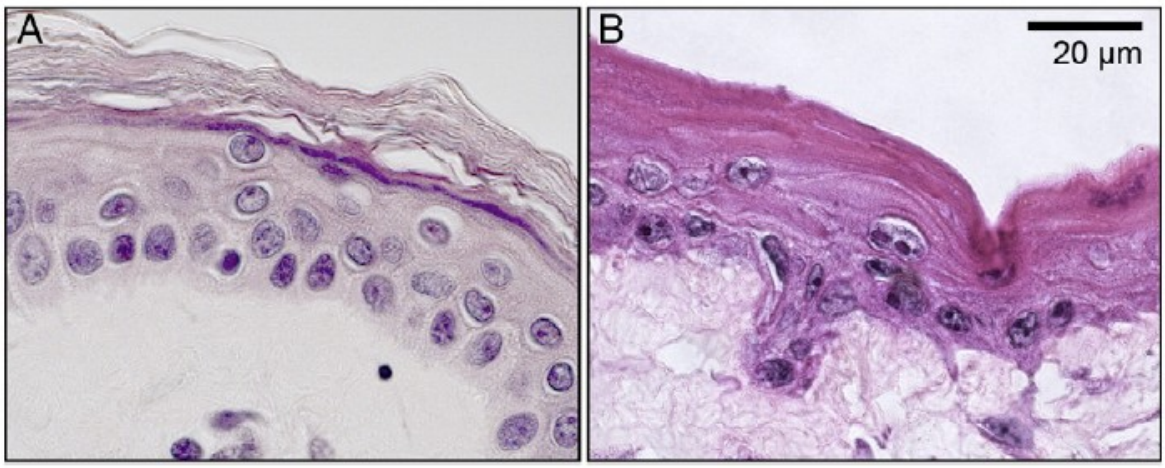

Figure 8.: histological staining of *in vivo* skin (A) and *in vitro*-engineered epidermal/dermal skin substitute (B). Scale bar equals 20 µm.[2]

Epidermal substitutes in vitro model

The human skin is exposed to a great amount of different chemicals that need to be classified according to their capacity to harm the skin. Utilizing conventional test methods, the necessary number of toxicity tests will be extremely time and cost consuming. In contrast, skin *in vitro* models offer a viable and cost-effective alternative for the hazard assessments of the substances under REACH (European programm for Registration, Evaluation, Authorization and Restriction of Chemicals) regulatory. Two living skin equivalent models have been validated according to ECVAM regulatory for corrosion testing [86–88]. Unlike the assays for acute corrosion, skin irritation tests are more complex and need not only the measurement of cytotoxicity, but also of metabolic reactions such as cytokines and enzyme release.

In response to physical or chemical stresses, keratinocytes release various substances such as interleukin-1α F(IL-1 α), interleukin-8 (IL-8), tumor necrosis factor α (TNF- α), interleukin-6 (IL-6), interleukin-7 (IL-7), and interleukin-15 (IL-15) *in vivo* [55]. Employing *in vitro* skin substitutes, a dose dependent release of the cytosolic enzyme lactate dehydrogenase (LDH) and IL-1α was observed in response to the application of various cosmetics [61].

However many drugs and cosmetics are applied to the skin, but the amount of the substances that reach the targeted site remains often unclear. Hence, for the cosmetic industry, it is of great interest to have an *in vitro* system, which can determine how much of a cosmetic formula penetrates through the epidermal layer into the skin [62]. Penetration assays can thereby help to determine the risk/benefit ratio of certain chemicals such as glucocorticoids [64]. Currently, researchers are investigating the penetration of substances through artificial stratum corneum (SC) [63], epidermal reconstructs [62] and epidermal/ dermal [65] reconstructs. A great

advantage of these artificial models is not only that the healthy state of the skin can be mimicked, but also that it is possible to simulate diseased states [66]. However, a major difference between *in vivo* skin and skin substitutes is the presence of skin appendages such as hair follicles, sweat glands and sebaceous glands. These appendages represent openings, which can increase the permeability of the skin. Percutaneous absorption of drugs is due to two different routes of passive diffusion. The transepidermal diffusion uses an inter- or transcellular pathway across the stratum corneum, whereas the transappendageal diffusion follows the route through the hair follicles and their associated sebaceous glands [67]. The importance of skin appendages and their ability to act as a conduit for drug transport have been recognized [68,69] and could be confirmed by experiments on a tissue-engineered human skin equivalent with hair [70]. This model was designed from human fibroblasts and keratinocytes in which complete pilosebaceous units, obtained by thermolysin digestion of hairy skin, were inserted. In a hydrocortisone diffusion test, this model could show a significantly increased rate of penetration in comparison to the control (skin equivalent with sham hair insertion). The skin is exposed to potentially harmful irradiation that can cause serious alterations in the skin. To protect the exposed cells, the natural skin is pigmented with melanin that is able to absorb harmful UV radiation (UVA and UVB) and can scavenge formed radical oxygen species [71]. Melanin itself is produced in melanocytes and distributed to the surrounding keratinocytes through dendritic extensions [72]. Hence, the investigation of skin reactions to sunlight requires the addition of melanocytes in order to mimic the *in vivo* situation correctly (fig .9) [73].

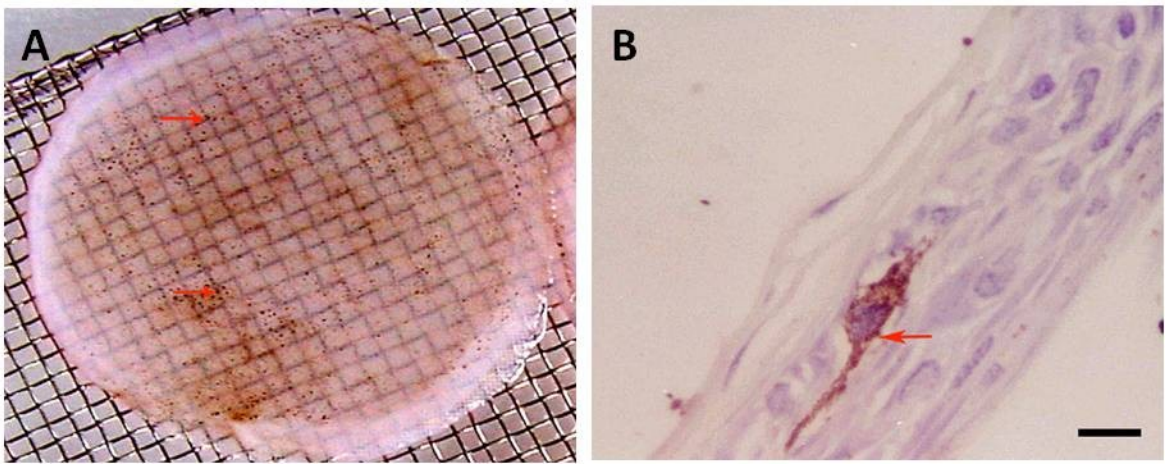

Figure 9.: epidermal layer *in vitro* with melanocytes ;(A) Brown appearance of the tissue-engineered skin containing melanocytes; pigmented spots could be seen; (B) DOPA staining of the tissue-engineered skin containing melanocytes, and stained with hematoxylin; melanocytes located in the basal layer of the skin equivalents. Obvious pigmentation could be seen in the cytoplasm. Scale bar 25 µm.[73]

By introducing melanocytes into skin substitutes, the natural process of pigmentation could be successfully recreated. To protect natural skin *in vivo* from damaging radiation, sun-blocking lotions can be applied topically. To develop improved photo protective agents, skin substitutes can be used as easy manageable *in vitro* test systems [74]. The combination of systemically or topically applied drugs together with sun irradiation can also result in adverse skin reaction. This phototoxicity can result in amplified erythema and inflammatory responses *in vivo*. To predict the phototoxic effects of substances, skin substitutes can be exposed to drugs and UVB irradiation *in vitro*. It has been demonstrated that epidermal skin substitutes are able to discriminate between phototoxic and non-phototoxic substances and are thus a suitable alternative test method for phototoxicity [75].

Full thickness in vitro models

Although the great majority of the skin substitutes used in pharmacological research are only composed of an epidermal layer, these skin substitutes could be further improved by the addition of a dermal layer containing fibroblasts. In this context,

fibroblasts have only recently begun to receive more attention. It was discovered that skin fibroblasts are far from being homogeneous and it was speculated that some chronic wounds are due to a change in the composition of the fibroblast population [76]. Using standard cell culture, it was shown that fibroblasts positively influence keratinocyte growth *in vitro*, most likely due to the fact that these cells secrete soluble growth factors [77]. In natural skin, the interaction between fibroblasts and keratinocytes plays a major role in processes such as wound healing [78] and the formation of the base membrane [79,80]. Using skin substitutes, it was demonstrated that fibroblasts play a crucial role in the natural epidermal histogenesis. Without fibroblasts, the keratinocyte differentiation is severely affected and results only in few layers of highly differentiated epithelial cells [51,52]. Interestingly, keratinocytes have also a positive effect on the proliferation of fibroblasts [51]. This interaction of epidermal and dermal cells is hypothesized to be due to a double-paracrine mechanism that regulates the growth of keratinocytes and fibroblasts [81,82]. According to this hypothesis, keratinocytes secrete IL-1 that stimulates the skin fibroblasts to secret keratinocyte growth factor (KGF) and granulocyte-monocyte colony-stimulating factor (GM-CSF), which in turn positively in"uence the proliferation of the keratinocytes. Furthermore, dermal fibroblasts play an essential role in the remodeling of the skin, in the contraction of acute wounds [83,84] and they can increase the resistances of keratinocytes to toxic chemicals [85]. Based on these findings, one could conclude that in order to gain meaningful data from toxicological *in vitro* studies, the isolated focus on a keratinocyte-containing epidermal layer alone is not sufficient, making the use of a full-thickness skin model essential. In contrast, epidermal substitutes might be more suitable for the determination of the penetration coefficient through the skin. In routine *in vitro* penetration studies (= percutaneous absorption testing), a defined area of a skin substitute separates a donor from an

acceptor chamber. The leak-proof connection of the skin substitute to the experimental setup is important. Collagen-based full-thickness skin substitutes are not ideal for such tests since they do not seal the whole surface area due to a low mechanic resilience, thus resulting in open edges, through which the substance under investigation can openly diffuse. Bell et al. described the first process for generating an *in vitro* test system with a dermal and an epidermal component [84]. In this process, allogeneic fibroblasts were seeded into a matrix of bovine collagen type I. In order to generate a natural epidermis, keratinocytes were cultured on the surface of this matrix at an air–liquid interface [86]. This skin substitute has been used under the name Apligraft™ (fig.10) for the treatment of chronic wounds and was marketed under the name TESTSKIN™ as an *in vitro* test system [87].

To date, different techniques for the formation of a dermal layer ex vivo have been described. Fibroblasts are seeded into a hydrated gel of collagen [88], a fibrin gel [89] or a scaffold composed of collagen/chitosan/ chondroitin-4–6-sulfates [90]. In another approach, high densities of fibroblasts were seeded onto a synthetic membrane. Over time, the fibroblasts generated their own matrix, which could then be inoculated with keratinocytes to form a skin substitute (self assembly method). The advantage of this method is that no cross-species scaffold is needed for the formation of a dermal layer. Furthermore, synthetic polymers such as polylactic-co-glycolic acid (PLGA) [91], polycaprolactone (PCL) [92], a combination of PLGA/ PCL [93] or PLGA and PCL with naturally derived collagen [94] were used to generate the dermal skin layer. The advantages of these polymers include a greater mechanic stability and no risk of pathogen transfer. However, major pitfalls of these materials are a lack of natural adhesion and signaling molecules

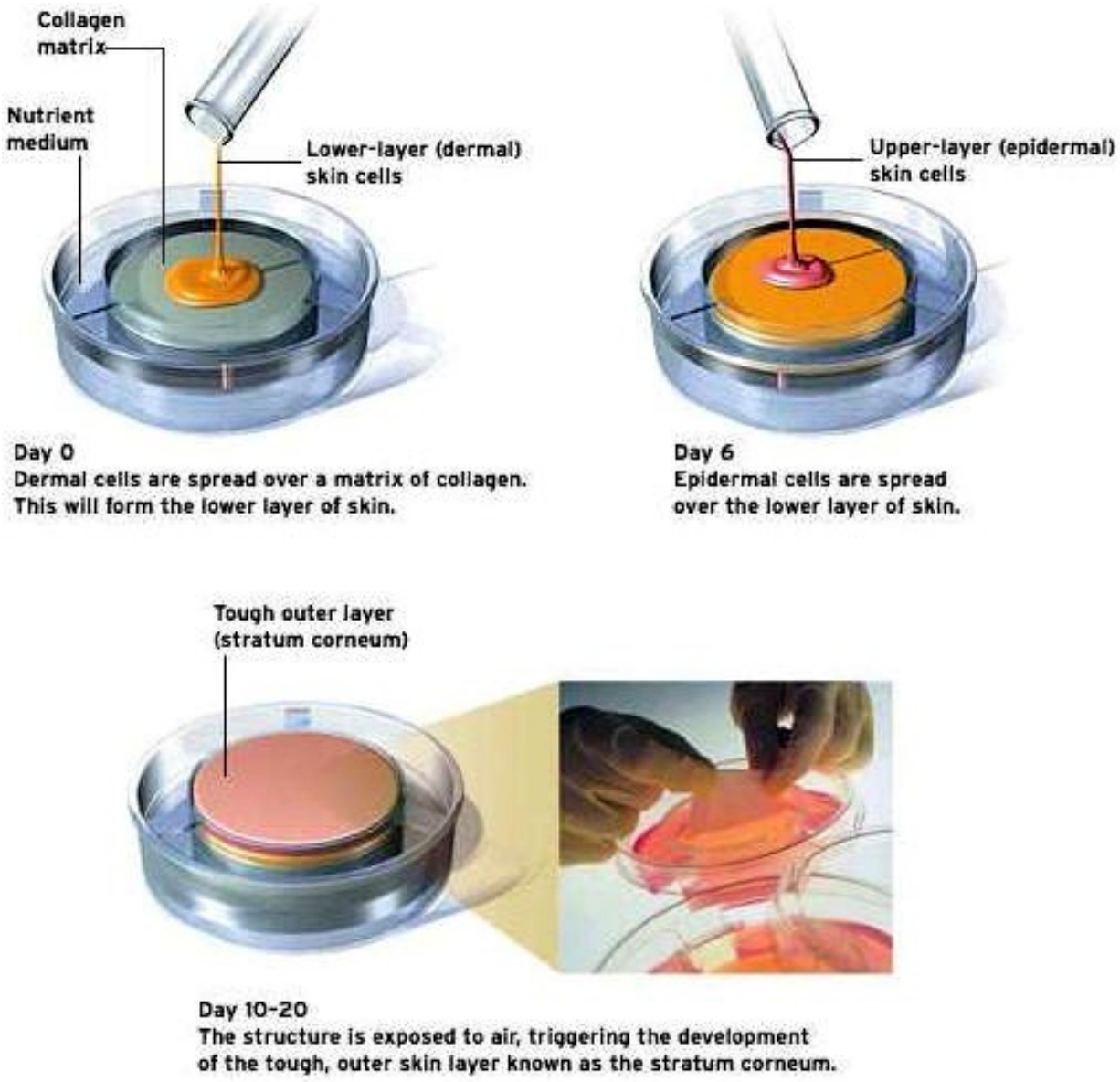

Figure 10.: Apligraft prosessing

Full-thickness skin substitutes are of great value for the investigation of complex dermatological questions, where the molecular crosstalk between the keratinocytes and the fibroblasts is crucial. Furthermore, full-thickness skin substitutes are necessary for the investigation of processes where the epidermis and the dermis are equally involved. In order to test possible immunological reactions on skin, Langerhans cells (LCs) can be introduced into full-thickness skin substitutes. The function of these specialized dendritic cells (DCs) of the skin is to capture and process antigens that come into contact with the skin. LCs reside as immature cells

in epidermal niches [95]. Upon binding to an antigen, these cells migrate from the epidermis into local dermal lymph nodes. During this migration, the LCs differentiate into mature DCs and can present the processed antigen to T-cells in the lymph nodes [96]. As reported, first attempts of the integration of epidermal LCs into a skin substitute failed and resulted only in round pycnotic cells in the upper layers of the epidermis [97]. However, to overcome these problems, researchers integrated non-differentiated CD34-positive (CD34+) hematopoietic progenitor cells (HPCs) and CD34+ HPCs that were differentiated into LCs by granulocyte macrophage growth factor and tumor necrosis factor-α (TNF- α), into a pigmented skin substitute [97]. The integration of differentiated as well as non-differentiated cell populations resulted in suprabasally located cells that exhibited LC typical markers. These results provided evidence for the influence of the keratinocytes in the LC differentiation from CD34+ HPCs [97] [92]. In another approach, epidermal biopsies were placed directly onto a dermal substitute of collagen and fibroblasts. The epidermal keratinocytes and the LCs migrated out of the biopsies and covered the dermal compartment. After culture on an air–liquid interface, a functional epidermis was formed that contained LCs with an immature phenotype. To simulate the early contact with an allergen, these skin substitutes were treated with the LCs promoting GM-CSF and the immunosuppressive agent cyclosporine-A (SC-A). GM-CSF was found to increase the migration, but not the density of the LCs, whereas SC-A did not influence the density of immature LCs [98].

In vitro skin models are currently employed for identifying skin corrosive or -toxic substances and have been proven to be very useful tools for the investigation of basic developmental processes as well as for the identification of pathological conditions. Although the design of the epidermal and/or dermal layer-mimicking *in vitro* skin substitutes is today nearly state-of-the-art, there are clearly differences

between these models and native *in vivo* skin [99]. Future developments in *in vitro* skin substitutes should include the addition of skin appendages. The integration of sweat glands or hair follicles will help to mimic a more realistic *in vivo* situation, thus offering a more correct experimental setup.

REFERENCES

1.Lydia Sorokin**.**The impact of the Extraacellular matrix on inflammation. Nature review Immunol. 2010 Vol. 10

2. Hugo Fernandes,Lorenzo Moroni,Extracellular matrix and tissue engineering applications. Journal of Material Chemistry.

3. J. Myllyharju and K. I. Kivirikko, Trends Genet., 2004, 20, 33–43.

4. K. Gelse, E. P€oschl and T. Aigner, Adv. Drug Delivery Rev., 2003, 55, 1531–1546.

5.M. J. Buehler, Proc. Natl. Acad. Sci. U. S. A., 2006, 103, 12285– 12290.

6 F. W. Keeley, C. M. Bellingham and K. A. Woodhouse, Philos. Trans. R. Soc. London, Ser. B, 2002, 357, 185–189.

7 D. W. Urry, T. Hugel, M. Seitz, H. E. Gaub, L. Sheiba, J. Dea, J. Xu and T. Parker, Philos. Trans. R. Soc. London, Ser.B, 2002, 357, 169– 184

8 A. Lamure, M. F. Harmand and C. Lacabanne, J. Biomed. Mater. Res., 1990, 24, 735–747

9. Serini, G. & Gabbiani, G. Mechanisms of myofibroblast activity and phenotypic modulation. *Exp. Cell Res.* **250**, 273–283 (1999

10. G. C. Gurtner, S. Werner, Y. Barrandon and M. T. Longaker, Nature, 2008, 453, 314–321.

11. Lavker RM. Cutaneous aging: chronologic versus photoaging. In: Gilchrest BA, ed. Photoaging. Cambridge, Mass.: Blackwell Science, 1995: 123-35.

12. Braverman IM, Fonferko E (1882) Studies in cutaneous aging: I.the elastic fibre network. JInvest dermatol 78:434-443

13. Barbara A. Gilchrest, Jeand Krutman Skin Aging

14. R. Langer and J. P. Vacanti, Science, 1993, 260, 920–926.

15. Niklason LE, Gao J, Abbott WM, Hirschi KK, Houser S, Marini R, Langer R. Functional arteries grown *in vitro*. Science 1999;284(5413):489–93.

16. Gooch KJ, Blunk T, Courter DL, Sieminski AL, Vunjak-Novakovic G, Freed LE. Bone morphogenetic proteins-2, -12, and -13 modulate *in vitro* development of engineered cartilage. Tissue Eng 2002;8(4): 591–601.

17. Kelm JM, Djonov V, Ittner LM, Fluri D, Born W, Hoerstrup SP, et al. Design of custom-shaped vascularized tissues using microtissue spheroids as minimal building units. Tissue Eng 2006;12(8):2151–60.

18 McGuigan AP, Sefton MV. Vascularized organoid engineered by modular assembly enables blood perfusion. Proc Natl Acad Sci U S A 2006;103(31):11461–6

19. Khademhosseini A, Langer R, Borenstein J, Vacanti JP. Microscale technologies for tissue engineering and biology. Proc Natl Acad Sci U S A 2006;103(8):2480–7

20. McGuigan AP, Sefton MV. Vascularized organoid engineered by modular assembly enables blood perfusion. Proc Natl Acad Sci U S A 2006;103(31): 11461

21. Kelm JM, Djonov V, Ittner LM, Fluri D, Born W, Hoerstrup SP, et al. Design of custom-shaped vascularized tissues using microtissue spheroids as minimal building units. Tissue Eng 2006;12(8):2151–60.

22.Nakazawa K, Izumi Y, Fukuda J, Yasuda T. Hepatocyte spheroid culture on a polydimethylsiloxane chip having microcavities. J Biomater Sci 2006;17(8): 859–73.

23 Torisawa YS, Takagi A, Nashimoto Y, Yasukawa T, Shiku H, Matsue T. A multicellular spheroid array to realize spheroid formation, culture, and viability assay on a chip. Biomaterials 2007;28(3):559–66.

24 Sodunke TR, Turner KK, Caldwell SA, McBride KW, Reginato MJ, Noh HM. Micropatterns of matrigel for three-dimensional epithelial cultures. Biomaterials 2007;28(27):4006–16.

25 Gottwald E, Giselbrecht S, Augspurger C, Lahni B, Dambrowsky N, Truckenmuller R, et al. A chip-based platform for the *in vitro* generation of tissues in three-dimensional organization. Lab Chip 2007;7(6):777–85.

26 Mironov V, Kasyanov V, Markwald RR, Prestwich GD. Bioreactor-free tissue engineering: directed tissue assembly by centrifugal casting. Expert Opin Biol Ther 2008;8(2):143–52.

27. Torisawa YS, Chueh BH, Huh D, Ramamurthy P, Roth TM, Barald KF, et al. Efficient formation of uniform-sized embryoid bodies using a compartmentalized microchannel device. Lab Chip 2007;7(6):770–6.

28 *Yukiko T. Matsunaga , Yuya Morimoto , and Shoji Takeuchi*Molding Cell Beads for Rapid Construction of Macroscopic 3D Tissue Architecture *Adv. Mater.* 2011, *23*, H90–H94

29. Y. T. Matsunaga, Y. Morimoto and S. Takeuchi, Molding cell beads for rapid construction of macroscopic 3D tissue architecture, Adv. Mater., 2011, 23(12), H90–H94.

30. P. Calvert, Printing cells, Science, 2007, 318(5848), 208–209.

31. C. Norotte, F. S. Marga, L. E. Niklason and G. Forgacs, Scaffold-free vascular tissue engineering using bioprinting, Biomaterials, 2009, 30(30), 5910–5917.

32. V. Mironov, R. P. Visconti, V. Kasyanov, G. Forgacs, C. J. Drake and R. R. Markwald, Organ printing: tissue spheroids as building blocks, Biomaterials, 2009, 30(12), 2164–2174.

33. H. Onoe, R. Gojo, Y. Tsuda, D. Kiriya, M. Kato-Negishi and S. Takeuchi, Cell fibers: construction of centimeter-scale 3D tissues by weaving, 14th International Conference on Miniaturized Systems for Chemistry and Life Sciences, 2010, pp. 629–631.

34. Wu MH, Huang SB, Cui Z, Cui Z, Lee GB. A high throughput perfusion-based microbioreactor platform integrated with pneumatic micropumps for threedimensional cell culture. Biomed Microdevices 2008;10(2):309–19.

35. Yates C, Shepard CR, Papworth G, Dash A, Beer Stolz D, Tannenbaum S, et al. Novel three-dimensional organotypic liver bioreactor to directly visualize early events in metastatic progression. Adv Cancer Res 2007;97: 225–46.

36. Figallo E, Cannizzaro C, Gerecht S, Burdick JA, Langer R, Elvassore N, et al. Micro-bioreactor array for controlling cellular microenvironments. Lab Chip 2007;7(6):710–9.

37 Wong AP, Perez-Castillejos R, Christopher Love J, Whitesides GM. Partitioning microfluidic channels with hydrogel to construct tunable 3-D cellular microenvironments. Biomaterials 2008;29(12):1853–61.

38. Yu H, Meyvantsson I, Shkel IA, Beebe DJ. Diffusion dependent cell behavior in microenvironments. Lab Chip 2005;5(10):1089–95.

39. Salazar-Ciudad I, Jernvall J, Newman SA. Mechanisms of pattern formation in development and evolution. Development 2003;130(10):2027–37.

40. Nelson CM, Bissell MJ. Of extracellular matrix, scaffolds, and signaling: tissue architecture regulates development, homeostasis, and cancer. Bull Math Biol 2006;22:287–309.

41. Lecuit T, Le Goff L. Orchestrating size and shape during morphogenesis. Nature 2007;450(7167):189–92.

42. Florian Groeber, Monika Holeiter Skin tissue engineering — *In vivo* and *in vitro* applications Advanced Drug Delivery Reviews 128 (2011) 352–366

43. S. MacNeil, Progress and opportunities for tissue-engineered skin, Nature 445 (2007) 874–880

44. M. Ponec, Skin constructs for replacement of skin tissues for *in vitro* testing, Adv. Drug Deliv. Rev. 54 (Suppl 1) (2002) S19–S30.

45. C.A. Vacanti, A.G. Mikos, Tissue Eng. 1 (1995) 1–2.

46. F.W. Falkenberg, H. Weichert, M. Krane, I. Bartels, M. Palme, H.O. Nagels, H. . Fiebig, *In vitro* production of monoclonal antibodies in high concentration in a new and easy to handle modular minifermenter, J. Immunol. Meth. 179 (1995) 13–29.

47. R. Schade, C. P!ster, R. Halatsch, P. Henklein, Polyclonal IgY Antibodies from Chicken Egg Yolk—An Alternative to the Production of Mammalian IgG type Antibodies in Rabbits, Fund for the Replacement of Animals in Medical Experiments, ATLA, Nottingham, 1991, pp. 403–419.

48. T. Sun, S. Jackson, J.W. Haycock, S. MacNeil, Culture of skin cells in 3D rather than 2D improves their ability to survive exposure to cytotoxic agents, J. Biotechnol.122 (2006) 372–381.

49. D. Asselineau, B. Bernard, C. Bailly, M. Darmon., Human epidermis reconstructed by culture: is it “normal”? J. Investig. Dermatol. 86 (1986) 181–186.

50 E. Johnson, S. Meunier, C. Roy, N.L. Parenteau, Serial cultivation of normal human keratinocytes: a de!ned system for studying the regulation of growth and differentiation, *In Vitro* Cell. Dev. Biol. 28 (1992) 429–435.

51. K. Boehnke, N. Mirancea, A. Pavesio, N.E. Fusenig, P. Boukamp, H.-J. Stark, Effects of fibroblasts and microenvironment on epidermal regeneration and tissue function in long-term skin equivalents, Eur. J. Cell Biol. 86 (2007) 731–746.

52. A. El-Ghalbzouri, S. Gibbs, E. Lamme, C. Van Blitterswijk, M. Ponec, Effect of fibroblasts on epidermal regeneration, Br. J. Dermatol. 147 (2002) 230–243.

53. Y. Xie, S.C. Rizzi, R. Dawson, E. Lynam, S. Richards, D.I. Leavesley, Z. Upton, Development of a three-dimensional human skin equivalent wound model for investigating novel wound healing therapies, Tissue Eng. C Meth. 16 (2010) 1111–1123.

54. R. Roguet, Use of skin cell cultures for *in vitro* assessment of corrosion and cutaneous irritancy, Cell Biol. Toxicol. 15 (1999) 63–75.

55. T. Welss, D.A. Basketter, K.R. Schroder, *In vitro* skin irritation: facts and future. State of the art review of mechanisms and models, Toxicol. *In Vitro* 18 (2004) 231–243.

56 J. Draize, G. Woodard, H. Calvery, Methods for the study of irritation and toxicity of substances applied topically to the skin and mucous membranes, J. Pharmacol. Exp. Ther. 82 (1944) 377–390.

57 R.L. Campbell, R.D. Bruce, Direct comparison of rabbit and human primary skin irritation responses to isopropylmyristate, Toxicol. Appl. Pharmacol. 563 (1981) 555–563.

58. L. Phillips, et al., A comparison of rabbit and human skin response to certain irritants, Toxicol. Appl. Pharmacol. 21 (1972) 369–382.

59. EU, Seventh Amendment to the EU Cosmetics Directive 76/768/EEC, in: The European Parliament and the Council of the European Union (Ed.), Brussels, 2003.

60. R.A. Becker, C.J. Borgert, S. Webb, J. Ansell, S. Amundson, C.J. Portier, A. Goldberg, L.H. Bruner, A. Rowan, R.D. Curren, W.T. Stott, Report of an ISRTP workshop progress and barriers to incorporating alternative toxicological methods in the U.S, Regul. Toxicol. Pharmacol. 46 (2006) 18–22

61. M.A. Perkins, R. Osborne, F.R. Rana, A. Ghassemi, M.K. Robinson, Comparison of *in vitro* and *in vivo* human skin responses to consumer products and ingredients with a range of irritancy potential, Toxicol. Sci. 48 (1999) 218–229.

62. S. Gabbanini, E. Lucchi, M. Carli, E. Berlini, A. Minghetti, L. Valgimigli, *In vitro* evaluation of the permeation through reconstructed human epidermis of essentials oils from cosmetic formulations, J. Pharm. Biomed. Anal. 50 (2009) 370–376.

63 M.D. Jager, W. Groenink, J.V.D. Spek, C. Janmaat, G. Gooris, M. Ponec, J. Bouwstra, Preparation and characterization of a stratum corneum substitute for *in vitro* percutaneous penetration studies, 1758 (2006) 636–644.

64. A.Gysler, B. Kleuser,W.Sippl, K. Lange, H.C. Korting, H.D.Höltje,M. Schäfer-Korting, Skin penetration and metabolism of topical glucocorticoids in reconstructed epidermis and in excised human skin, Pharm. Res. 16 (1999) 1386–1391. 65. K.

65. Ackermann, S. Lombardi Borgia, H. Korting, K. Mewes, M. Schäfer-Korting, The Phenion® full-thickness skin model for percutaneous absorption testing, Skin Pharmacol. Physiol. 23 (2009) 105–112.

66 J.A. Bouwstra, M. Ponec, The skin barrier in healthy and diseased state, Wide Angle Q. J. Film Hist. Theory Criticism Pract. 1758 (2006) 2080–2095.

67. R.J. Scheuplein, Mechanism of percutaneous absorption. II. Transient diffusion and the relative importance of various routes of skin penetration, J. Invest. Dermatol. 48 (1967) 79–88.

68. J. Kao, J. Hall, G. Helman, *In vitro* percutaneous absorption in mouse skin: influence of skin appendages, Toxicol. Appl. Pharmacol. 94 (1988) 93–103.

69. B. Illel, H. Schaefer, J. Wepierre, O. Doucet, Follicles play an important role in percutaneous absorption, J. Pharm. Sci. 80 (1991) 424–427.

70. M. Michel, N. L'Heureux, R. Pouliot, W. Xu, F.A. Auger, L. Germain, Characterization of a newtissue-engineered human skin equivalentwith hair, *In Vitro* Cell. Dev. Biol. Anim. 35 (1999) 318–326.

71. M. Brenner, V.J. Hearing, The protective role of melanin against UV damage in human skin, Photochem. Photobiol. 84 (2008) 539–549.

72. G. Chen, T. Sato, H. Ohgushi, T. Ushida, T. Tateishi, J. Tanaka, Culturing of skin fibroblasts in a thin PLGA-collagen hybridmesh, Biomaterials 26 (2005) 2559–2566.

73. Yuan Liu a, Fumihiko Suwa. Reconstruction of a tissue-engineered skin containing melanocytes. Cell Biology International 31 (2007) 985e990

74. F. Bernerd, D. Asselineau, An organotypic model of skin to study photodamage and photoprotection *in vitro*, J. Am. Acad. Dermatol. 58 (2008) S155–S159.

75. D. Lelièvre, P. Justine, F. Christiaens, N. Bonaventure, J. Coutet, L. Marrot, J. Cotovio, The episkin phototoxicity assay (EPA): development of an *in vitro* tiered strategy using 17 reference chemicals to predict phototoxic potency, Toxicol. *In Vitro* 21 (2007) 977–995.

76. S.V. Nolte, W. Xu, H.-O. Rennekampff, H.P. Rodemann, Diversity of fibroblasts—a review on implications for skin tissue engineering, Cells Tissues Organs 187 (2008) 165–176.

77. R.I. Freshney, Culture of Animal Cells, A Manual of Basic Techniques, Wiley Liss, New York, 2000.

78. V. Falanga, C. Isaacs, D. Paquette, G. Downing, N. Kouttab, J. Butmarc, E Badiavas,J. Hardin-Young, Wounding of bioengineered skin: cellular and molecular aspects after injury, J. Investig. Dermatol. 119 (2002) 653–660.

79. F. Andriani, A. Margulis, N. Lin, S. Griffey, J.A. Garlick, Analysis o microenvironmental factors contributing to basement membrane assembly and normalized epidermal phenotype, J. Investig. Dermatol. 120 (2003) 923–931.

80. D.-Y. Lee, K.-H. Cho, The effects of epidermal keratinocytes and dermal fibroblasts on the formation of cutaneous basement membrane in three-dimensional culture systems, Arch. Dermatol. Res. 296 (2005) 296–302.

81. N. Maas-Szabowski, A. Shimotoyodome, N.E. Fusenig, Keratinocyte growth regulation in fibroblast cocultures via a double paracrine mechanism, J. Cell Sci. 112 (Pt 1) (1999) 1843–1853.

82. N. Maas-Szabowski, H.J. Stark, N.E. Fusenig, Keratinocyte growth regulation in defined organotypic cultures through IL-1-induced keratinocyte growth factor expression in resting !broblasts, J. Investig. Dermatol. 114 (2000) 1075–1084.

83. B. Coulomb, L. Dubertet, C. Merrill, R. Touraine, E. Bell, The collagen lattice: a model for studying the physiology, biosynthetic function and pharmacology of the skin, Br. J. Dermatol. 111 (Suppl 27) (1984) 83–87.

84. E. Bell, H.P. Ehrlich, D.J. Buttle, T. Nakatsuji, Living tissue formed *in vitro* and accepted as skin-equivalent tissue of full thickness, Science (New York, N.Y.) 211 (1981) 1052–1054.

85. T. Sun, S. Jackson, J.W. Haycock, S. MacNeil, Culture of skin cells in 3D rather than 2D improves their ability to survive exposure to cytotoxic agents, J. Biotechnol. 122 (2006) 372–381

86. E. Bell, S. Sher, B. Hull, C. Merrill, S. Rosen, A. Chamson, The reconstitution of living skin, J. Investig. 81 (1 Suppl) (1983) 2s–10s.

87. D.A. Laska, R.G. Poulsen, J.W. Horn, V.P. Meador, D.M. Hoover, An evaluation of TESTSKIN™: an alternative dermal irritation model, *In Vitro* Toxicol. 5 (1992) 177–189

88. N.L. Parenteau, P. Bilbo, C.J. Nolte, V.S. Mason, M. Rosenberg, The organotypic culture of human skin keratinocytes and !broblasts to achieve form and function, Cytotechnology 9 (1992) 163–171.

89 H.-J. Stark, K. Boehnke, N. Mirancea, M.J. Willhauck, A. Pavesio, N.E. Fusenig, P. Boukamp, Epidermal homeostasis in long-term scaffold-enforced skin equivalents, J. Investig. Dermatol. Symp. Proc. 11 (2006) 93–105.

90. F. Sahuc, K. Nakazawa, F. Berthod, Mesenchymal–epithelial interactions regulate gene expression of type V11 collagen and kalinin in keratinocytes and dermal– epidermal junction formation in a skin equivalent model, Wound Repair Regen. 4 (1996) 93–102.

91. K.W. Ng, D.W. Hutmacher, Reduced contraction of skin equivalent engineered using cell sheets cultured in 3D matrices, Biomaterials 27 (2006) 4591–4598.

92. P. Bruin, J. Smedinga, A.J. Pennings, M.F. Jonkman, Biodegradable lysine diisocyanate-based poly(glycolide-co-epsilon-caprolactone)-urethane network in artificial skin, Biomaterials 11 (1990) 291–295.

93. K.W. Ng, H.L. Khor, D.W. Hutmacher, *In vitro* characterization of natural and synthetic dermal matrices cultured with human dermal !broblasts, Biomaterials 25 (2004) 2807–2818.

94. N.T. Dai, M.K. Yeh, C.H. Chiang, K.C. Chen, T.H. Liu, A.C. Feng, L.L. Chao, C.M. Shih, H.K. Sytwu, S.L. Chen, T.M. Chen, E.F. Adams, Human single-donor composite skin substitutes based on collagen and polycaprolactone copolymer, Biochem. Biophys. Res. Commun. 386 (2009) 21–25.

95. R. Graf, M. Kock, A. Bock, M. Schubert-Zsilavecz, D. Steinhilber, R. Kaufmann, T. Gassenmeier, H. Beschmann, A. Bernd, S. Kippenberger, Lipophilic prodrugs of amino acids and vitamin E as osmolytes for the compensation of hyperosmotic stress in human keratinocytes, Exp. Dermatol. 18 (2009) 370–377.

96. I.R. Williams, T.S. Kupper, Immunity at the surface: homeostatic mechanisms of the skin immune system, Life Sci. 58 (1996) 1485–1507.

97. M. Régnier, M.J. Staquet, D. Schmitt, R. Schmidt, Integration of Langerhans cells into a pigmented reconstructed human epidermis, The Journal of investigative dermatology, 1997, pp. 510–512.

98. J. Fransson, L.C.Heffer,M. Tengvall Linder,A. Scheynius, Culture of human epidermal Langerhans cells in a skin equivalent, Br. J. Dermatol. 139 (1998) 598–604.

99. B.L. Allen-Hoffmann, S.J. Schlosser, C.A.R. Ivarie, C.A. Sattler, L.F. Meisner, S.L.O. Connor, Normal growth and differentiation in a spontaneously immortalized near-diploid human keratinocyte cell line, NIKS, Differentiation (2000) 444–455.

Chapter 2

Microscaffold degradation rate affects the assembly of *de novo* synthesized ECM in a 3D Dermis equivalent *in vitro*

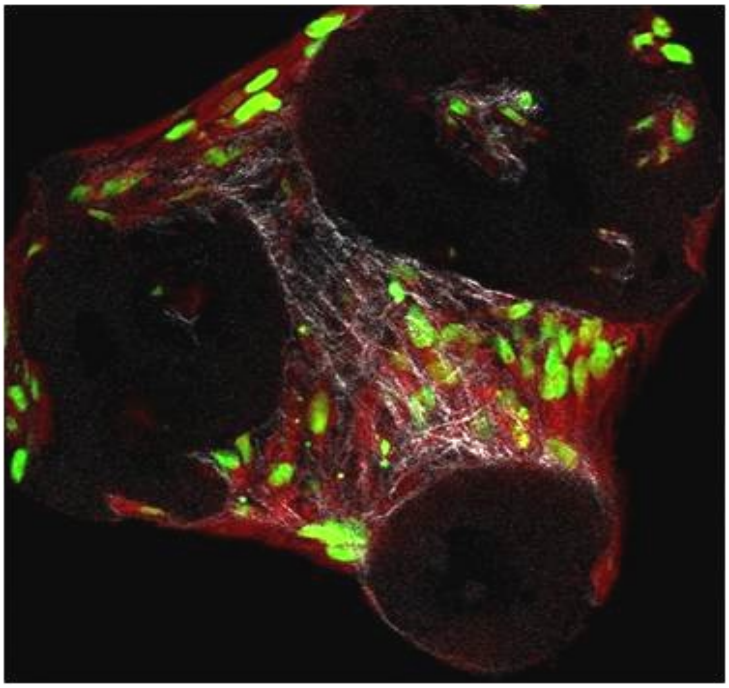

INTRODUCTION

One of the most challenging issues of cell-based tissue engineering is the implementation of strategies to successfully culture large construct *in vitro* mimicking the natural tissue organization. To reach this aim recent efforts have been concentrated on bottom-up tissue fabrication methods [1] using both scaffold-free [2-5] and scaffold-based micro-modules as building blocks [6-12] to generate a larger 3D tissue construct. However, while many studies focused their attention on the molding capability of building blocks [5-6, 8-10], at best of our knowledge few efforts have been spent to reach a deep understanding of their role in ECM organization as well as collagen assembly of the 3D tissue resulting by their bio-sintering. Scaffold free building blocks have been successfully used for the *in vitro* bio fabrication of high cell dense biological structure such as cardiac muscle and blood vessels [3-5]. Nevertheless some cell types are unable to produce sufficient ECM, migrate or form cell-cell junction when cultured without the guidance and signaling provided by the scaffold surfaces [1]. To address this challenge cells have been mixed with natural or artificial hydrogel or seeded on microcarriers to form modular tissues of specific geometries and mechanical properties. In this context, cell-laden hydrogel resembled the architecture of the target tissue at micron-scale, but scaling up the production to tissue level dimensions has not been proven yet [1,6]. On the contrary, a long time culture of 3D engineered tissue rich in endogenous ECM have been performed by molding cell-seeded microbeads [10-12]. Indeed this kind of scaffold-based building block, produced in order to be provided by cell-derived ECM layer essential for the cells to grow and differentiate in a tissue like environment, biologically fused in a 3D tissue equivalent under appropriate culture conditions. In this fashion, our has develpoed [11] a versatile strategy yielding 3D dermal tissue constructs of defined size and geometry by means of the biological sintering of cell seeded microscaffold so-called microtissue precursors (μTPs). Since μTPs were shown to spontaneously aggregate in a stable manner, a 3D viable tissue formation strategy based on the assembly of μTPs was proved feasible. Furthermore, we assessed that dynamic process conditions optimized in order to promote and to control the assembly of *de novo* deposited ECM lead to

the realization of a 3D dermal equivalent having mechanical properties close to bovine native dermis [12]. In this chapter the role of microscaffold properties in providing guidance to direct tissue morphogenesis has been investigated. To reach this aim we tuned the stiffness and degradation rate of the gelatin microscaffold by varying their crosslinking extent and assessed their different sensitivity to MMPs activity. As consequence each formulation of microscaffold realized, dynamically seeded with human dermal fibroblast, generated Human Dermal μTP (HD-μTP) having different features. We hypothesized that collagen deposition and in particular its assembly during the bio sintering process is strongly related to the evolving micro-scaffold properties, generating large dermal like tissue with different ECM composition. To reach this aim gelatin porous microcarriers were crosslinked with different concentrations of glyceraldehyde obtaining microscaffolds characterized by different stiffness and metalloproteinase's-mediated degradation kinetics. Human dermal fibroblasts (HDF) were dynamically seeded on each microscaffold formulation in order to realize HD-μTP having different features. To investigate the role of HD-μTP, and indirectly of the microscaffold, on the maturation of the 3D tissue equivalent, the micromodules realized have been used as building blocks for the fabrication of the corresponding macrotissue.

MATERIALS AND METHODS

Microscaffold production

Preparation of porous gelatin microbeads

Gelatin porous microbeads (GPMs) have been prepared according to a modified double emulsion technique (O/W/O) [13]. Gelatin (type B Sigma Aldrich Chemical Company, Bloom 225, Mw=l 76654 Dalton) was dissolved into 10 ml of water containing TWEEN 85 (6% w/v) (Sigma Aldrich Chemical Company). The solution was kept at 60°C. Toluene containing SPAN 85 (3% w/v) (Sigma Aldrich Chemical Company) was continuously added to the aqueous gelatin solution (8 % w/v) to

obtain primary oil in water emulsion. The added toluene formed droplets in the gelatine solution until saturation. Beads of gelatine containing droplets of toluene were produced through the addition of excess toluene (30 ml). The overload of toluene allowed the obtaining of a double emulsion (O/W/O). After cooling below 5°C, 20 ml of ethanol was added to extract toluene and stabilize GPMs. The resulting microspheres were filtered and washed with acetone and then dried at room temperature. Microspheres were separated selectively by using commercial sieves (Sieves IG/3-EXP, Retsch, Germany). GPMs with 75-150 μm size range were recovered and further processed. After sieving the number of microcarriers per milligram was determined by counting microbeads in cell culture dish (w/2 mm grid Nunc). Finally the microbeads morphology has been examined by means of Scanning Electron Microscopy (SEM).

Crosslinking of GPM

GPMs have been stabilized by means of chemical treatment with glyceraldehyde (GAL), in order to make them stable in aqueous environment at body temperature. In particular, GPMs were dispersed into acetone/water solution containing different amounts of GAL and mixed at 4°C for 24 h. Then microspheres were filtered and washed with acetone and dried at room temperature. The amount of crosslinks introduced during the stabilization step and the degradation rate of the gelatin microbeads have been modulated by varying the percentage of the crosslinking agent (GAL). Three different amounts of glyceraldehyde (3%, 4% and 5% w/w of the microbeads) have been used to obtain microbeads with different crosslinking degrees.

In vitro enzymatic degradation of GPM

Enzymatic degradation of the crosslinked GPM was performed using collagenase (Sigma Chemical Co.) with an activity of 0.250 U/mg solid. Degradation of GPM without collagenase was used as a control. Moreover degradation of commercial highly crosslinked gelatin microbeads (Percell Biolytica AB, Astorp, Sweden) was evaluated too. Triplicate samples of dry microspheres for each time point were weighted (W1) and then well immersed in a 0.001 U/mL and 4μg/ml collagenase solution (pH 7.5) and incubated at 37°C. Degradation of GMP was discontinued at five time points (60, 90, 120, 150 and 180 min), by withdrawn the surnatant collagen solution, and adding ethanol solution to dry microspheres. The weight loss of GPM due to degradation with or without collagenase was quantified as follows:

$$\text{Weight loss } (\%) = \frac{(W_1 - W_2)}{W_1 * 100}$$

where, W2 is the weight of degraded GPM at each time points after dehydratation by means of an incremental series of ethanol solutions (75%, 85%, 95% and 100%, and 100% again, each step 20 min at room temperature) and dried in oven at 45°C for 2 days. Successively, the morphology of GPM after enzymatic degradation was grossly examined using a scanning electron microscope as described above.

Scanning electron microscopy (SEM)

SEM was performed to analyze both the morphology of naked microbeads and microbeads after collagenase treatment. The former didn't need any dehydratation process so they were mounted onto metal stubs using double-sided adhesive tape and then gold-coated using a sputter coater at 15 mA for 20 min. Coated samples were then examined by scanning electron microscopy (SEM) (Leica S400). The latter needed to be dehydratated at the end of collagenase treatment, the dehydratation was carried out by gradually decreasing the water concentration and increasing the ethanol concentration (75%, 85%, 95% and 100%, and 100% again, each step 20 min at room temperature). Finally the samples were treated following the procedure explained above for dried samples.

HD-μTP

Dynamic cell seeding

Human dermal fibroblasts (neonatal HDF 106-05n ECACC) were sub-cultured onto 150 mm Petri dishes in culture medium (Eagle's BSS Minimum Essential Medium containing 20% fetal bovine serum, 100 mg/mL L-glutamine,100 U/mL penicillin/streptomycin, and 0,1 mM Non Essential Amino Acids). Cells were maintained at 37°C in humidified atmosphere containing 5% CO_2. HDF of passages 6-12 and GPM crosslinked at 3%, 4% and 5% (3% GPM, 4% GPM, 5% GPM) have been used for all experiments. Before using dry GPM were sterilized by absolute ethanol sub-immersion for 24h. Successively to remove completely the ethanol several washings in calcium-free and magnesium-free phosphate-buffered saline (PBS) were performed. Before cell seeding PBS was removed and replaced with the culture medium. HD-μTPs cultivation was initiated by inoculating HDF at 10 cells $bead^{-1}$. Paralle experiments were performed for seeding HDF on 3% GPM, 4% GPM and 5% GPM corrispondetly three types of HD-μTP were performed named 3% HD-μTP, 4% HD- μTP and 5% HD- μTP. The culture suspension was stirred intermittently at 30 rpm (5 min stirring and 30 min static incubation) for the first 6h post-inoculation for cell adhesion, and then continuously agitated at 30 rpm. The growth medium was replenished on the first day and every 2 days until the end of experiments (9 days in total). From the day 4^{th} 50μg/ml of ascorbic acid was added. HD-μTP samples were taken for assay at day 1, 3, 6 and 9.

Cell adhesion and proliferation assay

The rate of disappearance of free cells from inoculated microcarrier cultures was determined as an indication of cell attachment to microcarriers. During the intermittent stirring phase culture sample (500 μl) was taken each hour and allowed to settle for 1 min in an Eppendorf tube. The microcarrier-free supernatant was introduced into a hemocytometer for cell counting. After counting the free cells in the medium with a hemocytometer, the number of cells adhering to microbeads (cell / microbead ratio) was evaluated. About 1ml aliquots were

collected at day 1,3,6 and 9 from spinner culture for the cell adhesion assay on the microcarriers. Briefly, 300 μl of the same aliquots was transferred to a cell culture dish (w/2 mm grid Nunc) for microcarrier counting, experiments were performed in triplicate. After that the microcarriers suspension was placed in the 1,5ml eppendorf tube, gently washed twice with PBS, and then treated with trypsin solution to allow cell harvesting. Finally, the detached cells were counted using a hemocytometer.

Cell viability and ECM morphology

Over the entire dynamic cell culture period in spinner flask, 1 ml aliquots were collected at day 1,3,6 and 9 for cell viability as well as ECM morphology during HD-mTP formation and evolution. To this aim samples were investigated by Confocal Leica TCS SP5 II combined with a Multiphoton Microscope where the NIR femtosecond laser beam was derived from a tunable compact mode-locked titanium:sapphire laser (Chamaleon Compact OPO-Vis ,Coherent). Cell viability, proliferation and morphology in the HD-μTP were assessed by staining the samples with phalloidin tetramethylrhodamine B isothiocyanate (Sigma-Aldrich) and SYTOX® Green (INVITROGEN) the former stains the cell's cytoskeleton the latter cell's nucleic acid. For both analysis, the HD-μTP were fixed with 4% paraformaldehyde for 20 min at room temperature, rinsed twice with PBS buffer, and incubated with PBS-BSA 0.5% to block unspecific binding. For actin microfilaments and nucleus detections, after fixation, the samples were stained with phalloidin tetramethylrhodamine B isothiocyanate (phalloidin) and SYTOX® Green respectively. In particular the samples were incubated with SYTOX® Green stock solution (10 mg/mL in dimethyl sulfoxide) diluted in PBS (1/500 v/v) for 10 min at 37°C, and after rinsing in PBS, they were stained with phalloidin for 30 min at room temperature. Moreover two-photon excited fluorescence has been used to induce second harmonic generation (SHG) and obtain high-resolution images of unstained collagen structures in μTPs' ECM. Indeed the samples were observed in order to highlight the simultaneous excitation of the two different fluorophores used (SYTOX® Green λ_{ex} 504, λ_{em} 523nm; phalloidin λ_{ex}=540-545 nm, λ_{em}=570-573 nm) as well as to induce Second Harmonic

Generation (SHG) (λ=840nm). Moreover, for histological analysis at day 4 from the beginning of dynamic cell seeding, 1 ml of HD-μTP suspension was fixed in a solution of 10% neutral buffered formaline for 24 h, dehydrated in an incremental series of alcohol (75%, 85%, 95% and 100%, and 100% again, each step 20 min at room temperature) treated with xylene and then embedded in paraffin. Successively, the samples were sectioned at a thickness of 6μm, and stained with hematoxylin and eosin, finally the sections were mounted with Histomount Mounting Solution (INVITROGEN) on coverslips and the morphological features of constructs were observed with a light microscope (Olympus, BX53).

Transmission electron microscopy (TEM)

TEM was performed to observe cells and collagen in the HD-μTP at different time point. HD-μTPs were first fixed with 2.5% glutaraldehyde (Sigma-Aldrich) in sodium cacodylate buffer 0.1 M (pH 7.2), washed with sodium cacodylate buffer and then fixed with 1% aqueous osmium tetroxide (Electron microscopy sciences, USA). Afterwards, the samples were dehydrated in a graded series of ethanol (Sigma-Aldrich), block contrasted with 1% uranyl acetate (Merck, Germany) and embedded in EMbed 812 (Electron microscopy sciences, USA). The prepared ultra-thin sections (65 nm) were contrasted with 0.3% lead citrate (Merck, Germany) and imaged with a Philips CM12 transmission electron microscope at an accelerating voltage of 80 kV.

3D dermal equivalent

HD-μTP molding

As previously described [12] HD-μTPs suspension was transferred from the spinner flask to a 50 ml Falcon centrifuge tube and, after settling, transferred by pipetting into the maturation chamber to allow their molding in disc-shaped construct (1 mm in thickness, 10 mm in diameter). During the filling procedure, the maturation chamber was accommodated on a device connected with a vacuum pump to make the process faster and to assure that any

bubble was in the maturation space. Finally the assembling chamber was placed on the bottom of a spinner flask and completely surrounded by culture medium. The spinner was operated at 60 rpm and the medium was exchanged every 3 days. Depending upon the HD-μTPs used as building block the resulting dermal tissue equivalent was named 3% biohybrid, 4% biohybrid or 5% biohybrid.

3D dermal equivalent biohybrid characterization

Cell distribution

Cell distribution along the biohybrid's thickness was assessed by analyzing 4',6-diamidin-2-fenilindolo (DAPI) stained sections of biohybrid. At each time point the assembling chamber was opened and the biohybrids were fixed in a solution of 10% neutral buffered formaline for 24 h (see *Cell viability and ECM morphology of HD-μTP*). After the fixation and dehydratation procedure the biohybrid was embedded in paraffin to be sectioned transversally to the circular surface. The DAPI stock solution (10 mg/mL in dimethyl sulfoxide) was diluted in PBS (1/104 v/v) and the samples incubated for 10 min at 37°C. Samples were then rinsed three times with PBS and observed by an inverted fluorescence microscope (IX81; Olympus), using a 4x objective. The obtained images were then analyzed by using an image analysis software (Image J®) to quantify the spatial distribution of the cells into the different portions of the biohybrid, similar to the method described by Salerno et al. Briefly, each image was organized in three equal vertical zones, EDGE, CENTRE, and EDGE, subsequently, the number of cell nuclei in each portion was measured by using Image J®. These values were then divided by the overall cell number in the whole cross section for the quantification of the HDF spatial organization and to assess that any necrotic centre exists. The frequency number of cells in each zone was evaluated. Five images for each sample were used for the analysis.

ECM morphology and composition

ECM composition and morphology along the biohybrid's thickness were assessed by

performing histological analysis on transverse sections of biohybrid.

5mm transverse sections of samples were stained using hematoxylin-eosin (Bio Optica) solutions, Masson's trichrome (Sigma Aldrich) and Picro Sirius Red (PSR) (Sigma Aldrich) following standard procedure and analyzed by an optical microscope (BX53; Olympus). Moreover histological sections from adult human skin (from breast reduction surgery) stained with PSR were ulteriorly observed by using polarized microscope. Polarized light images of samples stained with PSR alone were acquired with an inverted microscope (BX53; Olympus) with a digital camera (Olympus DP 21). A linear polarizer was placed between the light source and the specimen, while the analyzer was installed in the light path between the specimen and the camera. It is known that the color of collagen fibers stained with picrosirius red and viewed with polarized light depends upon fiber thickness; as fiber thickness increases, the color changes from green to red [14,15]. To quantitatively determine the proportion of different colored collagen fibers, we resolved each image into its hue, saturation and value components by applying the software's "color threshold" function. Only the hue component was retained and a histogram of hue frequency was obtained from the resolved 8-bit hue images, which contain 256 colors. We used the following hue definitions; red 0-51, green 52-120 [14,15]. The number of pixels within each hue range was determined and expressed as a percentage of the total number of collagen pixels, which in turn was expressed as a percentage of the total number of pixels in the image. The analysis of fiber content and hue was applied to 20 PSR stained sections of each type of biohybrid at each time points, and about 5 region of interest (ROI) were examined for each section. Since the aim of imaging analysis was to investigate the evolution of endogenous ECM composition, it was necessary to exclude by ROI the areas occupied by the microscaffold when it was still present. This condition was verified only for the 5% biohybrid at each time point. For this reason in this sample the ROI appears irregular depending by the local arrangement as shown in figure 6a. Otherwise since only endogenous ECM are present in 3% as well as 4% biohybrid, ROI rectangular-shaped were randomly placed within the images. Since the 4% biohybrid was subjected to contraction with culture time, the ROI was

decreased proportionally to contraction. In this way it was avoided the “convective” transport of pixels within the ROI.

SHG imaging and ultra-structure analyses

SHG imaging were performed using a Confocal Leica TCS SP5 II femtosecond laser scanning system (Leica), coupled to a tunable compact mode-locked titanium:sapphire laser (Chamaleon Compact OPO-Vis ,Coherent). All observations were made using unprocessed and untreated biohybrid just withdrawn from the maturation chamber. SHG was induced using wave-lengths of 840 nm (collagen) as described previously. Following imaging samples were processed for TEM analysis as described earlier.

RESULTS AND DISCUSSIONS

Bottom up strategy and tissue assembly

In this study, a bottom-up approach was exploited to build up 3-D tissue constructs *in vitro* by using µTPs as functional building units. The process philosophy is schematized in figure 1. The optimized dynamic culture conditions used, coupled with sub-millimetric nature of the µTP, represent important features of this approach and allowed overcoming the transport limitations and enabled the massive production of viable and functional micrometric building block for bottom up tissue engineering application. Moreover, a particular attention it has been addressed to the role of micro-scaffold on the composition, organization and maturation of *de novo* synthesized ECM in the 3D human dermal equivalent tissues realized. To this aim, porous micro scaffolds (GPM) with different stiffness as well as different degradation kinetics have been produced by means of a modified double emulsion method [13] and used as microscaffold for HDF seeding in dynamic culture, in order to produce µTP having different properties. We tuned the degradation rate of GPM by changing the crosslinking extent (3% GPM, 4% GPM, 5% GPM) and assessed their different sensitivity to MMPs with collagenase treatment.

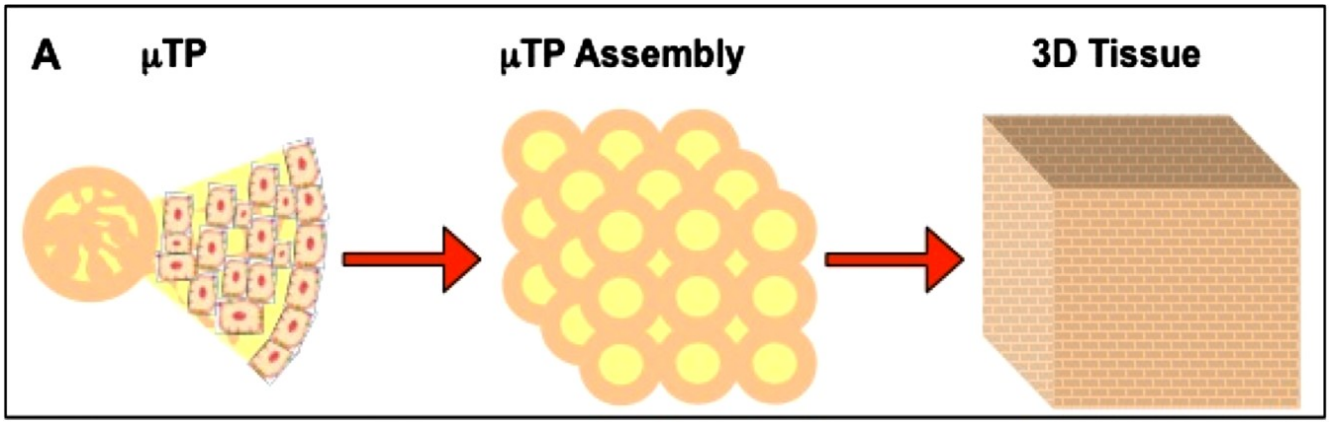

Figure 1A.: Scheme of the bottom-up process

As expected [11], the dynamic process conditions used for the production of HD-µTPs guaranteed both high seeding efficiency (95%) and high proliferation rate since the cells increased of 10 times in nine days of spinner culture. We have taken advantage of this condition to start the process by using smaller amount of cell compared with other techniques [10-12]. However, the dynamic spinner culture exploited to produce HD-µTP, was not a mere cell expansion phase, but a process in which cells underwent stimuli crucial for the production of functional building blocks. In particular, the addiction of ascorbic acid to the culture medium increased the proliferative rate and stimulated the synthesis and the secretion of appropriate ECM components [16]. Moreover, optimized dynamic culture conditions coupled with sub-millimetric nature of the µTP allowed overcoming the transport limitations and enabled the massive production of viable and functional micrometric building block for bottom up tissue engineering application

Microscaffold production and characterization

SEM micrographs revealed that the GPMs prepared by the modified double emulsion method showed a good sphericity and a highly porous surface (Fig.2A, B). Interconnected pores about 20 mm in diameter were distributed uniformly both on the whole surface and in the bulk of GPM. Three different percentages of crosslinker (GAL) have been explored for stabilizing gelatin (3% GPM, 4% GPM and 5% GPM). As detected by SEM micrographs the presence of the GAL didn't induce any change in 5%GPM macroscopic morphology

compared to the untreated one (Fig.2A, B), the same behavior has been observed for 3%GPM as well as 4%GPM (data not show).*In vitro* enzymatic degradation of GPM has been performed by means of collagenase and as shown by the fig. 1C GPM's weight loss was a function of time as well as percentage of crosslink. After one hour the 3 % GPM lost about 80% of their mass, 4% GPM about 60% and 5% GPM about 30%. At the end of the time slot (3 hours) 3% GPM and 4% GPM lost all their masses, while 5% GPM lost about 60% of their initial mass.

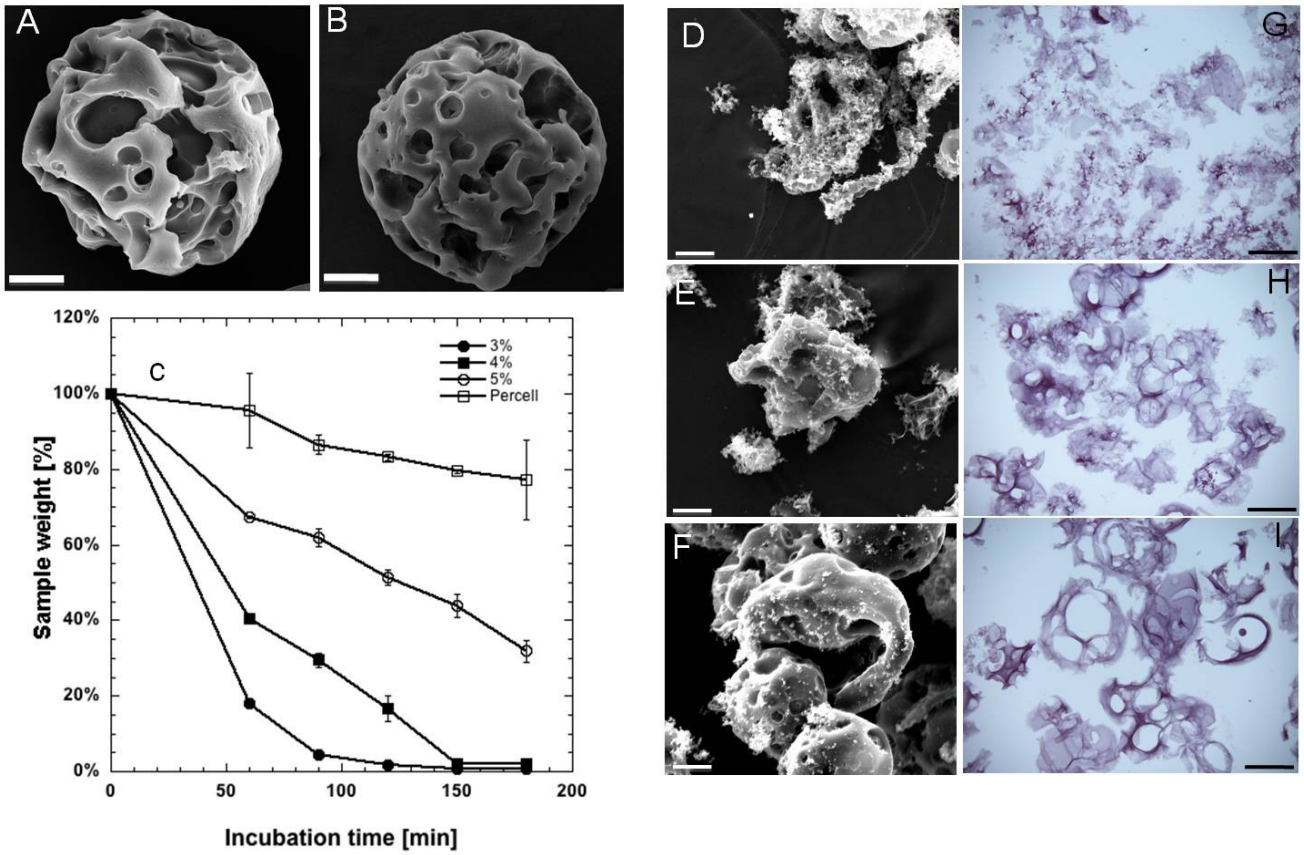

Figure 2.: GPM's morphology and degradation. SEM micrographs of 5%GPM (A) and w/o GAL (B). Time evolution of weight loss (C) of 3%GPM (full circle), 4%GPM (full square), 5%GPM (empty circle), and commercial GPM (empty square). SEM micrographs of 5%GPM (D), 4%GPM (E), 3%GPM (F), after 120 minutes under MMPs treatment. At same time point, the corresponding H&E for 5%GPM (G), 4%GPM (H), 3%GPM (I). Sale bar is 20µm for SEM micrographs and 100mm for H&E images

Any weight loss has been assessed for commercially available gelatin microcarriers (Percell) as well as for GPM treated with PBS without collagenase (data not show) within the time frame analyzed. The effect of degradation was qualitatively confirmed by means of

morphological inspection of the GPM after each time point of the enzymatic degradation assay. In the figure 2 SEM (Fig. 2D-F) as well as histological analyses (Fig. 2 G-I) of GPM at the second time point (90 min) of degradation assay are reported. The images showed the change in morphology of the GPM. In particular, the picture highlighted that the degradation due to the collagenase's effect was more evident at lower crosslink degree. Indeed at the same time point 3%GMP completely lost its initial morphology in terms of sphericity and porosity, while this effect was less evident as crosslinking extent increases. Lastly, the number of dry microcarriers per milligram was determined to be $5*10^3$ beads/mg and was evaluated in order to control the cell/microcarriers' ratio at the inoculum step of the spinner culture, as described below.

HD-µTP evolution and characterization

Cell adhesion and proliferation

The spinner flask was loaded with 10^5cell*ml^{-1} and 2mg*ml^{-1} of microbeads, corresponding to 10 cells per bead. The first 6 h of the seeding phase were characterized by intermittent stirring to improve the cell-to-bead distribution and to obtain a lower proportion of unoccupied beads [17]. The disappearance of free cells from the inoculated spinner cultures was considered to indicate the attachment of cells to the microcarriers. In the figure 3A is reported the seeding efficiency calculated as $[(C_0-C_t)*100]/C_0$ where C_0 is the concentration of the HDF at the inoculum time and C_t the concentration of the HDF in the culture medium at each hour of the intermittent seeding phase of spinner culture. It was possible to observe that seeding efficiency was not influenced by crosslinking degree, indeed at the end of the intermittent stirring the seeding efficiency was ≈95% for all three GPM's crosslinking extent. Moreover, the cell adhesion as well as cell proliferation during the spinner culture were evaluated at day 1, 3, 6 and 9. In the figure 3B was reported the cell/microbead ratio increasing up to ≈ 100 cell*bead^{-1}. Any relevant difference in cell adhesion and proliferation has been noted for the three kinds of GPM during the whole spinner culture. At the same time points transmission electron micrographs of ultrathin sections of colonized GPM

highlighted the different phases of cell attachment and collagen deposition (Fig. 3C-F). At day one a cell of round shape just settling onto the GPM surface is shown (Fig. 3C) as the time increases cell started to adhere and spread onto GPM surface (Fig. 3D). At 6 day of spinner culture (Fig. 3E) it was observed a multilayer of cells well adhered to each other and to microbeads surface.Cells inserted in the superficial pores of microbeads can be observed. Finally the last image (Fig. 3F) shows a layer/multilayer of cells embedded within collagen

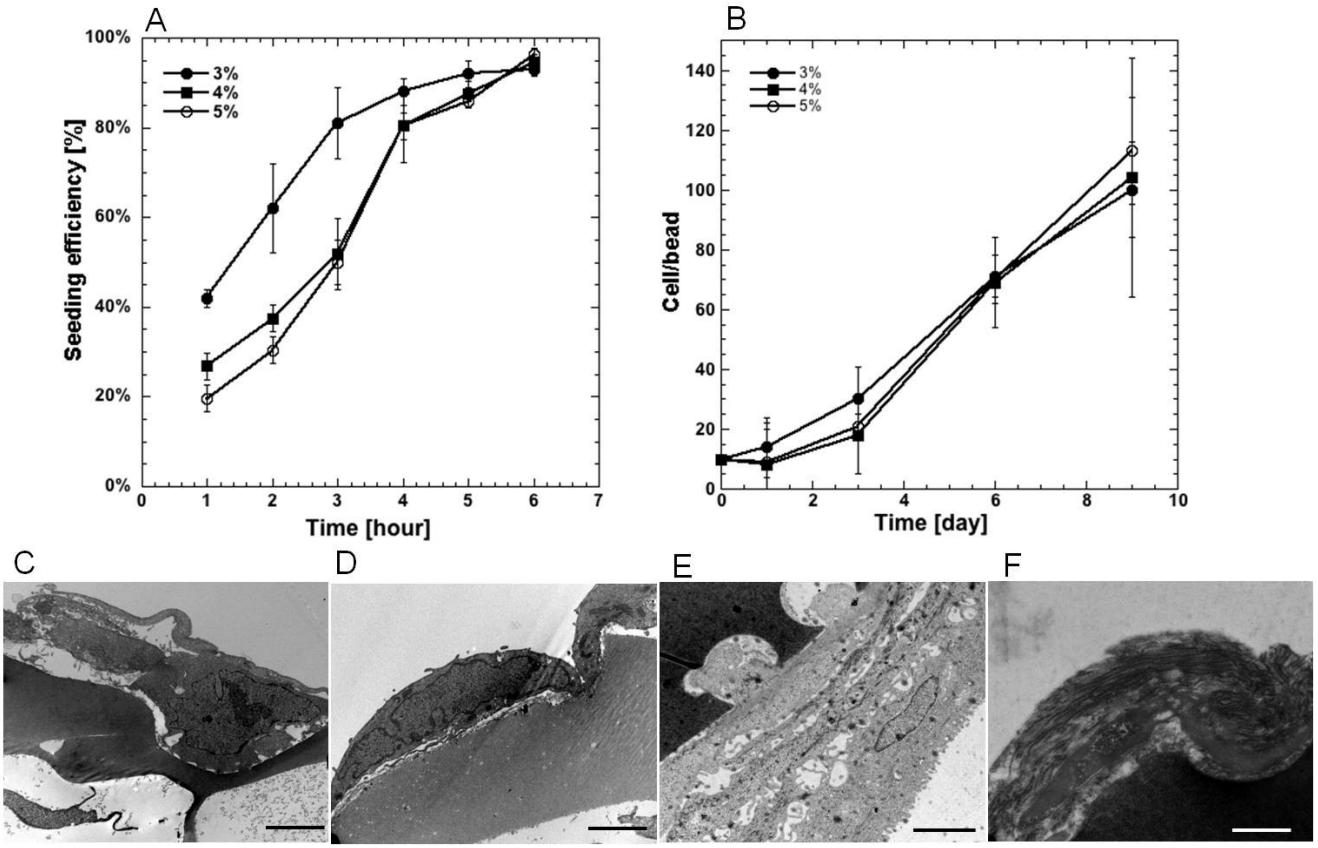

Figure 3.: growth of HDF on GPM. Cell seeding efficency (A) and cell proliferation (B) of HDF on 5%GPM (empty circle) 4% GPM (full square), 3% GPM (full circle). TEM micrograph of HDF behavior on 5%GPM at day 1 (C) scale bar is 750nm, day 3 (D) scale bar is 750nm, day 6 (E) scale bar is 500nm and day 9(F) scale bar is 250nm.

Cell viability and ECM morphology

The figure 4 reported the multichannel images of 3% HD-µTP, 4% HD-µTP and 5% HD-µTP at 3, 6 and 9 days of spinner culture highlighting cell's nuclei (green), cell's cytoskeleton (red) and unstained collagen (gray). Images showed the time evolution of µTP in terms of cells number increase, collagen deposition and cell-seeded GPM aggregate formation. In the first column the image of HD-µTP at 3 days of culture is reported and as expected few

cells are present and someone occupied the pores of the GPM but any signal of collagen presence has been detected.

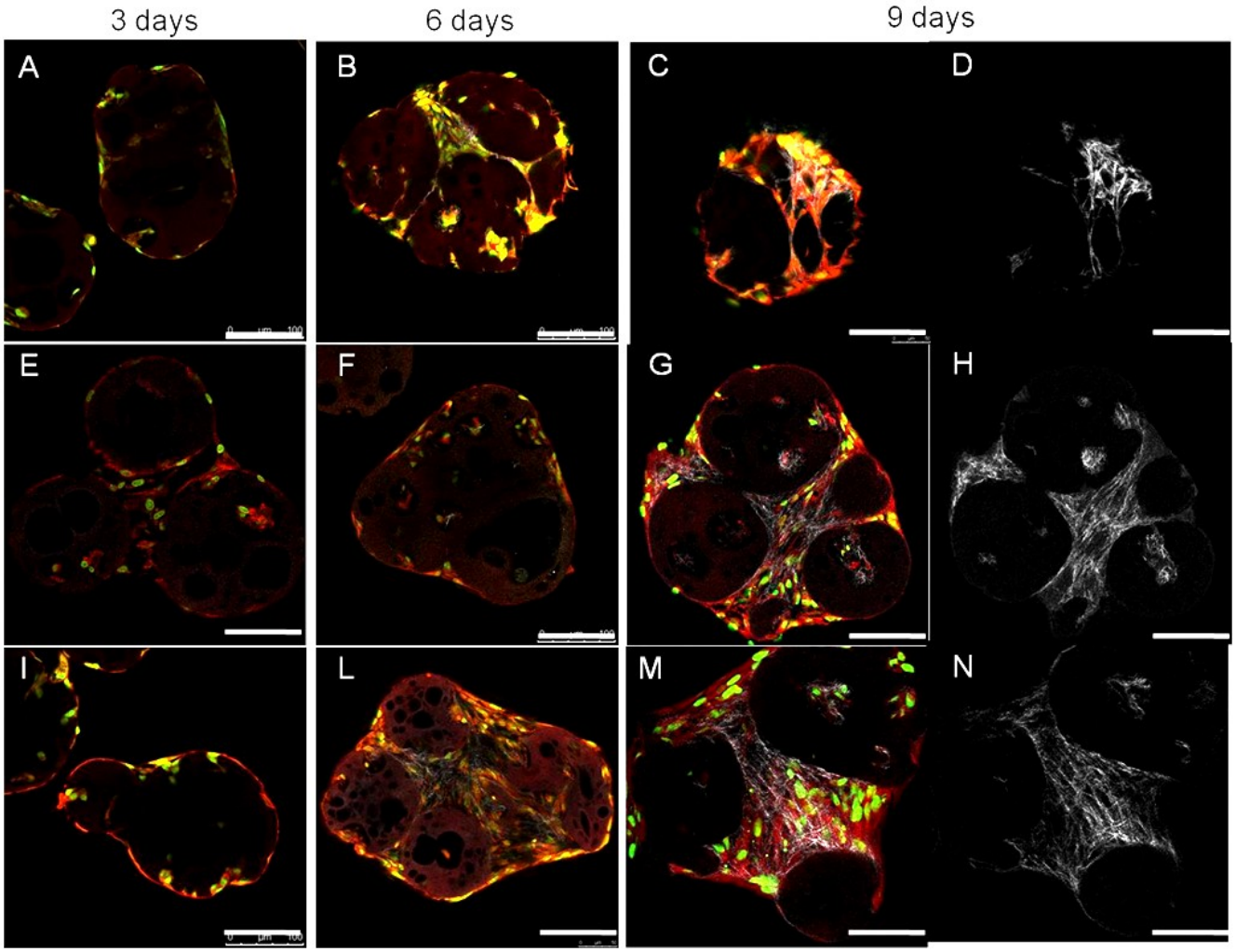

Figure 4.: multiphoton images of HD-µTP. Three channels images of HD-µTP at 3, 6 and 9 days and SHG image at 9 days of spinner culture of 3% HD-µTP (A-D), 4%HD-µTP (E-H) and 5%HD-µTP (I-N) respectively. Cell nuclei in green, actin in red, SHG collagen signal in gray. Scale bar is 100µm

Moreover the GPM's morphology appeared quite similar for the three crosslinking extent. By the sixth day the GPM morphology changed depending on the GPM's crosslinking degree. However the cells number increased with culture time as well as the neo-ECM deposition that works as glue among the single cell seeded GPM. Nevertheless, at 6 days of culture the SHG signal is quite weak indicating that the collagen deposition is low. In the third column the image of sample at the last day of spinner culture are shown. Both in 5% HD-µTP and in

4% HD-μTP it is possible to distinguish the single GPM that maintain the initial morphology, otherwise in the 3% HD-μTP the GPM porosity appeared collapsed and it is impossible to distinguish the single GPM. Finally in the last column only SHG multiphoton confocal images of all three kinds of HD-μTP at 9 days of spinner culture were reported showing a stronger collagen signal for all three formulation. Moreover confocal images highlighted that the morphology of HD-μTPs and their ECM organization depended upon the GPM's crosslinking extent. In general for each kind of HD-μTP as the time increased we observed cell proliferation, HD-μTPs aggregation, HD-μTP remodeling and ECM rich in collagen deposition as highlighted by SHG images (Fig. 4 D, H, N). In particular when the 3% GPM are used the HD-μTP are subjected to a strong contraction due to less stiffness of the GPM associated with their great deformability. At the same time when the GPM's cross-linking extent increased, stronger SHG signal in HD-μTP was detected (Fig. 4 D, H, N). This phenomenon can be explained by the different stiffness of the substrate that affecting gene expression of cytoskeleton proteins can regulate the morphology as well as the collagen synthesis of the cells [18].The images show that extensively elongated cells with stretched actins bridged the adjacent GPM together and indicated very strong cell-GPM interactions

3D dermal equivalent

Macroscopic analyses

The maturation space was disk shaped (1 mm in thickness, 10 mm in diameter) inserted in a dynamic environment allowing tangential flow that guarantee optimal nutrient supply and waste removal through the maturation space during the culture time. Three kinds of dermal equivalent tissues have been realized starting from 3%-HD-μTPs, 4%-HD-μTPs and 5%-HD-μTPs as building blocks respectively. Three culture times have been explored 2, 4 and 6 weeks. At each culture time, morphological inspection, cell viability, collagen deposition as well as collagen maturation index have been evaluated. As shown in the figure 5B biohybrid obtained by assembling 3% HD-μTPs (3%biohybrid) is subjected to a strong contraction at 2 weeks of maturation culture, so any further culture time has been explored. The image of

biohybrid obtained by assembling 4% HD-µTPs (4%biohybrid) and 5% HD-µTPs (5%biohybrid) at 2 and 6 weeks of culture are reported in the figure 5C,D and figure 5E,F respectively. At 2 weeks of culture it was evident by the image that both the 4% and 5% biohybrid retained the disc shape of the mold, are compact and can be handled without any damage. At 6 weeks of culture while the 5% biohybrid retained shape and thickness the 4% biohybrid is subjected to a thinning.

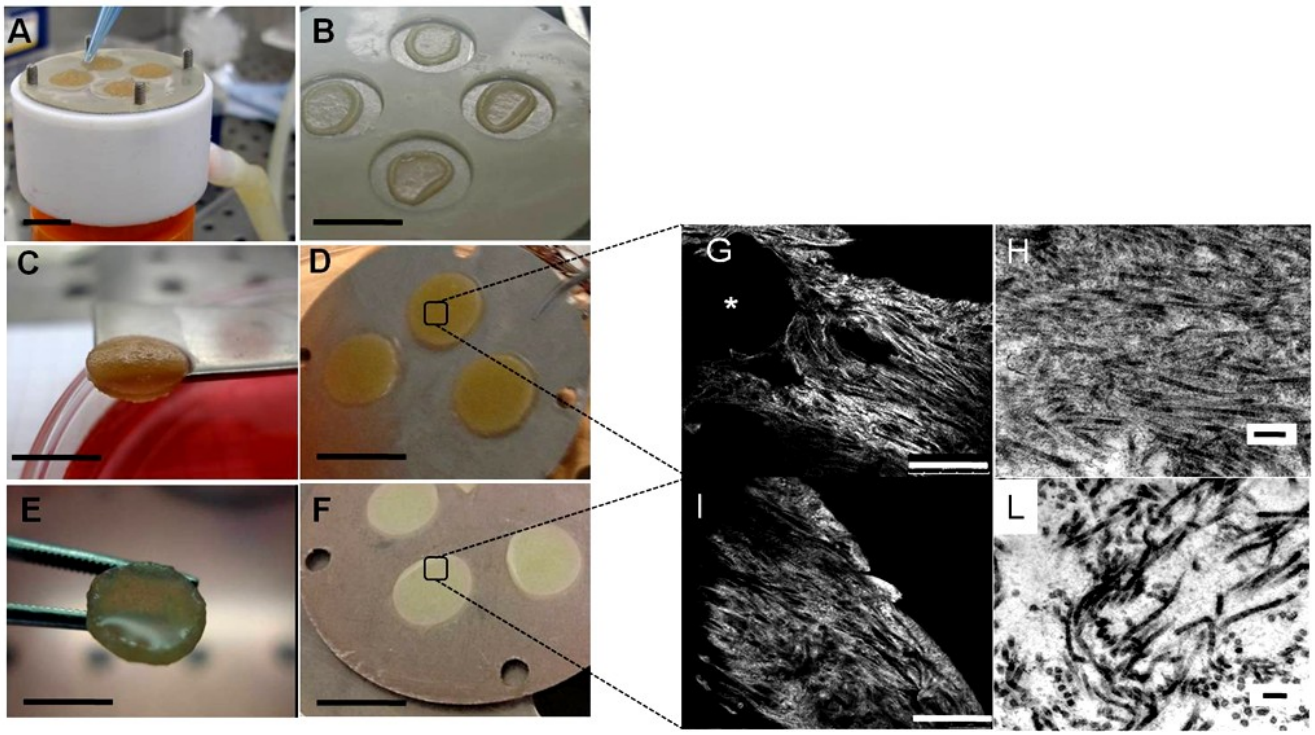

Figure 5.: HD-µTP molding and tissue releasing. Molding 5%HD-µTP in maturation chamber (A), Macroscopic view of 3% Biohybrid at 2 weeks of culture (B), 4% Biohybrid at 2weeks of culture (C), 4% Biohybrid at 6 weeks of culture (D), 5% Biohybrid at 2 weeks of culture (E), 3% Biohybrid at 6 weeks of culture (F), scale bar is 1 cm. Tissue equivalent's collagen morphology: SHG image at 6 weeks of 5% biohybrid (G) and 4% biohybrid (I) respectivEly, asterisk indicates a GPM still present in 6% biohybrid, scale bar is 100µm. TEM micrograph showing collagen organization at 6 weeks in 5% biohybrid (H) and 4% biohybrid (L) respectively, scale bar is 200nm.

Microscopic analyses

In the figure 5G-I representative images of collagen fibers of 4% biohybrid as well as 5% biohybrid at 6 weeks of culture are shown. It is known that collagen fibers produce high SHG signal that can be used to measure their organization and the strength of signal is directly correlated to the degree of collagen maturation [18,19]. For this reason SHG imaging of the

collagen network was investigated by exploiting multiphoton microscopy with the advantage of fast in situ visualization of collagen fibers in intact, non fixed and non-sliced biohybrid tissues (Fig. 5 G, I). The figure 5G and 5I reported the SHG images of 5%biohybrid and 4%biohybrid respectively, the signal was strong in both images, anyway in the former the collagen fibers appear better organized in collagen bundle. In order to gain information on the ultrastructure, the same samples were fixed, embedded, sliced and stained, followed by TEM (Fig. 5 H,L). The TEM images of both the sample (Fig.5 H, L) show that collagen is correctly assembled in fibrils, which display the characteristic banded pattern (i.e. 67nm). The fibril diameter is of the same order of magnitude of that one found in native tissues about 20-30 nm. Anyway TEM image of 5% biohybrid confirms that collagen fibrils within the sample are closely packed while in the 4% biohybrid they appear fine and randomly organized so it isn't possible to discern higher order structures like fiber bundles. In figure 6 histological images (Masson Trichrome) concerning all kinds of biohybrids at each time point (i.e. 2, 4, and 6 weeks) are reported. In fig 6(A-C) cross section of 5% biohybrid at each time point are reported. From the images it is possible to see that collagen (in blue) is present along the whole thickness up to 6 weeks of culture, any necrotic regions are present and microbeads (in purple) are still present at the end of culture time. Any significant change in thickness has been observed. In figure 6 (D-F) cross section of 4% biohybrid at each time point are reported. It is possible to assess that microscaffold degradation took place at 2 weeks of culture and the biohybrid was made up principally by endogenous material. Relevant differences could be assessed with culture time, indeed in this case the biohybrid's thickness changed over the time showing a thinning of 75% at 6 weeks, indicating that while the microbeads degradation is taking place the biohybrid is subjected to a contraction process even if new collagen is synthesized. It is interesting to highlight that after the second weeks of culture the tissue is completely made-up of endogenous ECM.

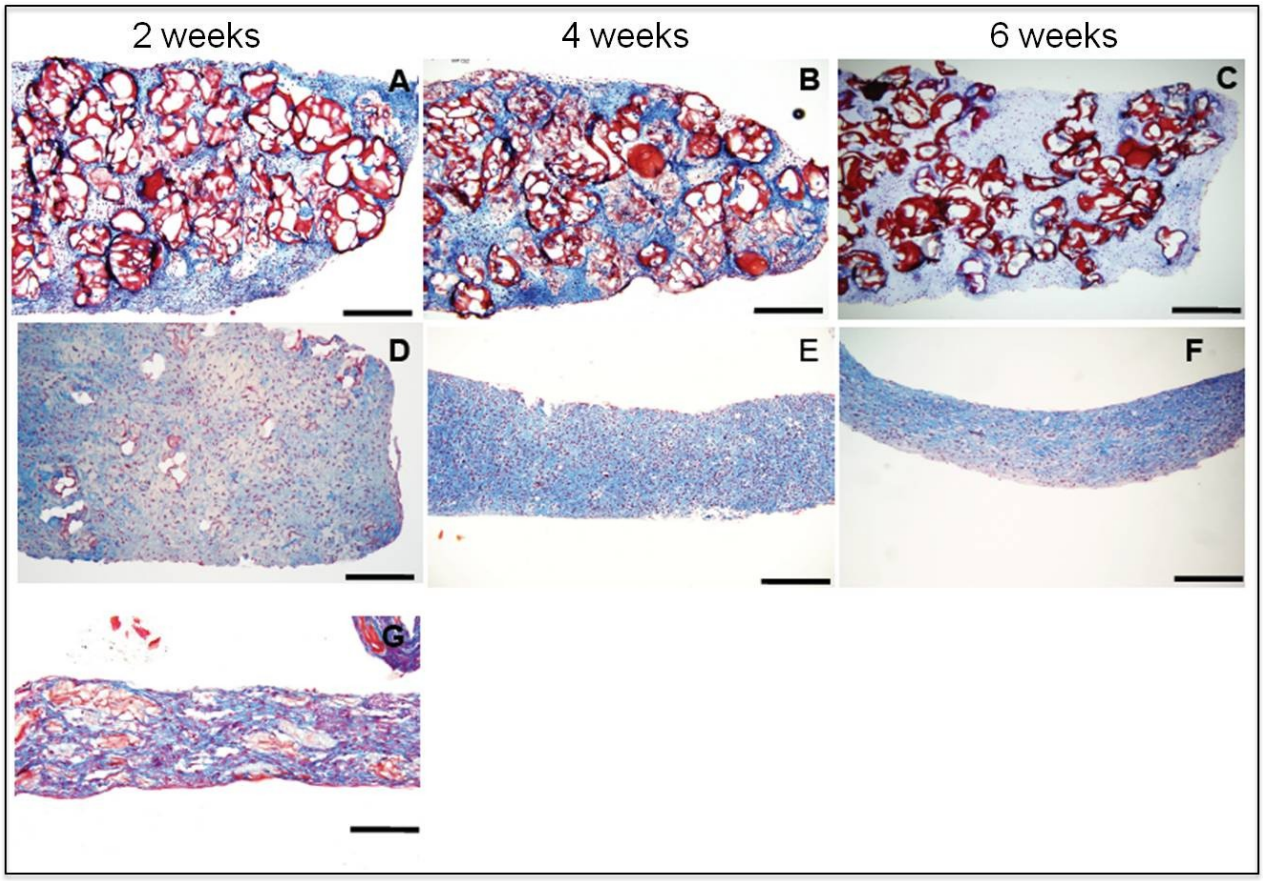

Figura 6.: histological analyses. Masson trichrome stained cross section of 5%biohybrid at 2 weeks (A) scale bar is 200μm, 4 weeks (B) scale bar is 200μm, 6 weeks (C) scale bar is 200μm; 4%biohybrid at 2 weeks (D) scale bar is 200μm, 4 weeks (E) scale bar is 100μm, 6 weeks (F) scale bar is 100μm; 3%biohybrid at 2 weeks(G) scale bar is 100μm.

Finally, the figure 6H shows that 3%biohybrid was subjected to a very strong and rapid contraction (around 90%) before arriving at 2 week of culture, but the tissue, as in the case of 4% biohybrid, is completely made-up of endogenous components. Similar observations, can be made by analyzing the H/E histology (data not show). It is possible to establish that depending upon the type of μTP used as building block the resulting biohybrid changed strongly its macroscopic aspect as well as ECM morphology (Fig. 5 B-F; Fig. 6 A-H). In particular the difference found in biohybrid can be correlated with the different initial stiffness, degradation kinetics, as well as MMPs sensitivity of the microscaffold (GPM) used to produce the HD-μTP. Indeed when the less degradable microscaffold (5% GPM) is used the biohybrid retained its shape and thickness until the sixth weeks of culture and GPM were still present (Fig. 6 A-C). By using the most degradable microscaffolds (3% GPM) the

biohybrid lose both thickness and shape at two weeks of culture (Fig. 6H), whilst using 4% GPM the corresponding biohybrid shown an intermediate behavior (Fig. 6 D-F): it was completely made up by endogenous ECM just after two weeks of culture and it was more stable than 3% biohybrid retaining its shape for longer time. This is probably due to more packed collagen fibers that hinder contractile action exerted by cells. Indeed, by investigating the micro as well as ultra-structure of 4% and 5% biohybrid (Fig. 5 G-L) it was possible to observe some interesting differences about collagen maturation and organization. Indeed, SHG images of 5% and 4% biohybrid confirmed that in the former collagen was more packed than in the latter, this condition was ulteriorly confirmed by ultra-structure analyses performed by TEM (Fig. 5). At the light of these results it is conceivable to hypothesize that microscaffold play a crucial role in guiding and sustaining the organization of *de novo* synthesized ECM. Therefore the contraction of the biohybrid was due not only to the disappearance of the microscaffold, but to the lack of an organized and mature ECM able to sustain biohybrid shape and thickness while microscaffold degradation took place. However, due to the very strong contraction of the 3% biohybrids, only 4% biohybrids and 5% biohybrid have been analyzed. In figure 7, DAPI's stained section of biohybrid showed a uniform cell distribution along biohybrid thickness at each time point.

Indeed, by subdividing the biohybrid in three distinct zones (edge, center, edge) the cell frequency in each section appeared constant and it did not change over time (table 1). This result suggests that the process condition guaranteed culturing of 3D tissue equivalent without cell necrosis up to 6 weeks

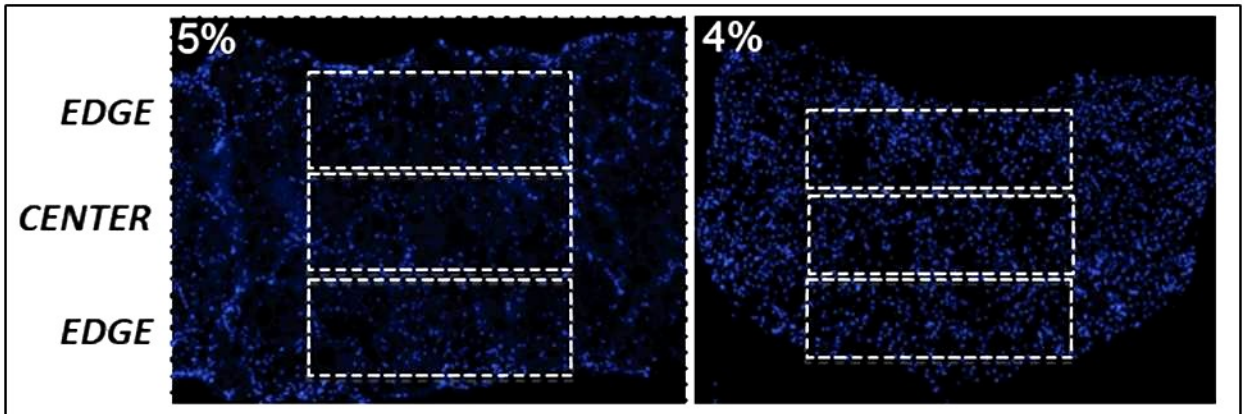

Table 1

	5%			4%		
	2 W	4 W	6 W	2 W	4 W	6 W
EDGE	35.30±0.23	34.63±0.18	33.63±0.18	34.42±0.25	32.50±0.28	34.50±0.28
CENTER	33.39±0.26	30.90±0.21	32.89±0.21	32.62±0.25	34.30±0.32	33.30±0.32
EDGE	35.54±0.35	34.47±0.32	33.47±0.32	32.94±0.23	33.19±0.31	32.19±0.31

Figure 7.: DAPI staining. Nuclei distribution in cross section of 5%biohybrid (A) and 4%biohybrid (B). The dotted line indicated the ROI in which the nuclei were counted. Table 1.: Cell's frequency in each part of biohybrid has been calculated. Data have been reported as mean ± SD.

ECM maturation analyses

Picrosirius red staining allowed monitoring collagen maturation with time. In the figure 8 A-C representative images of Picrosirius red stained biohybrid's cross-section are reported. The reported images are related to the 6 weeks of culture for 5% and 4% biohybrid, and to 2 weeks of culture for 3% biohybrid. According to the histological analyses microscaffolds are still present only in 5% biohybrid. In order to investigate the collagen 'status' (immature *vs.* mature) we exploited polarization microscopy with picrosirius red. This method has been widely used to measure the molecular and fiber orientation of collagen and to characterize collagen fiber arrangement in several kinds of tissues *in vitro* as well as *in vivo* [20-24], and it was also found that there was a good correlation between the volumetric collagen content assessed by biochemical assay and the collagen fraction estimated by videodensitometry [20].The figure 8D shows the results from imaging process of Picrosirius red images

assessing that collagen is present at each time point for all the biohybrid type. In particular in 5% biohybrid at 2 weeks of culture the proportion of green (thin/immature collagen fibers) and red (thick/mature collagen fibers) is quite similar 0.04±0.02 and 0.03±0.02, respectively. As the time increases the proportion of green fibers slightly decreases from 2 week to 4 week, but there is no change from 4 week to 6 week. Otherwise the proportions of red fibers increase with time reaching at six weeks the value of 0.35±0.09. Interestingly, the red fiber content of 5% biohybrid at six weeks of culture approached the value found for the skin (i.e. 0.43). In the 4% biohybrid the proportion of both red fibers and green fibers presents the same trend found in 5% biohybrid, nevertheless the red fibers content reached lower value than that found in 5% biohybrid at each time point. Indeed the maximum value found at six weeks of culture is 0.16±0.03 versus 0.35±0.09 found at six weeks for 5% biohybrid, statistical analyses confirmed that the values are different. At last, in the 3% biohybrid the analysis was performed only at 2 week, and the difference between red and green collagen was statistically different and similar at the value found in the 4% biohybrid as well as 5% biohybrid at the same time point.

By observing the behavior of mature collagen (red fraction) in the figure 8D it is possible to see that in the 5% biohybrid the collagen assembling process is faster than in 4% biohybrid. This result suggests that the collagen composition evolution over culture time presented in fig. 8D indicated that cells were engaged in synthesizing their own ECM by assembling and remodeling the immature collagen (thin fiber/green fraction) in a mature collagen (thick fiber/red fraction) with a velocity depending upon the initial micro-scaffold property. Indeed, the fraction of neo-synthesized collagen remained constant over the time, indicating a continuous collagen synthesis

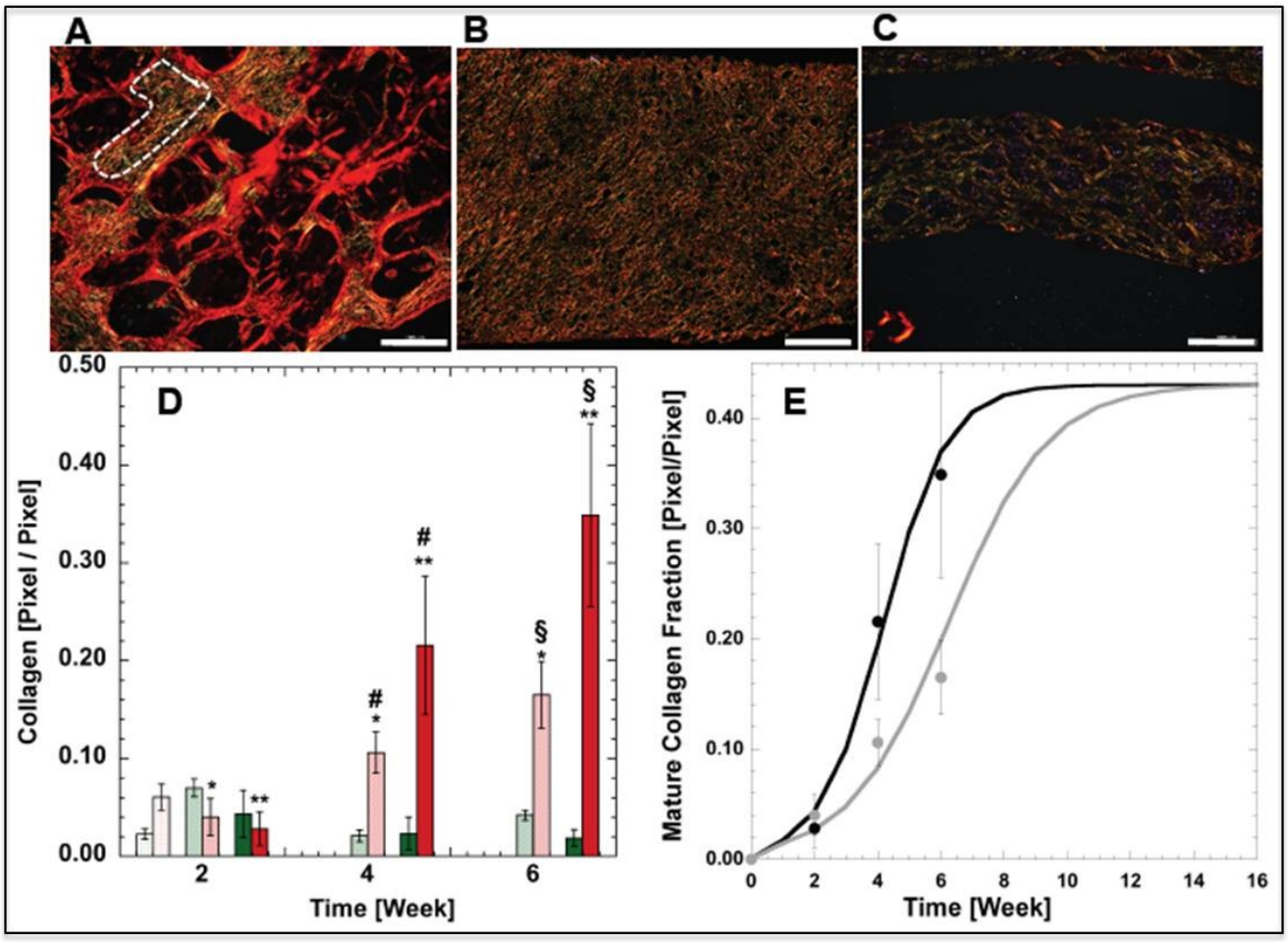

Figure 8.: ECM maturation analyses. Picro Sirius red stained cross section of 5% biohybrid at 6 weeks (A) scale bar is 100 µm, 4% biohybrid at 6 weeks (B), scale bar is 200 µm; 3% biohybrid at 2 weeks (C) scale bar is 200 µm. Time evolution of collagen red fraction and collagen green fraction (D): 3% biohybrid (slight green intensity/ slight red intensity); 4% biohybrid (medium green intensity/medium red intensity); 5% biohybrid (strong green intensity/strong red intensity). Behavior of red fraction collagen: experimental data of 5% biohybrid (black circles) and 4% biohybrid (gray circle), equation 1 evaluated by using curve fitted parameters reported in table 1 for 5% biohybrid (black lines) and 4%biohybrid (gray line).

By contrast, analyzing the data concerning the mature collagen we observed a continuous increase over the time, for both biohybrids. Nevertheless there was a difference in the collagen kinetic assembly: 5% biohybrid approached faster than 4% biohybrid the composition of human dermis The evolution of kinetics parameters related to collagen assembly process, has been carried out by using data from red fraction evolution shown in figure 8D for 5% and 4% biohybrid with equation 1

$$y = \frac{Y_{\max}}{2}\left[1 - \tanh(\beta t - \alpha)\right] \qquad \text{Eq. 1}$$

subjected to following conditions:

$$y(0) = 0$$
$$y(\infty) = Y\max \qquad \text{Eq.2}$$

where *y* represents the red collagen fraction, Y_{max} the maximum collagen assembled fraction, t the culture time and α and β two kinetic parameters. The equation 1 is a sigmoid shaped saturation law and its use, together with equation 2 in fitting the data related to collagen assembly, is justified by the following considerations: (i) at early time of the collagen assembling process, the value of mature collagen is very close to zero (y(0)= 0); (ii) as time increases, the fraction of the mature collagen increases (Fig. 8D); (iii) at the longer culture time the assembly process has to reach a steady state [20], and the fraction of mature collagen approaches a value that in this case is the fraction of assembled collagen in native dermis (y(∞)=Ymax). The data of red collagen were then fitted with equation 1 and equation 2 using a fitting procedure implemented in Mathematica®, and the results are reported in table 1. The parameter β [time^{-1}] can be related to the rate of collagen assembly, while the parameter α [dimensionless], is related to the inflection point of the function hyperbolic tangent. When the argument of the equation 1 is zero (βt-α = 0), the fraction of mature collagen, y, is the half of the maximum collagen fraction, in this condition the time defined by the equation 3

$$T_s = \frac{\alpha}{\beta} \qquad \text{Eq. 3}$$

can be seen as an index of collagen maturation, representing the 'setting time' of the collagen in ECM. The plot in the fig. 8E, shows the behavior of mature collagen in 5% biohybrid (black curve) and 4% biohybrd (gray curve) as well. As expected the kinetic of collagen maturation in 5% biohybrid is faster than 4% as confirmed by fitting parameters reported in table 2. The values of the rate of the collagen assembly (β) are 0.5 and 0.3 week^{-1} for 5% and 4% biohybrid respectively. Furthermore, the collagen 'setting time' (Ts) is lower in the 5% than in 4% biohybrid (30 days *vs*. 40 respectively). The values fall in the intervals reported in literature for collagen turnover [25]. These results indicated that the microscaffold properties affected the collagen assembly rate. In particular, longer degradation rate sped-up the collagen assembly process and such phenomenon can be correlated both with the

scaffold stiffness and with the growth of ECM in a confined space. The former observation agrees with literature data reporting the influence of substrate stiffness in up-regulating collagen synthesis and organization [26, 27]. The latter hypothesizes that when collagen monomers are secreted in to a confined space the higher collagen concentration induces a control on matrix organization and packing [21], before to reach a contact inhibition condition [28]. These two events are verified in 5% biohybrid where the stiffer GPM being still present into biohybrid until the 6 weeks of culture allowed the tissue growth only in confined space.

Different case is verified in 3% biohybrid where the use of 3% GPM having the shortest degradation rate, induces their degradation at two weeks of culture. Although 3% biohybrid is composed by endogenous collagen (Fig. 6H) its maturation as well as organization (Fig. 8 C-D) is not able to prevent the tissue contraction due to cellular traction. It is commonly believed that the control over tissue growth is obtained by matching degradation rates of tissue scaffolds to the rate of various cellular processes [29]. At light of our results, we suggested that kinetic of collagen assembly is one of the most important cellular process at which is necessary to refer to. To highlight this concept we introduced a graphical illustration (Fig. 9) relaying upon scaffold design criteria for engineering soft tissue *in vitro* arisen by the observed phenomena. According to the strategy proposed by Hutmacher [30] the total mechanical integrity of the cellular construct (P_{MAX}), is composed by the contribution arising by the scaffold (P_s) and the growing tissue (P_{ECM}), as described by the equation 4

$$P_{ECM}(t) + P_S(t) = P_{\mathrm{MAX}} \qquad \text{Eq. 4}$$

At the beginning of the process scaffold architecture guides cell growth and premature tissue development, so at early stage of the process is verified the condition $P_S = P_{MAX}$.

During the cellular construct culture, scaffold gradually vanishes leaving sufficient space for cell invasion and new tissue in growth. However, physical support by the 3D scaffold should be maintained until the engineered tissue has sufficient mechanical integrity to support itself verifying the condition $P_{ECM} = P_{MAX}$. The property P_{ECM}, can be related to the collagen fraction in the growing tissue (y), and it has to approach P_{MAX} as the time is increasing [31,32]. As a consequence P_{ECM} can be expressed by means of equation 5:

$$P_{ECM}(t) = \frac{P_{MAX}}{Y_{max}} y$$ Eq. 5

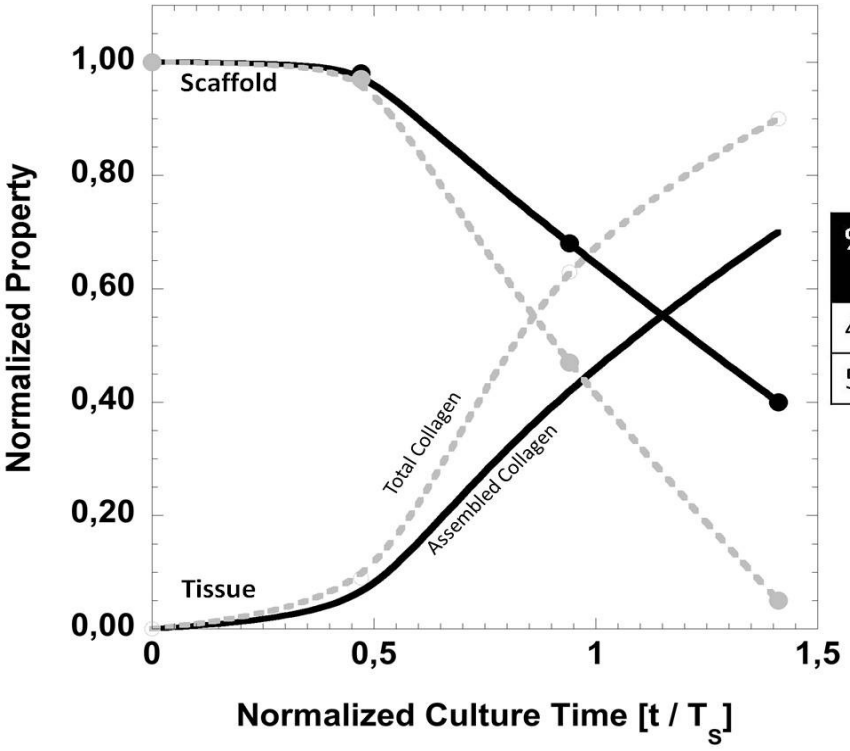

Table 2

%	α	β [Week^{-1}]	Tc [d]
4	1.7	0.3	40
5	2.1	0.5	30

Figure 9.: scaffold design criteria. Evolution of P_{ECM} and P_s versus dimensionless culture time (t/T_s): P_{ECM} by using $y = y_{red}$ (black line), $y = y_{red}+y_{green}$ (gray dotted line) in equation 4; P_S by using $y = y_{red}$ (black circle), $y = y_{red}+y_{green}$ (gray circle) in equation 5. Table 2.:Kinetics parameters obtained by curve fitting red-collagen data of 4% and 5% biohybrid with equation 1 and equation 2. b, rate of collagen assembly [week^{-1}]; T_s, 'setting time' [day].

By combining equation 4 and equation 5, the time evolution of the PS normalized to P_{MAX}, can be expressed according to equation 6:

$$\frac{P_S(t)}{P_T} = \left(1 - \frac{y}{Y_{max}}\right)$$ Eq. 6

In fig. 9 we reported the behavior of Eq. 5 and Eq. 6 by using mature collagen values ($y = y_{red}$) and total collagen values (mature + immature, $y = y_{red} + y_{green}$) of 5% biohybrid taken by figure 8D. The cross over between Eq. 5 and Eq. 6 should indicate the characteristic degradation time of the scaffold. Interestingly, by using the mature collagen value, $y = y_{red}$ in the equation 5 and 6, the cross over falls above the setting time ($T_2 < T_s$). Otherwise by using

total collagen values, $y = y_{red} + y_{green}$, the crossover falls before the ECM setting time ($T_1 > T_s$). Therefore it is possible to argue that if the microscaffold is designed in order to match its degradation time (T_d) with the total collagen synthesis, it will degrade before collagen assembly occurred ($T_d / T_s << 1$) and this condition doesn't guarantee that the engineered tissue has a sufficient mechanical integrity to support itself. In contrast by matching the scaffold degradation time with assembly collagen time, most probably the ECM has sufficient maturation degree to prevent tissue contraction ($T_d / T_s >> 1$). At light of this observation in our study, the 3% GPM verified the condition of $T_d / T_s << 1$ consequently 3%biohybris resulted in a fast shrinkage; the opposite condition $T_d / T_s >> 1$ is verified for 5% GPM indeed the 5% biohybrid didn't show any contraction, exhibited the highest collagen maturation degree, and retained microscaffold during the time of culture. Otherwise the 4% GPM verified a condition in which T_d / T_s is just below the unity, consequently the 4% biohybrid is able to sustain the tissue contraction for longer time compared to 3% biohybrid, thanks to a superior collagen maturation of the neo-ECM able to support the integrity of the biohybrid in the absence of microscaffold. Probably the gold standard condition $T_d/T_s \approx 1$ (i.e. endogenous tissue and shape retention) can be reached by exploring a cross-linking extent ranging between 4%GAL and 5%GAL and this issue is actually under investigation. So, morphological analyses showed that endogenous ECM was present in each 3D tissue equivalent realized, but its time evolution, organization and collagen assembly kinetics strongly depend upon the microscaffold formulation used. The increase of the microcarriers' crosslinking extent sped up collagen assembly kinetic obtaining stiffer ECM able to balance both scaffold's mass loss and cell traction in a limited time window. Taken together our results indicate that by tuning the degradation rate of micro scaffold, it is possible to modulate the properties of the ECM of the final 3D tissue. Moreover HD-µTP, produced under optimized dynamic conditions, can be molded to produce a 3D human dermal equivalent made up of endogenous ECM able to sustain a long-time culture *in vitro*. Despite of other approaches relaying the realization of building block used in bottom up tissue engineering, the HD-µTP realized in this study are rich in ECM essential for the cell to grow

and differentiate in a tissue like environment. To reach this aim the initial presence of micro scaffold has a crucial importance [10-12], to promote the synthesis of ECM. In order to guarantee not only the collagen synthesis but also its organization a key issue of this study is the modulation of initial micro-scaffold properties. Indeed while many studies focused their attention on the molding capability of building blocks, at best of our knowledge any efforts have been spent to reach a deep understanding of their role in ECM organization as well as collagen assembly of the 3D tissue resulting by their biosintering.

CONCLUSION

In conclusion, we have demonstrated that μTP precursor assembly approach can be exploited to build-up human dermal tissue equivalent *in vitro* completely made up by endogenous ECM components. Moreover we assessed that the microscaffold degradation rate plays a fundamental role in the collagen maturation and provides the possibility to tune the properties of the final 3D tissue. Finally we found key parameters of collagen assembly's process, useful to address a more efficient scaffold design for *in vitro* soft tissue engineering. These parameters aid to identify the trade-off between too short (mechanical failure, endogenous material) and too long scaffold persistence (shape retention, partially endogenous material).

REFERENCES

1. Nichol JW and Khademhosseini A. Modular Tissue Engineering: Engineering Biological Tissues from the Bottom Up. Soft Matter. 2009;5:1312-1319.

2. Yang J, Yamato M, Kohno C, Nishimoto A, Sekine H, Fukai F, Okano T. Cell sheet engineering: recreating tissues without biodegradable scaffolds. Biomaterials 2005;26:6415-6422.

3. Shimizu T, Yamato M, Kikuchi A, Okano T. Biomaterials. Cell sheet engineering for myocardial tissue reconstruction. Biomaterials 2003;24:2309-2316.

4. Gwyther TA, Hu JZ, Christakis AG, Skorinko JK, Shaw SM, Billiar KL, Rolle MW.

Engineered Vascular Tissue Fabricated from Aggregated Smooth Muscle Cells. Cells Tissues Organs 2011;194:13-24.

5. Norotte C, Marga FS, Niklason LE, Forgacs G. Scaffold-free vascular tissue engineering using bioprinting. Biomaterials 2009;30:5910-5917

6. Khademhosseini A and Langer R. Microengineered hydrogels for tissue engineering. Biomaterials 2007;28:5087-5092

7. Naito H, Melnychenko I, Didié M, Schneiderbanger K, Schubert P, Rosenkranz S, Eschenhagen T, Zimmermann WH. Optimizing Engineered Heart Tissue for Therapeutic Applications as Surrogate Heart Muscle. Circulation 2006;114:I-72-I-78.

8. Matsunaga YT, Morimoto Y, Takeuchi S. Molding Cell Beads for Rapid Construction of Macroscopic 3D Tissue Architecture. Adv. Mater. 2011;23:H90–H94.

9. McGuigan AP, Leung B, Sefton MV. Fabrication of cells containing gel modules to assemble modular tissue-engineered constructs. Nature Protocols 2006;1:2963-2969

10. Chen M, Wang X, Ye Z, Zhang Y, Zhou Y, Tan WS. A modular approach to the engineering of a centimeter-sized bone tissue construct with human amniotic mesenchymal stem cells-laden microcarriers. Biomaterials 2011;32:7532-7542.

11. Palmiero C, Imparato G, Urciuolo F, Netti PA. Engineered dermal equivalent tissue *in vitro* by assembly of microtissue precursors. Acta Biomat 2010;62:548–2553.

12. Urciuolo F, Imparato G, Palmiero C, Trilli A, Netti PA. Effect of Process Conditions on the Growth of Three-Dimensional Dermal-Equivalent Tissue Obtained by Microtissue Precursor Assembly. Tissue Eng. 2011;17:155-64.

13. Nilsson K, Buzsaky F, Mosbach K. Growth of anchorage-dependent cells on macroporous microcarriers. Nature Biotech. 1986;4:989-990.

14. Rich L, Whittaker P. Collagen and picrosirius red staining: a polarized light assessment of fibrillar hue and spatial distribution. Braz. J. morphol. Sci. 2005;22:97-104.

15. Nadkarni SK, Mark CP, Park BH, De Boer JF, Whittaker P, Bouma, BE et al.Measurement of Collagen and Smooth Muscle Cell Content in Atherosclerotic Plaques Using Polarization-Sensitive Optical Coherence Tomography. Journal of the American College of Cardiology 2007;49: 1475-1481.

16. Salerno A., Guarnieri D, Iannone M, Zeppetelli S, Netti PA. Effect of Micro- and Macroporosity of Bone Tissue Three-Dimensional-Poly(ε-Caprolactone) Scaffold on Human Mesenchymal Stem Cells Invasion, Proliferation, and Differentiation *In Vitro* Tissue Engineering 2010;16:2661-2673

17. Ng YC, Berry JM, Butler M. Optimization of physical parameters for cell attachment and growth on macroporous microcarriers. Biotech and Bioeng 1996;50:627–35.

18. Konig K, Schenke-Layland K, Riemann I, Stock UA. Multiphoton autofluorescence imaging of intratissue elastic fibers. Biomaterials 2005; 26: 495–500.

19. Konig K. Clinical multiphoton tomography. J. Biophoton. 2008;1:13-23.

20. Obradovic B, Meldon JH, Freed EL, Vunjak-Novakovic G. Glycosaminoglycan deposition in engineered cartilage: Experiments and mathematical model. AIChE Journal 2000;46:1860–1871.

21. Xiaoqing G, Hutcheon AEK, Melotti SA, Zieske JD, Trinkaus-Randall V, Ruberti JW. Morphologic Characterization of Organized Extracellular Matrix Deposition by Ascorbic Acid–Stimulated Human Corneal Fibroblasts. IOVS 2007;48:4050-4060.

22. Zhu XH, Tabata Y, Wang CH, Tong YW. Delivery of Basic Fibroblast Growth Factor from Gelatin Microsphere Scaffold for the Growth of Human Umbilical Vein Endothelial Cells. Tissue Eng. 2008;14:1939-1947.

23. Pickering JG, Boughner DR. Fibrosis in the transplanted heart and its relation to donor ischemic time. Assessment with polarized light microscopy and digital image analysis. Circulation 1990;81:949-958

24. Noorlander LM, Melis P, Jonker A, Van Noorden CJF. A Quantitative Method to Determine the Orientation of Collagen Fibers in the Dermis. The Journal of Histochemistry & Cytochemistry 2002; 5:1469-1474.

25. Rosati P, Colombo R, Maraldi N. Istologia. Edi. Ermes 2006

26. Ventre M, Causa F, Netti PA. Determinants of cell-material crosstalk at the interface: towards engineering of cell instructive materials. J. R. Soc. Interface 2012;9:2017-2032.

27. *In Vivo* Stimulation of *De Novo* Collagen Production Caused by Cross-linked Hyaluronic Acid Dermal Filler Injections in Photodamaged Human Skin. Arch Dermatol. 2007;143:155-163.

28. Dubey N, Letourneau PC, Tranquillo RT. Guided neurite elongation and Scwann cell invasion into magnetically aligned collagen in simulated peripheral nerve. Regen Exp Neurol 1999;158:338-350.

29. Hubbell JA. Bioactive biomateriale. Current Opinion in Biotechnology. 1999;10: 123–129.

30. Hutmacher WD. Scaffolds in tissue engineering bone and cartilage. Biomaterials 2000; 21:2529-2543

31. Vunjak-Novakovic G, Martin I, Obradovic B, Treppo S, Grodzinsky J, Langer R, Freed L. J Orthop Res. 1999;17:130-138.

32. De Rosa E, Urciuolo F, Borselli C, Gerbasio D, Imparato G, Netti PA. Time and space evolution of transport properties in agarose-chondrocyte constructs. Tissue Eng. 2006;12:2193-201.

Chapter 3

3D HUMAN DERMIS EQUIVALENT *IN VITRO* AS A LIVING BIOLOGICAL TEST PLATFORM

INTRODUCTION

The classical tissue engineering approach to produce viable *in vitro* tissues by seeding cells into preformed, porous, and biodegradable scaffolds presents several shortcomings, mainly due to the difficulty in reproducing, at the pericellular level, adequate microenvironmental conditions in a three-dimensional (3D) thick structure [1,2]. New results demonstrated the importance of tissue micro-architecture on the resulting function of engineered tissue constructs [3]. Therefore, devising new biomimetic techniques for generating engineered tissues with micrometer-scale resolution is of great scientific interest. Microfabrication technologies have been applied to cell culture techniques in the effort to better direct tissue formation and function. As cell–cell and cell–extracellular matrix (ECM) interactions play critical roles in cell and tissue function, control over the cellular microenvironment could be key to fabricate biomimetic tissue structures [4]. The tissue microarchitecture in the human body is often made of repeating functional units. As a result, self-assembling of micrometer-scale tissues in order to create the native microarchitecture of natural tissues is a promising approach for the fabrication of functional complex tissue constructs. In this chapter we used a bottom-up approach to produce 3D dermis equivalent construct. A lot of different dermis equivalent models have been proposed in literature in the past decade, some including living fibroblast and other not including cell population. In these models, several materials such as, bovine collagen,[5] glycosaminoglycan,[6] human dead dermis,[7,8] synthetic polymers [9] and cell sheet confluent [10] have been used. Among the main drawbacks of the human dermis equivalent models used until now, are the presence of exogenous materials, the inappropriate mechanical properties, the difficult to obtain large and tick tissues, and the problem related to infection and rejection in clinical applications.

However one of the most used model in literature to mimic the native dermis is based on the cellularized fibrillar collagen. Nevertheless, even if this model is very close to native dermis's morphology it is too simplified to mimic the intricate pathway that *in vivo* plays a fundamental role in phenomena such as aging, photoaging or other events in which the structural proteins of ECM are involved. Many studies in literature reported that in photoaged skin *in vivo*, collagen fibrils are disorganized and abnormal elastin-containing material is accumulated [11]. Biochemical studies have revealed that in photoaged skin, levels of type I and III collagen precursor and crosslinks are reduced, whereas elastin levels are increased [12]. Moreover a large number of studies, unambiguously demonstrate that the UV radiation leads to enhanced and accelerated degradation and /or decreased synthesis of collagen fibers. This occurs because the UV irradiation plays a fundamental role in the induction of matrix metalloproteinases (MMPs), enzymens able to degrade matrix proteins such as collagen and elastin. Under basal conditions, MMPs are part of a coordinated network and are precisely regulated by their endogenous inhibitors, i.e. TIMPs which specifically inactivate certain MMPs. An imbalance between activation of MMPs and their respective TIMPs could lead to excessive proteolysis. It is now very well established that UV radiation induces MMPs without affecting expression or activity of TIMPs [13]. In a very simplified scheme, UVA radiation acts indirectly through the generation of free radicals and reactive Oxygen Species (ROS), in particular singlet oxygen, which subsequently can exert a multitude of effects such as lipid peroxidation, activation of transcription factors and generation of DNA strand breaks and cellular necrosis in the dermal layer [14]. In the light of these evidences in order to have an *in vitro* human dermal model able to recapitulate the events occurring *in vivo* after photo-damage it is fundamental produce a model having endogenous ECM. Since our dermis equivalent meets this need, in the study

presented in this chapter, we assessed the capability of our model to respond to external stimuli such as the UVA irradiation. We focused particular attention to the effect of irradiation on the organization of structural proteins such as collagen and elastin by multiphoton microscopy MPM, a new non invasive microscopic techniques that guarantee high resolution capability [15]. It allows the visualization of unstained structural bio-molecule such as collagen and elastin. Because the intensity of the signals and the organization of the ECM are strongly related with the status of the tissue (healthy *vs*. damaged), the use of MPM in combination with image analysis algorithms is becoming a very powerful diagnostic tool [16]. Many works have been published demonstrating that the organization of collagen network can be quantified by using Second Harmonic Generation (SHG) / Two Photon Elastin Fluorecence (TPEF) [17] images coupled with texture analysis performed with Grey Level Co-occurrence Matrix (GLCM) and/or Fast Fourier Transform (FFT) [18, 19]. However, currently the studies related to collagen or stromal modification occurring under pathological conditions have been performed on patients or tissue biopsies and, no reports exist concerning *in vitro* tissue models made-up by endogenous ECM.

MATERIALS AND METHODS

Spinner cell culture

Macroporous gelatin microbeads were obtained by using a double emulsion technique. Glyceraldehydes has been used as gelatin crosslinker at 4% w/w of the microbeads, only this percentage has been used in order to obtain a tissue completely endogenous without the presence of microbeads at the 6 week. The microbeads/fibroblasts cultures were propagated in spinner flasks (100ml, Belco) for 96 hours, in order to obtain a human demis-microtissues precursor (HD-µTPs), the stirring mode was set at 30rpm, 30 minutes pause and 5 minutes running, for the first

6 hours of seeding; continuous stirring for the following hours of culture. The spinner cultures were incubated at 37°C in 5% CO2.

Tissue assembling in sheet-shape

HD-µTPs suspension was transferred from the spinner flask to a 50 ml Falcon centrifuge tube and, after settling, transferred by pipetting into the maturation chamber to allow their molding in sheet shape. The filling is carried out vertically with the maturation chamber immersed in the culture medium. In the hollow space of the chamber are inserted through a syringe the µTP along the slot available, taking care to fill all the necessary volume. The maturation chamber showed in fig. 1 is home made and similar at the maturation chamber used to realized a disc shape but the size is a square with an area of 25 square centimeters.

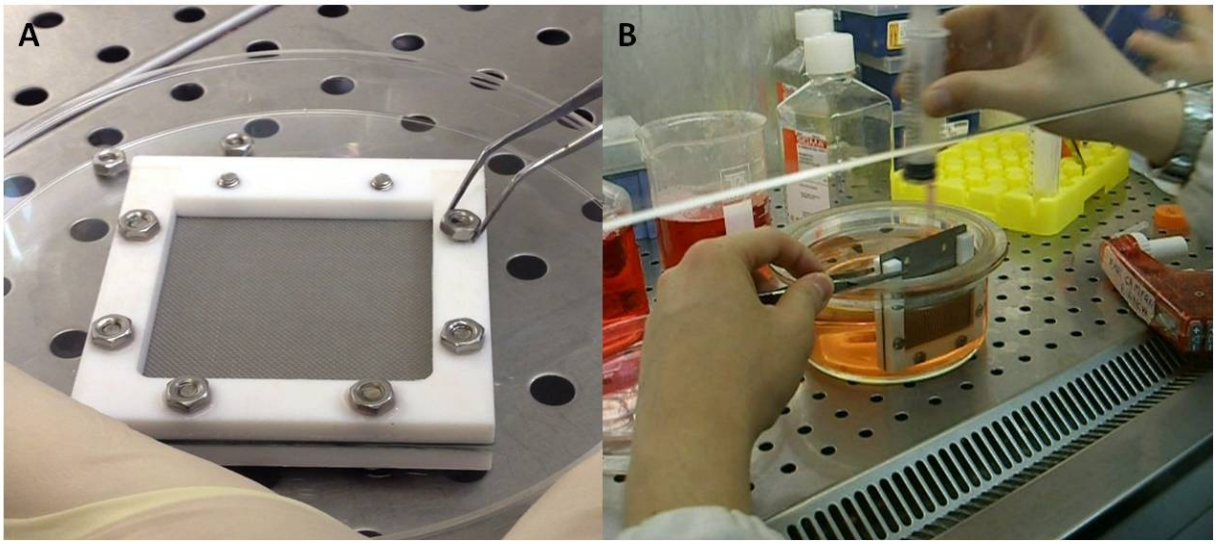

Figure 1.: procedure of tissue assembly. (A) maturation chamber, (B) vertical filling system

Only one hand, the occurrence of the vertical filling, is closed only at the end of the filling process. Finally the assembling chamber was placed on the bottom of a particular spinner flask home made showed in figure 2.

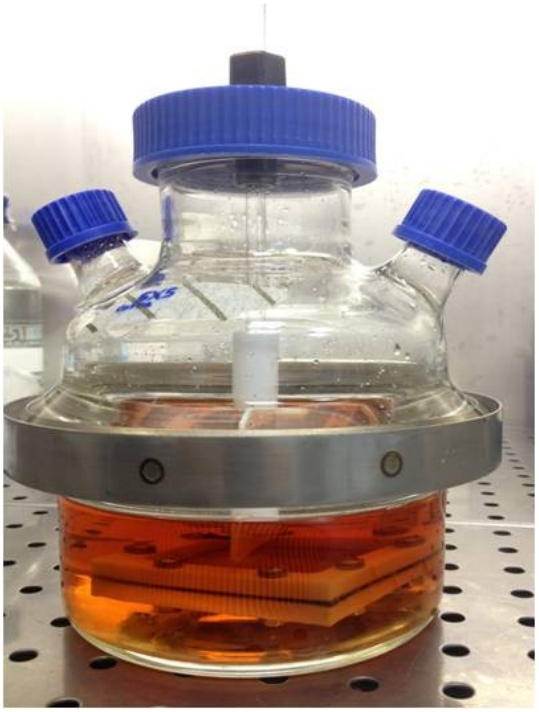

Figure 2.:spinner flask or bioreactor of tissue maturation

The bioreactor is formed by two part connected by fixing flange and in figure 2 it is showed completely surrounded by culture medium. The spinner was operated at 60 rpm and the medium was exchanged every 4 days

Morphological extra cellular matrix characterization

Histological analyses and immufluorescences

ECM composition and morphology along the peace of the sheet thickness were assessed by performing histological analysis on transverse sections of biohybrid.

5µm transverse sections of samples were stained using hematoxylin-eosin (Bio Optica) solutions, Masson's trichrome (Sigma Aldrich), following standard procedure and analyzed by an optical microscope (BX53; Olympus). The samples that will be included in Tissue Tek are fixed in 4% paraformaldehyde for 30 min at room temperature, wash them in PBS and after can be placed into a sucrose 2M solution that was prepared in water. Tissues should be soaked with sucrose at room

temperature not more than 24h; this part of procedure is more important for frozen preservation. Indeed we discarged the sucrose 2M and place the sample in the Tissue Tek Killik in the suitable mold named Peel-A (Ted Pella INC) that we submerge in liquid nitrogen vapors for 1 min and then remove and store in -80 °C. The immunofluorescences are performed on sample that were cuts in slices (5-8 μm) with criomicrotome (Leica CM 1850) and were used for the SHG analysis of the structures such as collagen and elastin. The cut was oriented so as to view the cross section of the samples. Moreover fibronectin, laminin, elastine, dermal markers were performed respectively : anti-fibronectin monoclonal antibody (Sigma), Anti-laminin polyclonal antibody (Sigma), anti-elastine polyclonal antibody (Sigma). Every antibody monoclonal were produced in mouse and the polyclonal antibody were produced in rabbit. The nuclear stain was Sytox Green (Invitrogene). The secondary antibodies that we used were: Alexa Fluor 546 mouse anti-rabbit IgG (H+L) (diluition 1:500; Life technologies), Alexa Fluor 488 mouse anti-rabbit IgG (H+L) (diluition 1:500; life technologies), Alexa Fluor 488 goat anti-mouse IgG (H+L) (diluition 1:500; life tecnologie), Alexa Fluor 546 goat anti-mouse. IgG (H+L)

Scanning electron microscopy (SEM) with Energy-Dispersive Spectroscopy (EDS)

SEM/EDS was performed to analyze both the morphology of peace of sample on surface and along thickness after the rift. The sample prepartation was described in the Chapter 1 Coated samples were then examined by scanning electron microscopy (SEM) (Leica S400).

Second Harmonic Generation (SHG) and two-photon excited fluorescence (TPEF) for sample imaging: SAAID index and GLCM matrix

To this aim samples of foreskin at 30 and 80's years old and the our human equivalent dermis were investigated by Confocal Leica TCS SP5 II combined with a Multiphoton Microscope where the NIR femtosecond laser beam was derived from a tunable compact mode-locked titanium:sapphire laser (Chamaleon Compact OPO-Vis ,Coherent). The samples for nonlinear imaging were prepared by freezing them and by cutting them in a compact routine cryostat. Slices ranging from 50 to 100 mm thickness were obtained. Before imaging, samples were unfrozen and closed with a microscope coverslide together with some PBS droplets in order to maintain the natural tissue osmolarity. The excitation was accomplished using a wavelength of 740 nm for TPEF and 840 nm for SHG and a mean laser power at the sample between 10 and 40 mW, depending on the depth of recording. These power levels are sufficiently low to avoid photobleaching and photodegradation effects, as demonstrated also in in-vivo multiphoton skin imaging [22]. SHG or TPEF detection was accomplished by switching the excitation wavelength between 740 nm and 840 nm. TPEF-SHG images were acquired with 512x512 pixels or 1024x1024 pixels spatial resolution, from 60 mm to 200 mm lateral dimension, using a pixel dwell time of 5 μs. The scanning time was approximately 1.3 s and 5 s for 512 and for a 1024-pixels image, respectively. For Second harmonic to Autofluorescence Aging Index of Dermis (SAAID) scoring images were processed with analysis software (Image J®). The calculated score is the geometrical mean of the value calculated from 10 different 50 mm side squared ROI for each sample. We have characterized the morphology of part of tissues by measuring the SAAID score. The SAAID value is a measure of the ratio between collagen and elastic tissue. It can be used to evaluate

intrinsic and extrinsic skin aging, as well as to give a measure of the fibrotic status of the dermis. It is defined as follows:

$$\mathbf{SAAID=}\frac{\mathbf{SHG.coll-TPEF.elast.}}{\mathbf{SHG.coll+TPEF.elast.}} \quad (1)$$

In the equation 1 SHG coll represents the intensity distribution of the SHG signals due to collagen matrix and the TPEF elast represents the intensity distribution of the TPEF signal due to elastic fibers. SAAID index were evaluated both from 3D-HDE UVA- ($SAAID_0$) and 3D-HDE UVA+ ($SAAID_{UVA}$) and reported as the ratio

$$\Sigma = \frac{SAAID_0}{SAAID_{UVA}} \quad (2)$$

GLCM matrix was calculated from human skin of 80 years old an 30 years old and 3D-HDE UVA+ and 3D-HDE UVA- by SHG images. We performed gray-level co-occurrence matrices (GLCMs) texture analysis to SHG images. Based on gray-level statistical patterns between neighboring pixels, the GLCMs can provide texture features. In particular, by indicating the fibril and separation, the correlation feature, a measure of intensity correlation as a function of pixel distance, relates to collagen fibril structure. In detail, if the correlation falls off sharply with pixel distance, the collagen matrix presents distinct, linear fibrils; if it remains elevated as pixel distance is increased, the collagen matrix has less defined fibrillar structure. In this experiment, we calculated the correlation for distances ranging from 1 to 60 pixels (0.4 μm to 24.0 μm) in the horizontal direction of each optical section. [23].

As in the case of SAAID index the ratio of the correlation length between 3D-HDE UVA- and 3D-HDE UVA+ samples was evaluated.

$$\Lambda = \frac{L_0}{L_{UVA}} \quad (3)$$

Tensile properties measurements.

From 5x5 mm tissue equivalent were harvested bone dog shaped sample to perform the tensile mechanical tests. The samples were 1mm thick. 5 mm large with a measure length of 22 mm. The sample was placed between mechanical grips and mechanical test were performed by means of Instron 5566.

The test was carried out under displacement control with a two velocities of 0,5mm/min and 10mm/min. The force was measured by a load cell (2,5 N). The force and displacement data were converted in stress and deformation respectively. The stress was obtained by force data by dividing the force by initial cross sectional area (5x1 mm^2). The deformation was obtained by the displacement data normalized to the initial length of 22mm. From Stress-Strain curve it was evaluated: tangent elastic modulus E_{tan}, by evaluating the slope of the initial part of the whole curve; the deformation at breaker, as the value of the deformation corresponding the failure of the sample

RESULTS AND DISCUSSIONS

Human dermis equivalent: macroscopic aspect and mechanical testing

As show in figure 3 (A, B, C, D) human dermis equivalent obtained by assembling of HD-µTPs having 6 weeks of maturation appears ductile, flexible, strong and resistant to torsion stress and at the pull. Also the color of material is similar to human dermis and this aspect play a fundamental role in a hypothetical surgery application.

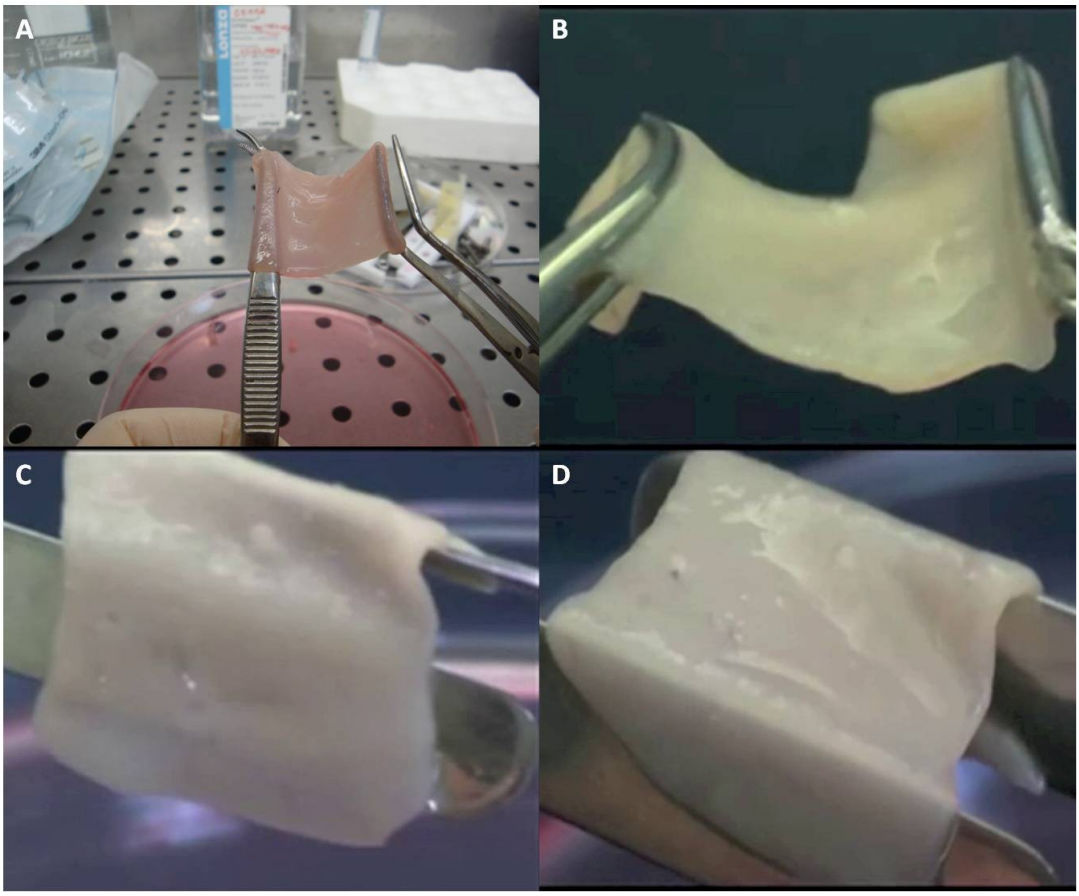

Figure 3.: images of human dermis equivalent

SEM images (Fig. 4A, B, C, D) show equivalent human dermis completely made by cells and ECM forming large 3D tissue equivalents. In figure 4B is highlighted the thickness of construct and in figure 4A and C it is possible to note the bundle of collagen on the surfaces. Moreover it is possible to detect the organic composition in percentage of carbon and oxygen by using EDS module, an analytical technique used for the elemental analysis or chemical characterization of a sample. The value indicated in table, 68,6% C and 31,4% O, demonstrates that the surface of sample also in percentage is very similar to native dermis

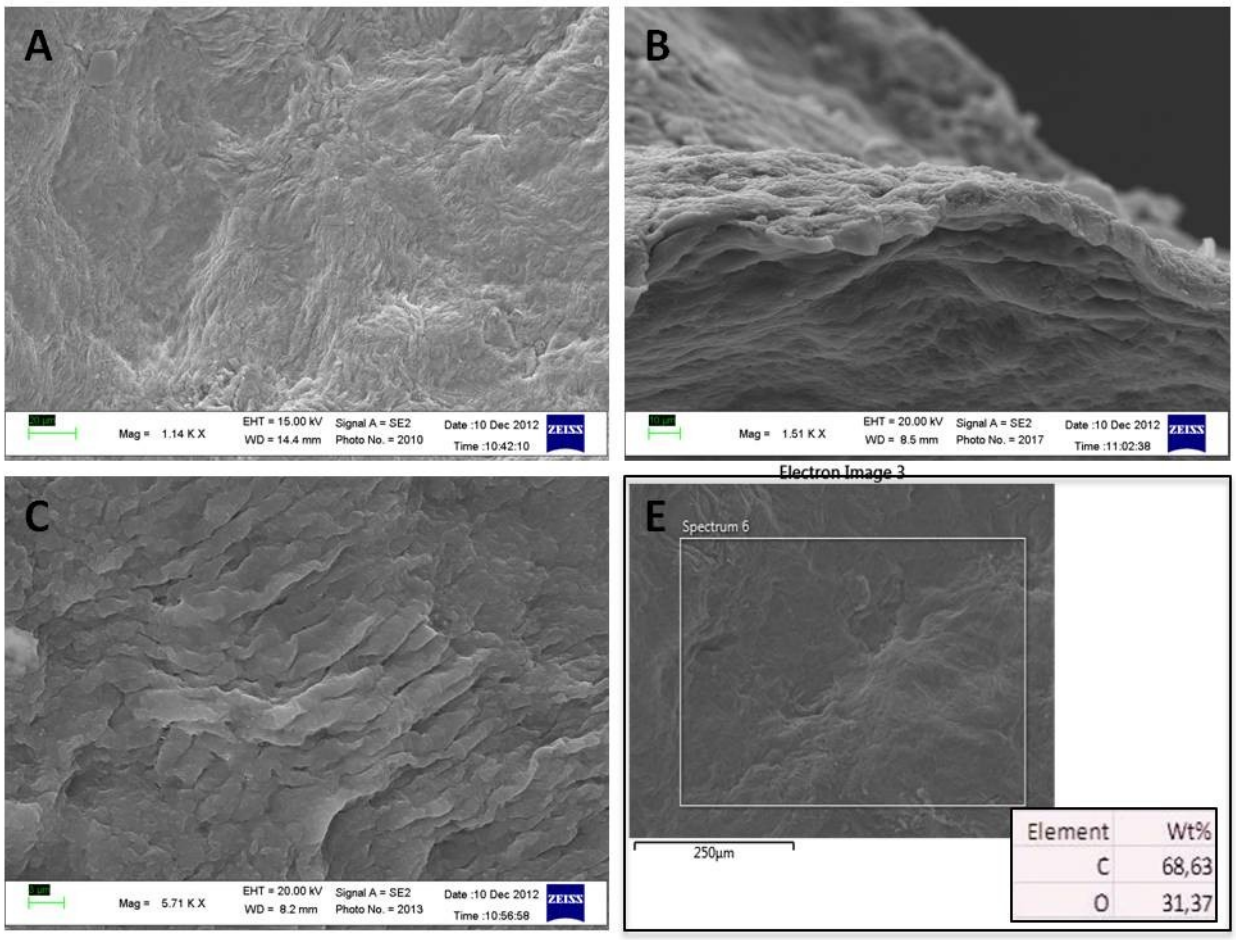

Figure 4.: scanning electron microscopy micrographs of human dermis equivalent;(A) surface, (B) and thickness, (C) bundle of collagen on the surface, (D) combination of the SEM image and table that indicates the percentage of element in the white area

In graph 1 we show the curve of mechanical stress of small sample dog-bone shaped obtained from derma equivalent sheet. We have performed two constant deformation rate, 0,5 mm/min and 10mm/min; in the table under graph is shown the values of tangent elastic module (E_{tan}) calculated in initial and linear portion of the curve, maximum strain (S_{max})and maximum stress.(σ_{max}). As shown in the table by increasing deformation rate also increases the Young module (E_{tan}). This trend is typical of elastic no linear materials. Indeed the test starts with an evident deformation of the sample until arriving at the point of maximum stress that is 0.70 KPa, at which the breakage occurring.

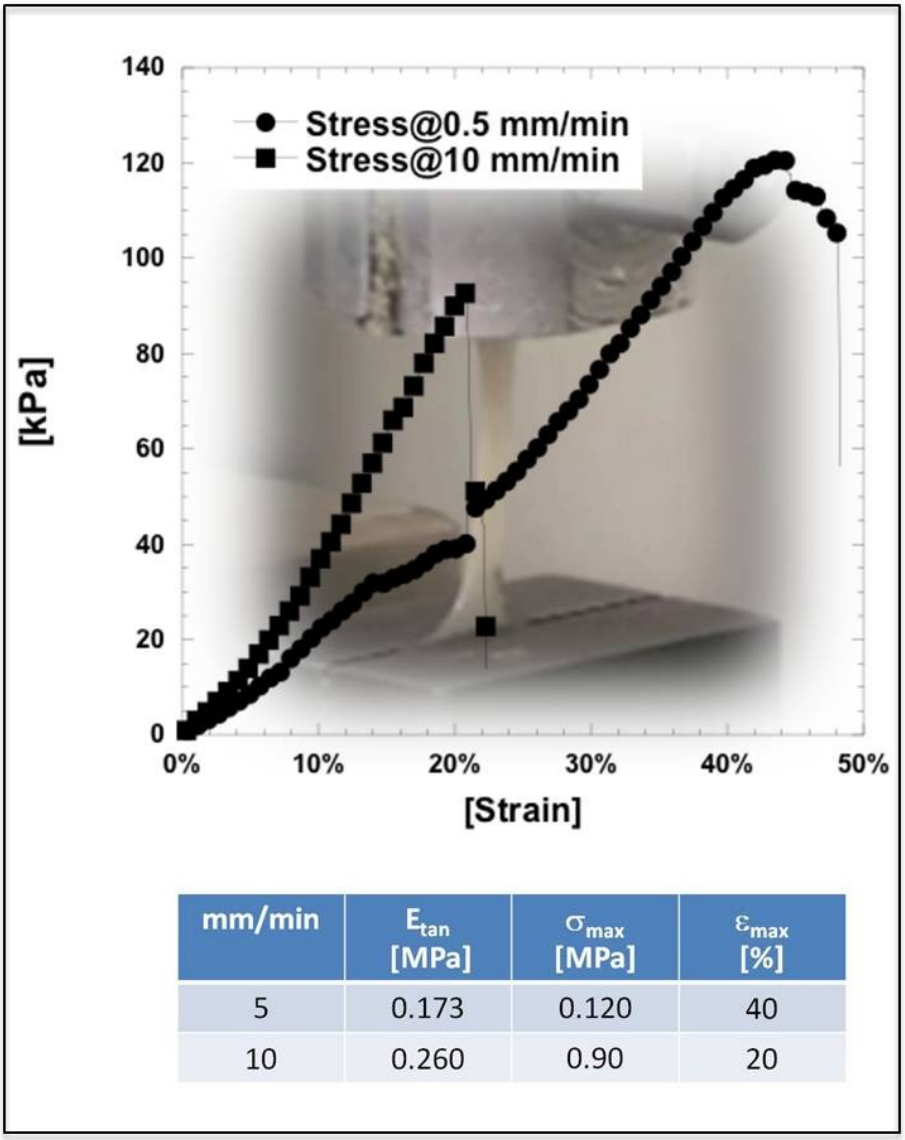

mm/min	E_{tan} [MPa]	σ_{max} [MPa]	ε_{max} [%]
5	0.173	0.120	40
10	0.260	0.90	20

Graph 1.: mechanical properties of human dermis equivalent. Graph show the strain *vs* stress at two deformation rate (0,5 mm/min at 10mm/min) and the table under shoe the parameters of Young module (E_{tan}), stress max(σ_{max}) and strain max (ε_{max}) in percentage and normalized to initial length.

By increasing the deformation rate the maximum stress that the sample can sustain increase too arriving at 200 g/cm^2

Morphological analysis of ECM

In the panel reported in figure 5, histological images of Hematoxylin-Eosin (fig 5A, B, C) and Masson Trichrome (fig 5C, D, F) concerning human dermis equivalent at 6 weeks of maturation have been shown.

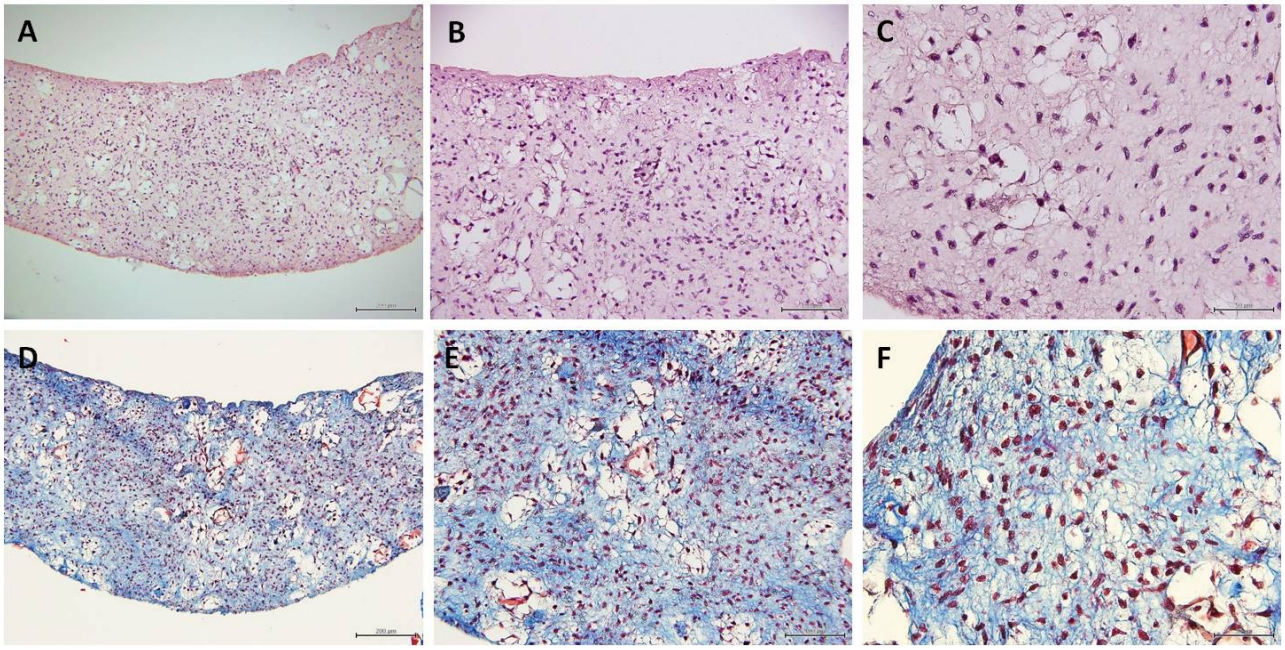

Figure 5.: histological analysis of human dermis equivalent (A, B, C) hematoxylin and eosin staining of transverse section thick 5µm and scale bars are indicated in the images. (D, E, F) Masson Trichrome staining of transverse section thick 5µm and the scale bars are indicated in the images.

In the figure 3D it is possible to observe that collagen (in blue) is present along the whole thickness of the sample (1mm), any necrotic region is present and microbeads are not present anymore at the end of culture time. In figure 5A and 5D any significant change in thickness has been observed compared to thickness of the chamber maturation. As shown in figure 5 B, it is possible to note that the fibroblasts are completely immerse in collagen matrix and the elongated nuclear morphology underlines the good condition of the cells in their own extracellular matrix. It is interesting to highlight that after 6 weeks of culture the tissue is completely made-up of endogenous ECM, and the contraction of thickness is not significant. As described

in previously chapter the collagen assembly kinetic in the 3D biohybrid suggested that the microscaffold play a fundamental role in the collagen maturation and indirectly in the 3D tissue shape retention. Moreover the close interdependence of matrix remodeling, mechanical properties and shape retention is fundamental to preserve the integrity in soft tissue [24-26].

In the figure 6 representative images of ECM markers of human dermis equivalent as well as native human dermis are shown. All immunofluorescence analysis are performed on transverse section 7μm thick and it has been matched with nuclear staining such as DAPI (fig 6 A, B, E, F) or SytoxGreen (fig 6 C, D). In particular in the image A and B is shown the laminin marker in red, so in the images C,D is shown the signal of the Second Harmonic Generation (SHG) of collagen network by exploiting multiphoton microscopy. Moreover in images E, F is shown the match of elastin (green) and fibronectin (red) signals. Immunofluorescence staining (fig 6A) demonstrated the presence of human laminin around cells in the ECM. Laminin presence on the edge of tissue show a signal intensity similar to that one found in the native tissue, suggesting that laminin accumulation is more strong on the endge of the sample assuming a morphology similar to the dermis-epidermal junction in native tissue. Obviously in native tissue laminin is also present in blood vessels [29], since our model is avascular we found laminin signal only on the edge of the sample and as spots within the ECM. Moreover in figure 6 C, D is demonstrated the presence of human collagen in the ECM and in particular around cells. The presence of human collagen secreted from human fibroblasts suggested that the cells not only proliferated but also works correctly like natural dermal fibroblasts by secreting and remodeling collagen [26]. The intensity of signal of collagen in human dermis equivalent and in native dermis is similar but the morphology of signals is different, indeed in the native dermis is possible to distinguish clearly the bundle of mature

collagen while in the tissue equivalent it is possible to distinguish the fibrills of the collagen but they are not still completely organizes.

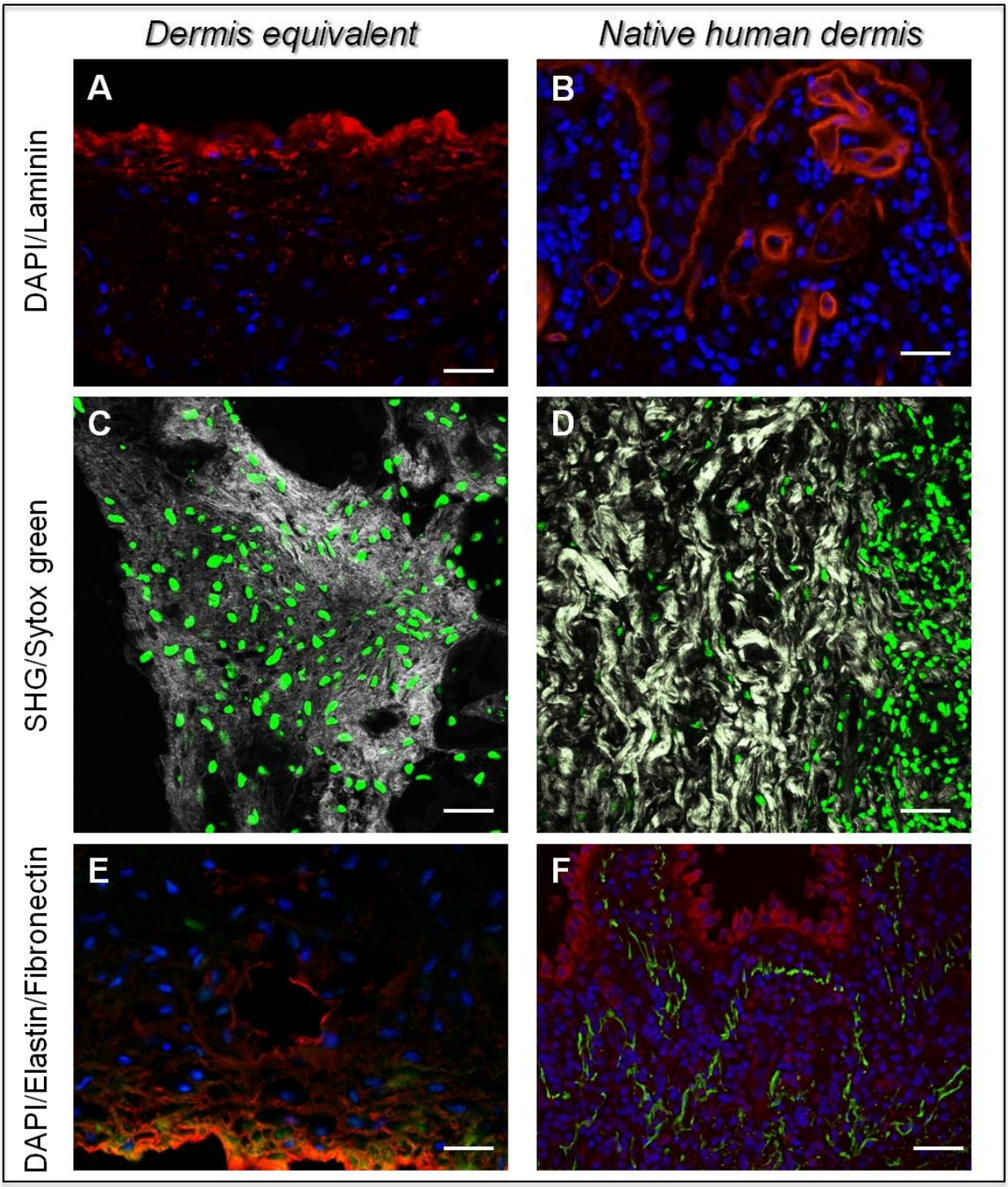

Figure 6.: immunofluorescence analysis of human dermis equivalente and native skin tissue. Frozen sections were immunostained for laminin (A, B)and DAPI as nuclear stain, collagen by SHG analisys (C, D) and Sytox green as nuclear stain, elastin in green and fibronectin in red (E, F) and DAPI as nuclear stain. (A-E) scale bare are 50µm,while in (F) scale bar is 100µm

Elastin and fibronectin constitute the two major components of the elastic tissue in normal human skin; so in tissue equivalents fibronectin is detected as shown in figure 6E and also the morphology of signal is similar to native tissue in fig. 6F. In the center of construct the intensity of fibronectin signal is low, but it is strong on the edge, this suggests that where the dermis is anchored on the grid the cells are able to produce more fibronectin and also the network of this proteins is more similar to native dermis. The signal of elastin is not very strong and it is relevant only on the edge of tissue equivalent where the elastin is deposited onto this microfibrillar network.

Healthy *vs* diseased model: *In vitro* platform for understanding collagen evolution

To test the hypothesis that 3D-HDE can be used as model to study the collagen remodeling occurring *in vivo* after solar exposure, UVA irradiation was delivered to 3D-HDE in order to mimic a daily UVA dose. The experiment was performed on tissue equivalent with disc shape by using µ-TPs of 5% GAL.

Cell apoptosis and dermal matrix alterations such as decreased synthesis and accelerated degradation of dermal matrix components, especially collagen fibers, are two important and well-known effects of photoaging. As shown in the figure 7C, D by the images of Sytox green stained sample, 3D-HDE UVA- reports a strong disappearance of fibroblasts and the presence of nuclei with irregular morphology indicating cells undergoing necrosis or apoptosis. According to this result H/E images of 3D-HDE UVA- and 3D-HDE UVA+ (fig.7A, B) show that the morphology of the ECM presents among the microbeads in the two samples are very different. In the 3D-HDE UVA+ typical bi-polarized fibroblast morphology is evident and eosin staining of ECM appears homogenous, differently 3D-HDE UVA- sample shows

piknotic cells and fragmented staining of ECM indicating that degeneration of collagen occurring.

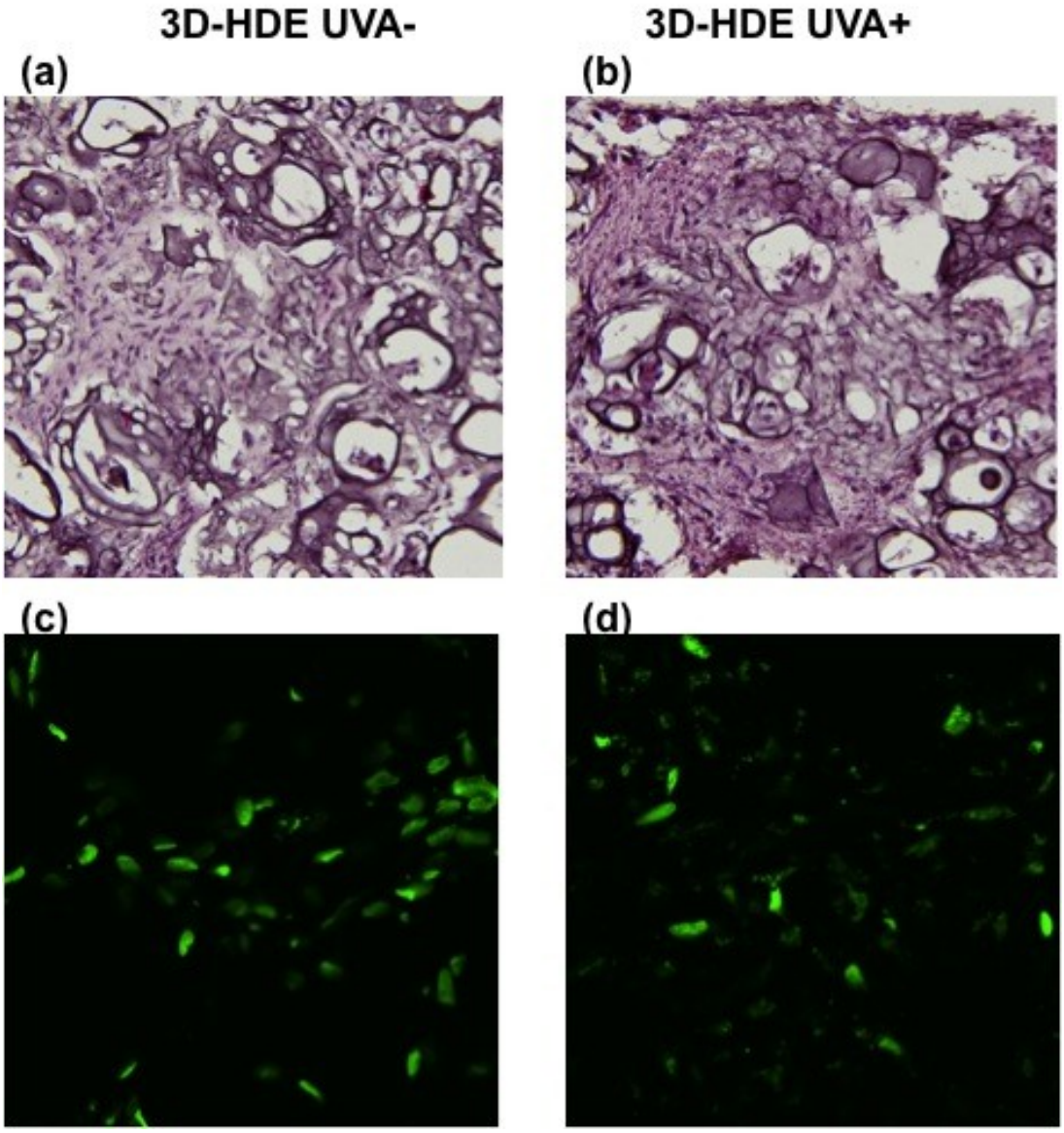

Figure 7.:histological analysis and nuclear staining on HDE UVA- and HDE UVA+. (a) hematoxilin and eosin on HDE UVA+, (b) hematoxilin and eosin on HDE UVA-.(c) Sytox green on UVA- and (d) Sytox green on HDE UVA+.

To better investigate the collagen suffering status after UVA irradiation MPM have been used to obtain useful parameter assessing the structural and compositional modification observed in the 3D-HDE UVA- and 3D-HDE UVA+. More specifically SAAID [18] index and correlation length are currently used as clinical indicator to detect ECM degeneration in damaged connective tissues [19, 20]. SAAID index

indicates the relative change in the collagen and elastin content after photo-damage and the decrease of SAAID index is observed in photo-aged dermis. Figure 8 reports the ratio of the SAAID index (S) as defined in the equation 2. In our 3D-HDE it was found that S is minor than unity indicating a re-distribution of ECM components as in the case of photo aged native dermis. The values are statistically different with a $p<0.05$ by performing a t-test.

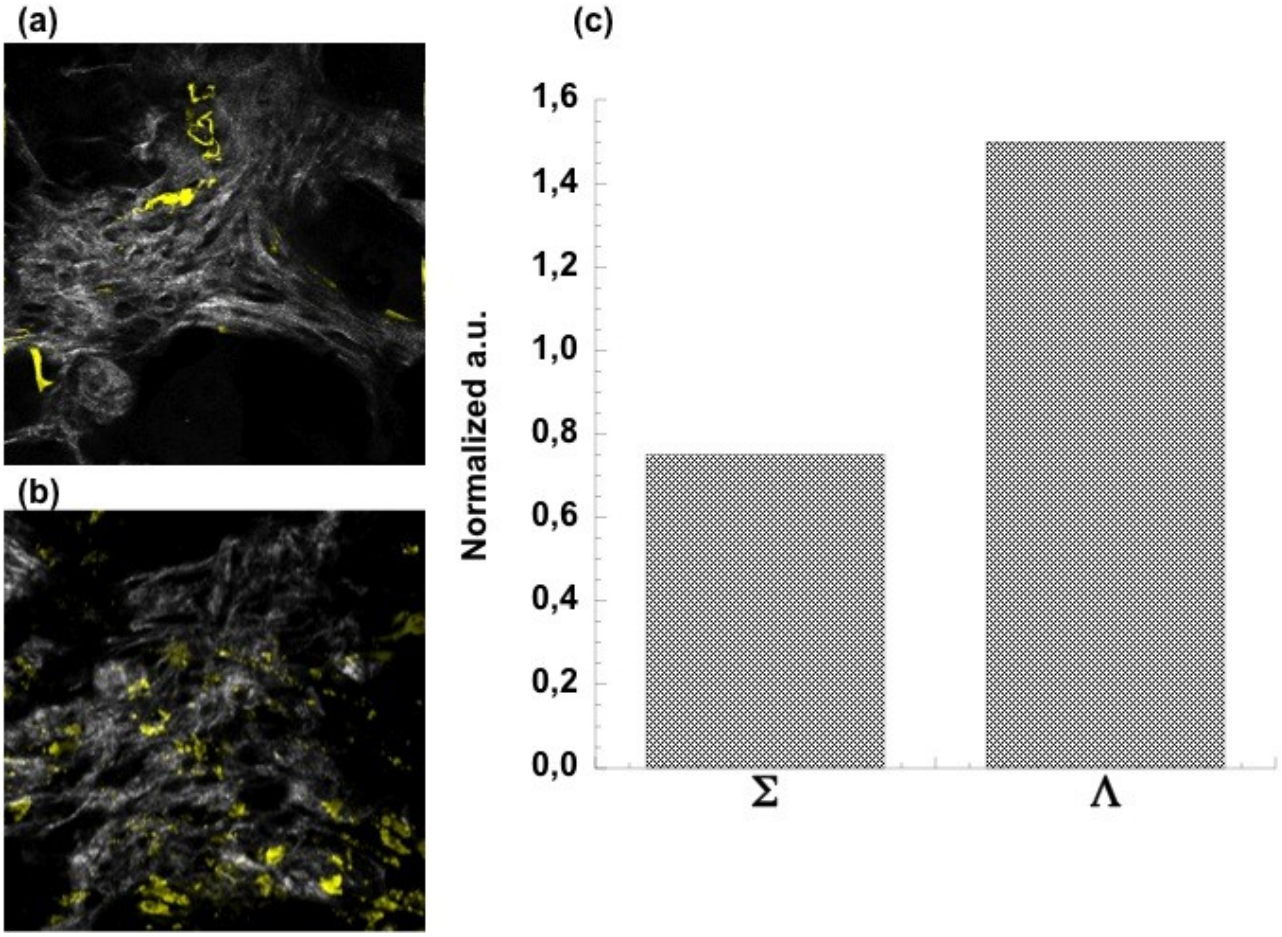

Figure 8.: analysis of SAAID index on human dermis equivalent UVA+ and UVA-(a) SHG of collagen in grey and elastin in yellow on HDE- by multiphoton microscopy analysis, (b) SHG of collagen in grey and elastin in yellow on HDE- by multiphoton microscopy analysis; in graph to the right is shown the value of SAAID index for Σ is described the HDE- and for Λ is indicated the HDE +

Correlation length is textural parameters indicating the roughness of the collagen matrix. Textural parameters of collagen network (correlation, entropy and contrast)

obtained from SHG images can be related with chrono-aging and photo-aging [20], development of arteriosclerotic plaques [21] and stroma modification due to tumor invasion and growth [22, 23]. Since a strictly correlation exists among mechanical/transport parameters of collagen network, its 3D architecture and its evolution in a pathologic status, several efforts have been carried out to relate collagen textural parameters to its elastic modulus [27] and bioactive agent diffusion [28]. By using this technique we investigated the young and healty and 3D-HDE UVA- and 3D-HDE UVA+ in order to assess if a irradiation with UVA have responsibility in terms of collagen architecture modification. Rough texture, or low correlation length is synonymous of fine structure with well defined collagen bundle and narrow distribution of bundle diameter. This is the condition of young and healthy dermis. Aging and in particular photo-aging, induces collagen degeneration causing change in textural features of collagen matrix. As a consequence, correlation length tends to increase because of collagen matrix coarsening. A way to measure the correlation length is to perform GLCM analysis and evaluate the Correlation over a length of interest that in our case it has been set to 42mm. In such spatial windows the distance at which the correlation function fall off represents the correlation length of the texture. In figure 9 is reported the ratio of the correlation length as defined in the equation 3. The value L is grater than unity indicating an increase in the correlation length after UVA exposure. The correlation length data of 3D-HDE UVA+ sample are statistically different from 3D-HDE UVA-, as confirmed by $p<0.05$ after t-test. Taken together these results indicated that our HDE are able to recapitulate *in vitro* relevant phenomena occurring in the human dermis during human daily life. The tissue realized resembles most of the native human dermis features in terms of composition, ultra structure, collagen network organization and mechanical

properties. The HDE can be imaged by means of non-linear optic techniques and it responds to external stimuli in a similar fashion as the native dermis.

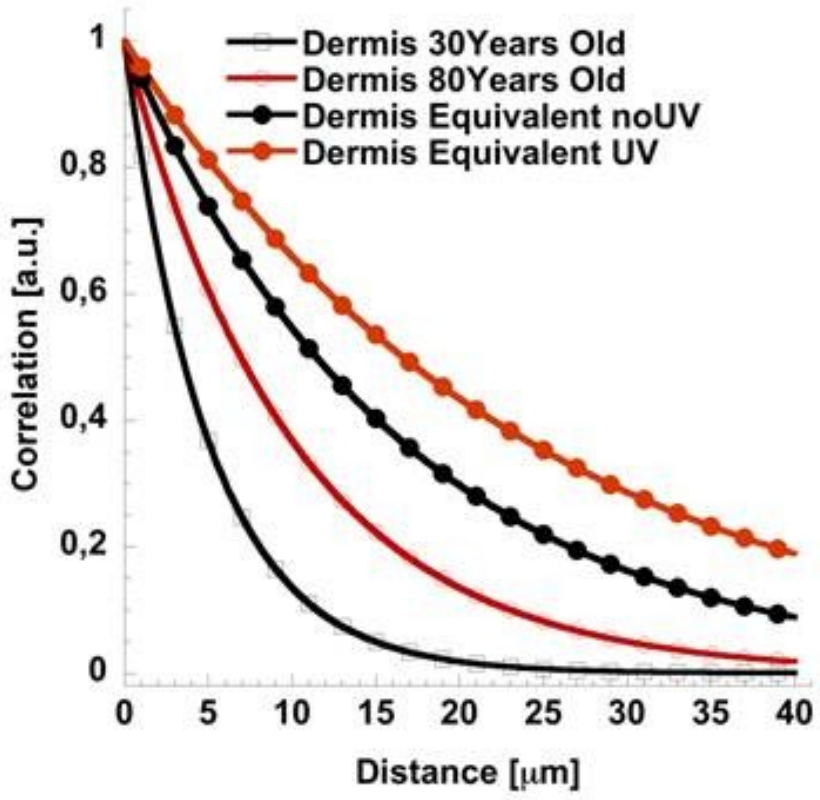

Figure 9.:Correlation distance in human dermis and in the HDE UVA+ and UVA- irradiation

By coupling the living nature of the HDE and non linear, non invasive a stain-free optical techniques such as SHG imaging, it will be possible to realize biological platform *in vitro*. In this work we have carried out studies on photoaging but the concept can be applied to a board range of cases: *in vitro* tumor model by realizing pathologic tissue, collagen re-organization after injury, to test the efficacy of therapeutics agents, to screen drugs to represent various disease states in a controlled environment and to evaluate new therapies targeted for a specific disease

CONCLUSION

We realized a 3D human dermis equivalent model *in vitro* having a surface of 25cm^2 and a thickness of 1mm, completely made up of endogenous extracellular matrix. This model represents a real innovation in tissue engineering and we have demonstrated that morphological, biochemical, and mechanical characteristics are very similar to native tissue. This new material could have applications in the medical field and our results about photoaging demonstrate that it can be used to study the biological mechanisms involved in diseases of the dermis. Complex mechanisms such as the response to UVA can be studied in *in vitro* models only if the biological living platform is made of structural proteins that form the native tissue, and our results that the model realized respond to this need.

REFERENCES

1. Freed, L.E., and Guilak, F. Engineering functional tissues. In: Lanza, R.P., Langer, R., and Vacanti, J., eds. Principles of Tissue Engineering.NewYork,NY: Academic Press, 2007, pp. 137–153.

2. Martin, I., Wendt, D., and Heberer, M. The role of bioreactor in tissue engineering. Trends Biotechnol 22, 80, 2004.

3. Yang, J., Yamato, M., Kohno, C., Nishimoto, A., Sekine, H., Fukai, F., and Okano, T. Cell sheet engineering: recreating tissues without biodegradable scaffolds. Biomaterials 26, 6415, 2005

4. A. Khademhosseini, R. Langer, J. Borenstein, J. P. Vacanti, Proc. Natl Microscale technologies for tissue engineering and biology. 2006, 103, 2480–2487.

5. Maruguchi T, Maruguchi Y, Suzuki S, Matsuda K, Toda KI, Isshiki N. A new skin equivalent: keratinocytes proliferated and differentiated on collagen sponge containing fibroblasts. Plast Reconstr Surg 1994; 93: 537–44.

6. Boyce ST, Michel S, Reichert U, Schroot B, Schmidt R. Reconstructed skin from cultured human keratinocytes and fibroblasts on a collagen-glycosaminoglycan biopolymer substrate. Skin Pharmacol 1990; 2: 136–43.

7. Lee DY, Cho KH. The effects of epidermal keratinocytes and dermal fibroblasts on the formation of cutaneous basement membrane in three-dimensional culture systems. Arch Dermatol Res 2005; 296: 296–302.

8. Lee DY, Ahn HT, Cho KH. A new skin equivalent model: use of a dermal substrate which combines de-epidermized dermis with fibroblast-populated collagen matrix. J Dermatol Sci 2000; 23: 132–7.

9. Bunsho Kao, M.D., Ph.D., Koichi Kadomatsu, M.D., Ph.D., and Yoshiaki Hosaka Construction of Synthetic Dermis and Skin Based on a Self-Assembled Peptide Hydrogel Scaffold. Tissue engineering: Part A Volume 15, Number 9, 2009

10. Yang J, Yamato M, Kohno C, Nishimoto A, Sekine H, Fukai F, Okano T. Cell sheet engineering: recreating tissues without biodegradable scaffolds. 2005 Nov;26(33):6415-22.

11. Smith JG, Davidson EA, Sams WM, Clark RD (1962) Alteration in human dermal connective tissue with age and chronic sun damage, J Invest Dermatol 39: 347-350

12. Braverman IM, Fonferko E (1882) Studies in cutaneous aging: I.the elastic fibre network. JInvest dermatol 78:434-443

13.Fisher GJ, Talware HS, Lin J et al (1998) retinoic acid inhibits induction of c-jun protein by ultraviolet radiation that occurs subsequent to activation of mitogen-activated protein kinase pathway in humanskin in vio. JClin Invest 101:1432-1440

14. Stewart SA, Ben-Porath I, Carey VJ, O'Connor BF, Hahn WC, Weinberg RA (2003) Erosion of the telomeric single-strand overhang at replicative senescence. Nat Genet 33:492-6

15. Konig K. Clinical multiphoton tomography. J. Biophoton. 2008;1:13-23

16. ShulianWu, Hui Li, Xiaoman Zhang, Zhifang Li, and Shufei Xu. Using multiphoton microscopi to analyze aging skin Spie News room 10.1117/2.1201012.003318

17. Sugata K, Osanai O, Sano T, Takema Y. Evaluation of photoaging in facial skin by multiphoton laser scanning microscopy Skin Res Technol. 2011 Feb;17(1):1-3.

18. Cicchi R, Kapsokalyvas D, De Giorgi V, Maio V, Van Wiechen A, Massi D, Lotti T, Pavone FS. Scoring of collagen organization in healthy and diseased human dermis by multiphoton microscopy. J Biophotonics. 2010 Jan;3(1-2):34-43

19. Zheng W, Li D, Li S, Zeng Y, Yang Y, Qu JY. Diagnostic value of nonlinear optical signals from collagen matrix in the detection of epithelial precancer. Opt Lett. 2011 Sep 15;36(18)

20. Koehler MJ, Preller A, Kindler N, Elsner P, König K, Bückle R, Kaatz MIntrinsic, solar and sunbed-induced skin aging measured *in vivo* by multiphoton laser tomography and biophysical methods. Skin Res Technol. 2009 Aug;15(3):357-63

21. Mostaço-Guidolin LB, Ko AC, Popescu DP, Smith MS, Kohlenberg EK, Shiomi M, Major A, Sowa MG. Evaluation of texture parameters for the quantitative description of multimodal nonlinear optical images from atherosclerotic rabbit arteries. Phys Med Biol. 2011 Aug 21;56(16):5319-34

22. Zhuo, Shuangmu Quantitatively linking collagen alteration and epithelial tumor progression by second harmonic generation microscopy, Applied Physics Letters

23. Lin SJ, Jee SH, Kuo CJ, Wu RJ, Lin WC, Chen JS, Liao YH, Hsu CJ, Tsai TF, Chen YF, Dong CY.Discrimination of basal cell carcinoma from normal dermal stroma by quantitative multiphoton imaging. Opt Lett. 2006 Sep 15;31(18):2756-8.

24.Brown, R. A. in *Future Strategies for Tissue and Orga Replacement* (eds Polak, J. M., Hench, L. L. & Kemp, P.) 51–78 (World Scientific Publishing, Singapore, 2002).

25. Brown, R. A., Prajapati, R., McGrouther, D. A., Yannas, I. V. & Eastwood, M. Tensional homeostasis in dermal fibroblasts: mechanical responses to mechanical loading in three-dimensional substrates. *J. Cell Physiol*. 175, 323–332 (1998)

26.*James J.Tomasek*,Giulio Gabbiani ‡,Boris Hinz‡,Christine Chaponnier‡ and Robert A.Brown§* Nature Myofibroblasts And Mechanoregulation Of Connective Tissue Remodelling Reviews | Molecular Cell Biology Volume 3 | May 2002 | 363

27. Raub CB, Mahon S, Narula N, Tromberg BJ, Brenner M, George SC.Linking optics and mechanic in an *in vivo* model of airway fibrosis and epithelial injury. J Biomed Opt. 2010 Jan-Feb;15(1):015004

28. Brown E, McKee T, diTomaso E, Pluen A, Seed B, Boucher Y, Jain RK.Dynamic imaging of collagen and its modulation in tumor *in vivo* by using second harmonic generation. Nat Med. 2003 Jun;9(6):796-800.

29. David J. Geer, B.S., Daniel D. Swartz, Ph.D., And Stelios T. Andreadis, Ph.D. *In Vivo* Model Of Wound Healing Based On Transplanted Tissue-Engineered Skin Tissue Engineering Volume 10, Number 7/8, 2004

Chapter 4

3D HUMAN SKIN EQUIVALENT

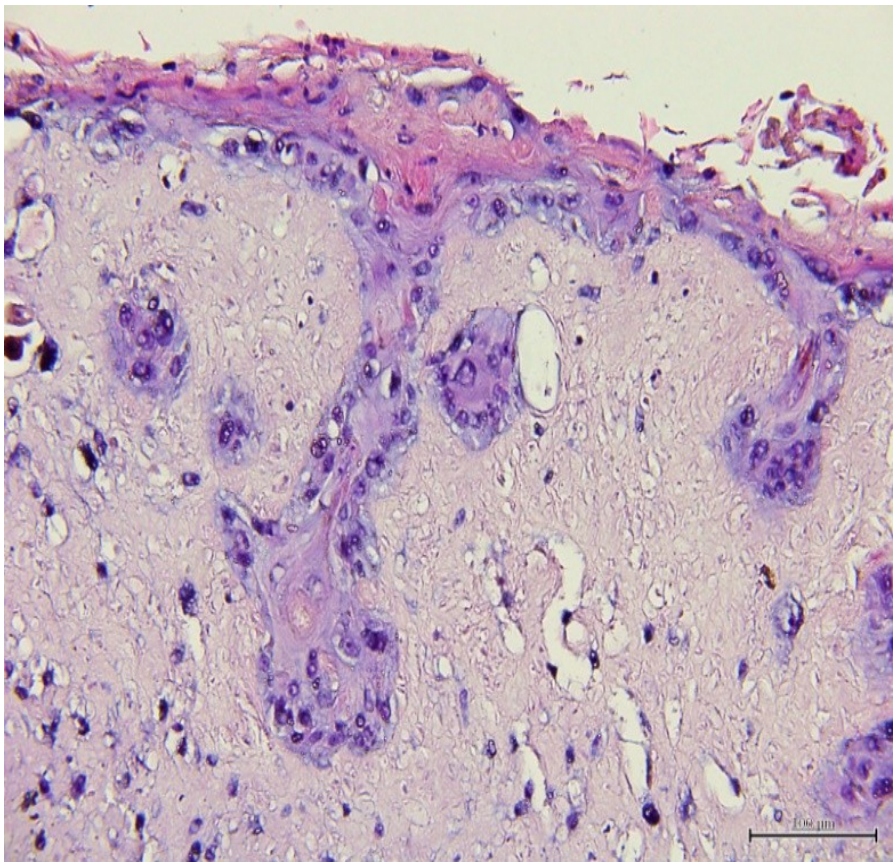

INTRODUCTION

Patients with 50 per cent total body surface area full-thickness wounds have only 50 per cent of undamaged skin left which could be used for split-thickness skin harvesting [1]. Donor sites would add to the total wound size resulting in a wound area covering 100 per cent of the body. An impaired epidermal barrier combined with reduced immunity of heavily burned patients can result in bacterial sepsis which is the main complication in deep extensive burns. In the case of a more extensive injury, donor sites are extremely limited and in such cases, meshing techniques can be used where grafted skin is uniformly perforated and stretched to cover greater areas of the wound. In such cases wounds are covered with temporary dressings or cadaver skin to form a mechanical barrier in order to prevent fluid loss and microbial contamination [1]. Alternative life-saving approaches in the treatment of extensive full-thickness wounds, include the use of cultured autologous keratinocytes and/or bioengineered skin substitutes. However, currently, there is a growing interest in skin equivalent production not only for surgery applications but also as alternative to animal testing. The scientific community argue animals are subjected to considerable pain and distress during toxicity testing with the final results scientifically unreliable because humans and animals can experience differing reactions to the same chemical. For this reason, animal testing for cosmetics has been banned within the European Union and a new legislation enforces also a sales ban on products from outside the EU tested on animals from March 2013 [2]. To meet these needs, significant progresses have been recently made in the development of 3D human skin model *in vitro*. One of the first model of skin equivalent *in vitro* related to the epidermal equivalent alone [3]. However, this model presented some limitations because of the lack of the dermal component. Thereafter, skin equivalents that were composed of both epidermis and dermis elements have been developed on the basis of a three-dimensional scaffold. As a substitute for normal skin *in vivo*, these models have been used in various fields of skin biology, pharmacotoxicology and also as a replacement for human skin in clinical applications[4-7]. Several biomaterial scaffolds have been applied as a dermal equivalent to develop more efficient skin equivalents. These biomaterials should be biodegradable, repairable and able to support the reconstruction of normal tissue, with similar physical and mechanical properties to the skin it replaces. It should provide pain relief, prevent fluid and heat loss from the wound surface and protect the wound from infection. It is also of great advantage if the skin substitute bio-construct is cost-effective, readily available, user-friendly and possesses a long shelf life. However, most of the skin equivalents realized contained exogenous materials in the dermal equivalents, such as bovine

collagen [8, 9], human allogenic dead dermis [10], synthetic polymers [11], these substances are expensive, difficult to obtain and are a source of infections, and not mimic the real structure of dermal tissue. So in the gold standard skin *in vitro*, the ultimate goal is the development of the skin *in vitro*, while preserving all its constituents' spatial and functional three-dimensional relations as well as cosmetic properties [12]. To satisfy this targets we developed a 3D human skin equivalent completely made of endogenous ECM in dermal and epidermal part. Moreover it presents a thickness close to that one of native dermis and it does not undergo significative shrinkage during culture time. Interestingly the model proposed can be built by using both fibroblasts and keratinocytes from the same patient

MATERIALS AND METHODS

Fabrication of 3D Human dermis equivalent

Exogenous collagen model (3D DEn)

Seed 1×10^6 human dermal fibroblast (HDF) in 10 ml fibroblast culture medium to a standard 10 cm2 cell culture dish so that they are almost confluent 1 day before incorporation into the collagen type I from bovine skin (Sigma Aldrich), and change the medium every 2 days.

After the fibroblasts have been passaged once from the frozen state, they will reach confluence in 3 days. The day of incorporation, prepare the acellular collagen mixture on ice, mixing 8 parts of chilled collagen solution with 1 part of $PBS10_X$. Use chilled pipets to prevent warming of collagen when it is mixed and avoid creating air bubbles when mixing. Collagen should be a transparent to matt color to ensure optimal gelation. If the color is not this , add a single drop of sodium hydroxide and check the pH is about 7,2-7,6. At this point add 300 µl acellular collagen matrix to each 6-well tissue culture plate insert. Ensure that the gel coats the entire bottom surface of the insert and allow it to gel 50 min in incubator. In the waiting time you can trypsinize the fibroblasts with trypsin/EDTA, count viable cells in an aliquot and resuspend the

fibroblasts to a final concentration of 1,2 × 105 cells/ml. then a total of 9,6 × 105 fibroblasts will be used per 8-well plate. Prepare the cellular collagen mixture on ice, adding the reagents in the order that show above and mix with cells , so that the cells will not be damaged by the acidic pH of the un-neutralized collagen. It is important to neutralize the collagen so that the cells will not be damaged by the acid pH that exists before neutralization.

Endogenous Biohybrid (3D DEn)

Spinner cell culture: macroporous gelatin microbeads were obtained by using a double emulsion technique. Glyceraldehydes has been used as gelatin crosslinker at 4% and 5% w/w of the microbeads, different percentage has been used in order to modulate microbeads degradation. The microbeads/fibroblasts cultures were propagated in spinner flasks (100ml, Bellco) for 96 hours, the stirring mode was set at 30rpm, 30 minutes pause and 5 minutes running, for the first 6 hours of seeding; continuous stirring for the following hours of culture. The spinner cultures were incubated at 37°C in 5% CO2.

Tissue equivalent assembly: tissue precursors obtained by previous step have been injected in maturation chamber to allow their molding in disc-shaped construct (1 mm in thickness, 11 mm in diameter) . After 4 weeks of culture, under dynamic conditions, the bio-hybrid obtained has been removed from the maturation chamber and seeded with keratinocytes in order to obtain the epithelial layer.

Keratinocyte and fibroblast extraction from foreskin

Day 1: separation of dermis from epidermis

Skin sample derived from reduction surgery with the informed consent of the patient. Take some ml of the transport solution as sterility control and incubate it in a culture flask over night at 37°C. Rinse the biopsy 3 times with PBS, remove the PBS but leave a little bit to avoid the biopsy to run dry. Remove hairs from the top and all fat and tissue remnants from the bottom side (the better you remove the fat/tissue remnants from the bottom side the easier the separation of dermis from epidermis will be the next day).Rinse with PBS again, till the PBS stays clear (about 3 times). Determine the size of the "purified" skin (important for the amount of enzymes dispase needed; do not determine the size before having removed all the fat because the skin will enlarge after the tissue remnants are removed). Cut skin into strips of about 3mm width. Transfer strips into new small petri dish, wash with PBS (important: do not use PBS with calcium and magnesium at this step). Incubate skin strips with Dispase solution (2U/mL; about 5-10 ml for 6cm² of skin) that all strips are covered with it; incubate over night for 16h to 18h

Day 2: fibroblast, endothelial and keratinocyte extraction

Check sterility control for contaminations; prepare 2 petri dishes with PBS (one for dermis, one for epidermis) Check after 16h if epidermis has removed from dermis (You can see this at the edge where epidermis is partly detached from dermis. If so: stop digestion by transferring skin strips to PBS; if not: incubate for 2 more hours; do not incubate the skin strips for more than 20h in Dispase as this will strongly harm your cells). After transferring the skin strips to PBS, wash them once to stop the Dispase reaction. Separate epidermis from dermis with tweezers, store both parts separately in the prepared petri dishes.

If needed: dermis can be used for extraction of microvascular endothelial cells and fibroblasts. Indeed you can scrape eight times on the both surfaces of dermal piece in PBS solution of and in this way you obtained the endotelial cells. Centrifuge 5 min 1200 rpm and resuspend the cell in Vasculife + Pen/Strep solution and count cells. Seed cells into flasks: $8*10^3$ cells per $cm^2$and change the media after 2 day. Vasculife® Basal Medium +10%FBS. Cells were maintained at 37°C in humidified atmosphere containing 5% CO2. Moreover you can take the dermal pieces remain and cut in small pieces and put in 30ml collagenase A solution (ROCHE) at concentration of 2mg/ml for 40 minutes at 37°C. After stop the collagenase solution with FBS and centrifuge 5 min 1200 rpm and resuspend the piece in a little volume of EMEM. Eagle's BSS Minimum Essential Medium containing 20% fetal bovine serum, 100 mg/mL L-glutamine,100 U/mL penicillin/streptomycin, and 0,1 mM Non Essential Amino Acids). In this in this way occurs the migration of fibroblasts on the surface of the petri .

Wash epidermal parts with PBS. Cut epidermis into small pieces, they should be about 4mm). Transfer pieces into preheated in 5mL 0,05% Trypsin/EDTA, wash petri dish with another 5 mL Trypsin/EDTA and transfer it to the tube- Incubate Trypsin/EDTA (with cutted epidermal pieces) for 5 min at 37°C water bath, vortex shortly every 1-2 min (important: the water bath temperature has to be 37°C, therefore do not place large cold flasks into it as this would reduce the temperature). Stop enzyme reaction by adding 1 mL FBS. Resuspend solution for 5 min (plastic single-use pipette) to separate cell clumps Strain solution by transferring it to new tube through cell strainer. Use the same pipette with prepared 10 mL PBS solution to wash the tube, the single-use pipette and finally transfer solution through cell strainer, too. Centrifuge: 5 min 1200 rpm. Resuspend cells in colture media and count cells. Seed cells into flasks: $8*10^3$ cells per cm^2.Important: full medium change after 4 h

(prepuce) or 24 h (adult skin); after 3 days 2nd medium change (cells should feature characteristic morphology now). Let cells culture up to 80% confluency before freezing (not more as keratinocytes will start to differentiate). Usefull notes to take during cell extraction: age of donor, gender, amount of cells extracted. Freezing of keratinocytes: colture media+ 20% FBS + 5% DMSO

Procedure 1: feeder layer tissue colture

1 week before the keratinocytes extraction is necessary to cultivate NIH 3T3 in DMEM low glucose plus or 10% fetal bovine serum. BD™ Collagen I, rat tail, may be gelled onto coverslips or tissue culture dishes, or used as a thin coating for cell attachment, and NIH 3T3 may be cultured on top of the gel that is prepared in this manner:

- the final volume of BD Collagen I rat tail solution may be used for one plate is 8 ml , and the final collagen concentration is 5 µg/ml. Place on ice a sterile tube of sufficient capacity to contain the final volume of BD Collagen I rat tail .add to the tube the following volume of 10X PBS:
- Final Volume /10 = mL 10X PBS

Calculate the volume of BD Collagen I, rat tail, to be used (do not add to the tube until step)

Final volume x Final collagen concentration in mg/mL / Concentration in bottle (see lot specific spec. sheet) = volume collagen to be added

Add to the 10X PBS the following volume of sterile ice cold 1 N NaOH (volume collagen to be added) x 0.023 mL = volume 1 N NaOH

Add to the 10X PBS/1 N NaOH the following volume of sterile ice-cold dH2O: (Final volume) - (Volume collagen) – (Volume 10X PBS) - (Volume 1 N NaOH) = Volume dH2O to add Mix the contents of tube and hold in ice.

- Add the calculated volume of BD Collagen I, rat tail, and mix. Leave on ice until ready for use. The BD Collagen I, rat tail, solution can be used immediately or held on ice for 2-3 hours.
- When ready to use, aseptically deliver the solution into the cell culture device and allow to gel at 37°C for 30 minutes.

Preparing the NIH 3T3 cells for use as a feeder layer

Once plate is confluent, treat with 10 µg/mL mitomycin C in complete medium for 2 hrs at 37oC.After treatment, wash plate with medium without serum at least 3 times, aspirating after each wash. Split the 3T3 cells by adding trypsin/EDTA; aspirate after 30-40 sec, incubate another 30 sec at RT, tap the plate to dislodge the cells, and resuspend them in complete medium. Spin the cell suspension down to obtain a cell pellet. Pellets can be used as feeder layers immediately, or The 3T3 cells must be used as feeder layers or frozen down within 2 days of being treated with mitomycin C

Splitting the feeder layer/epithelial plate:

Once the epithelial cells on the plate are 70-75% confluent, aspirate off medium and wash with pre-warmed 0.02% EDTA (0.68mM) in 1x PBS. This wash should be performed fairly rapidly and is done to remove the NIH 3T3 cells, but leave behind the epithelial cells. The EDTA wash is done ten times by pipetting 10-12mLs directly onto the cells on the outer perimeter of the plate, while rotating the plate. Then using this same EDTA again, do the same for the inner half of the plate cells. Aspirate off the EDTA from the previous washes, and repeat the 0.02% EDTA washes for the inner and outer halves of the plate. This makes a total of 40 washes. This EDTA wash protocol is for human keratinocytes, other cells may be less strongly adherent and the number of washes may have to be modified. Aspirate off the EDTA and look at the cells under the microscope and verify that all of the NIH 3T3 are washed away, if they are not then more EDTA washes should be performed. Trypsinize the

epithelial cells using their normal protocol (for keratinocytes trypsin 2 minutes RT, aspirate off the trypsin and then incubate for 5 min at 37oC, tap plate, resuspend in DMEM/F12). Epithelial cells should be plated back onto mitomycin C treated feeder layers in low density (250000 cell for a 100mm plate).

In this same way you can detach the epithelial cells and add it on the 3D organotypic colture with collagen matrix or on the our dermis equivalent sample. Moreover, the technique named “feeder layer/epithelial plate” is more used when the extraction of keratinocytes is done in the medium F12/DMEM that contain grow factor that sustain the grown of epithelial cell only on the NIH 3T3 feeder layer.

The composition of medium contain:

Ingredient	Stock concentration	Final concentration	Epidermalization I (ml)
DMEM low glucose			363
Ham's F12 supplements			120
L-glutamine	200 mM	4 mM	10
Adenine	18 mM	40 µM	1
Hydrocortisone	500×	1 µM	1
Triiodothyronine (T3)	500×	20 nM	1
Transferrin	5 mg/ml	10 µg/ml	1
Insulin	5 mg/ml	10 µg/ml	1
Progesterone	2 µM	2 nM	0.5
PES	500×	1×	1
Calcium chloride	0.5 M	1.8 mM	0
FBS			0.5

Table 1.: supplements for feeder layer/epithelial plate co-colture media

Procedure 2: keratinocytes monoculture

The choise of colture medium is crucial in order to obtain subculture of undifferentiated keratinocyte. For this reason we used the media KGM™-2,

convenient and easy to use. It is based on an optimised formulation and is serum-free. The growth medium contains the base medium, separate vial of calcium chloride and other supplement mix that are: BPE (bovine pitutary extract), hEGF, insulin (recombinant human), hydrocortisone, GA-1000 (gentamicin, amphotericin-B), epinephrine, transferrin. The formulation is optimised for initial seeding of 5000 cells / cm^2 up to subconfluence. Feeder-layer, extracellular matrix substrates or other substances are not necessary

Fabrication of human skin equivalent

Realization of epidermis layer

Dilute human fibronectin (Sigma Aldrich) in sterile balanced salt solution e concentration of 50 µg/ml than coat the dermis equivalent and cellular collagen matrix surface with a minimal volume(about 50µl for single well). Allow to air dry for at least 45 minutes at room temperature.Wash the keratinocyte 3 or 4 times with PBS/EDTA 0.01M leaving in contact for a few second and after, trypsinize keratinocyte colonies with trypsin/EDTA for 5 min at 37°C to obtain a single cell suspension. Once cells have detached, gently resuspend them in keratinocyte media, count cells and add the appropriate number of cells to a 15-mL tube so that there will be enough cells (400,000 cells/insert) to seed onto the desired number of inserts. Centrifuge at 1200rpm for 5 min and. At this time, the cells can be seeded directly onto the dermis equivalent and contracted collagen gels; resuspend the keratinocytes so that they are in the small volume needed for plating onto the matrix. It is important to resuspend cells in a small volume as 400,000 cells will be seeded onto the small surface area of the connective tissue (1.2 cm diameter). This is

performed by using a sterile, plastic 200-µL pipet to add 50 µL keratinocytes media to the 15-mL tube per 400,000 keratinocytes present. Gently dislodge the cell pellet and transfer it to a 1.5-mL sterile Eppendorf tube with a 1-mL plastic pipet. Gently resuspend the cell pellet in the eppendorf tube with a 200-µL pipetman until it is cloudy and well suspended and transfer 50 µL of the cell suspension to the center of the dermis equivalent and contracted collagen gel. Do not touch for 10 min to allow cells to begin to attach. Incubate at 37°C for 40–80 min without any media to allow the keratinocytes to fully adhere. At this point, in reference to the procedure used, the operator must continue to use the culture media related.

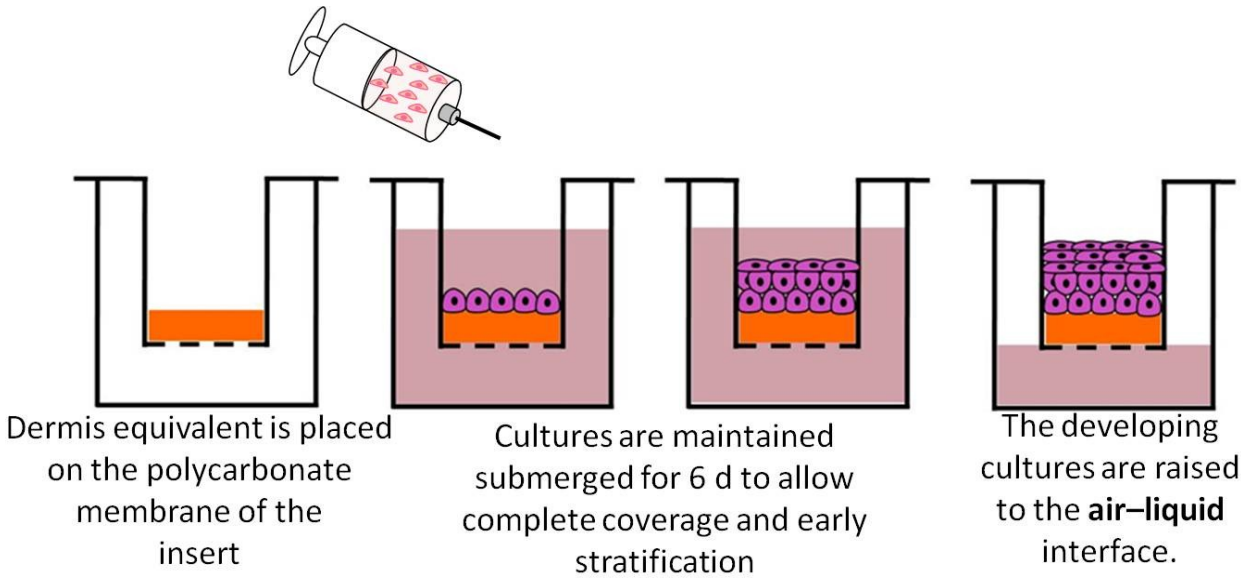

Figure 1.: fabrication of human skin equivalent

Procedure 1

Add Epidermalization I medium to each insert, adding a volume to the bottom of the well and after a volume gently into the insert on top of the keratinocytes. Incubate at 37"C. Feed each culture with medium every 2 days with appropriate HSE culture media as follows:

a. Day 4: Add a volume Epidermalization II medium.

b. Day 6 until termination of the experiment: add a volume Cornification medium to the bottom of the well so that the insert just contacts the medium every two days. Aspirate medium from the inside of the insert so that tissues can be grown at the air-liquid interface.

Ingredient	Stock concentration	Final concentration	Epidermalization I (ml)	Epidermalization II (ml)	Cornification (ml)
DMEM low glucose without calcium			363	363	237
Ham's F12 supplements			120	120	237
L-glutamine	200 mM	4 mM	10	10	10
Adenine	18 mM	40 µM	1	1	1
Hydrocortisone	500×	1 µM	1	1	1
Triiodothyronine (T3)	500×	20 nM	1	1	1
Transferrin	5 mg/ml	10 µg/ml	1	1	1
Insulin	5 mg/ml	10 µg/ml	1	1	1
Progesterone	2 µM	2 nM	0.5	0.5	0
PES	500×	1×	1	1	1
Calcium chloride	0.5 M	1.8 mM	0	1.8	1.8
FBS without calcium			0.5	0.5	10

Table2.: supplements for HSE Organotypic Media

To obtain DMEM low glucose and FBS without Calcium we used Chelex 100 (Sigma Aldrich)

Procedure 2

With this kind of procedure the time colture, modality and media are different to obtain HSE Human Skin Equivalent model, indeed the procedure is: add KGM gold media by adding before a volume to the bottom of the well or maturation chamber in plate and the rest of volume gently into the insert top of the keratinocytes and incubate cultures at 37°C (Fig. 1), Cultures are fed every 2 d in the following manner:

a KGM gold media: 3,5 ml for first 6day and change media every 2 day (submerged condition); b. cultures are raised to the air/liquid interface by adding only 1 ml to the bottom of the well so that the bottom of the insert just contacts the interface with the media. Additional feedings with KGM2 media without EGF and PTB but with CaCl2 concentration of 1.88 mM media are performed for 6 day.

Analyses of ECM: histologies and immufluorescences

Over the entire culture in submerged and air liquid condition, 3 sample were collected at day 6,12 and 18 for understand the morphology of tissue and the morphogenesis of the epidermal differentiation using histological and immunofluorescence technique. Indeed some samples will be included in paraffin and others in Tissue tek Killik (BiO Optical). Gently rinse organotypic collagen matrix cultures and our samples twice in PBS. Using a scalpel, cut away the insert membrane from the plastic insert, while for the our samples, using the thin palette, detach the sample from metallic grid and after were fixed in a solution of 10% neutral buffered formalin for 24h, but only samples that must be embedded in paraffin. The samples that will be included in Tissue Tek are fixed in 4% paraformaldehyde for 30 min at room temperature, wash them in PBS and after can be placed into a sucrose 2M solution that was prepared in water. Tissues should be soaked with sucrose at room temperature not more than 24h; this part of procedure is more important for frozen preservation. Indeed we discarged the sucrose 2M and place the sample in the Tissue Tek Killik in the suitable mold named Peel-A (Ted Pella INC) that we submerge in liquid nitrogen vapors for 1 min and then move and store in -80 °C.

The histologies and immunofluorescences are performed on samples embedded in paraffin e cut in slice (5-7 μm) with microtome (Thermo Scientific HM 355S) while the

samples included in Killiks were cut in slices (5-8 μm) with criomicrotome (Leica CM 1850) and were used for the SHG analysis of the structures such as collagen and elastin. in both procedures the cut of the was oriented so as to view the cross section of the samples. Hematoxsilin and eosin and Masson Trichromic stain were performed after deparaffination and hydratation of the sample, finally the sections were mounted with Histomount Mounting Solution (INVITROGEN) on coverslips and the morphological features of constructs were observed with a light microscope (Olympus, BX53) FIG. Furthermore, Keratin 10, keratin 14, P63, involucrin, loricrin, fillagrin epitheliar markers were performed using respectively: keratin 10 polyclonal antibody (diluition 1:500; Covance), keratin 14 polyclonal antibody (diluition 1:1000; Covance), Anti-p63 monoclonal antibody (diluition 1:50;abcam), involucrin monoclonal antibody (diluition 1:400; Sigma). loricrin polyclonal antibody (diluition 1:1000; Covance),anti-fillagrin polyclonal antibody (diluition 1:200; Sigma). Moreover fibronectin, and laminin dermal markers were performed respectively : fibronectin monoclonal antibody (Sigma) and Anti-laminin polyclonal antibody (Sigma) Every antibody monoclonal were produced in mouse and the polyclonal antibody were produced in rabbit. The secondary antibodies that we used were: Alexa Fluor 546 mouse anti-rabbit IgG (H+L) (diluition 1:500; Life technologies), Alexa Fluor 488 mouse anti-rabbit IgG (H+L) (diluition 1:500; life technologies), Alexa Fluor 488 goat anti-mouse IgG (H+L) (diluition 1:500; life tecnologie), Alexa Fluor 546 goat anti-mouse. IgG (H+L) (diluition 1:500; life technologies) The nuclear stain was 4',6-diamidin-2-fenilindolo (DAPI). Fundamental for the success of the immunostaining protocol is the pretreatment called unmasking with heat that is able to induce epitope retrieval. Indeed, place a 1L glass (Pyrex) beaker containing 500 mL of 0.01 M citrate buffer (Bio Optica) on a hot plate. Heat the buffer solution until it boils. (This step may be prepared before slide deparaffinization, as the buffer may take several minutes to

boil). Put the slides in a slide rack and place in the beaker with boiling buffer. Keep it boiling for 15 minutes. After heating, remove beaker from the hot plate and allow it to cool down for at least 15-20 minutes at room temperature. Rinse slides with PBS and begin the immunostaining protocol. Finally the sections were mounted with fresh buffered glycerol on coverslip and seal with nail polish and the morphological features of constructs were observed with a fluorescence microscope (Olympus, BX53).

RESULTS AND DISCUSSIONS

Morphology of 2D keratinocytes coltures

In this work we have explored different keratinocytes culture condition in order to find the method more efficient for our aim. Two major approaches are currently used for *in vitro* tissue engineering of the epidermis. The older technique of Rheinwald and Green (1975)[13], described in materials and methods and tested in the first time is based on the use of a serum-containing medium and of a feeder layer of mouse fibroblasts NIH 3t3 treated with mitomycin C. However the methods for *in vitro* culture of the keratinocytes co-coltures, have evolved until now and require: coating of culture surfaces with rat tail collagen I or fibronectin found in the extracellular matrix. These methods simulate *in vivo* conditions since collagens or extracellular matrix proteins serve as a substrate for keratinocytes growth [14,15]. The morphological result of cells in this first approach is shown in the figure 2, indeed the image (A) reports the typical morphology in petri of NIH 3t3 with collagen coating and image (B) is shown the morphology of NIH 3t3 treated with mitomycin C, a potent DNA crosslinker, act to stop the proliferation cell. Is evident that the cells treated with mitomycin have a large nucleus and a irregular morphology in which disappears the

bipolarity typical of the fibroblasts and also the volume of the cytoskeleton is increased. [13]

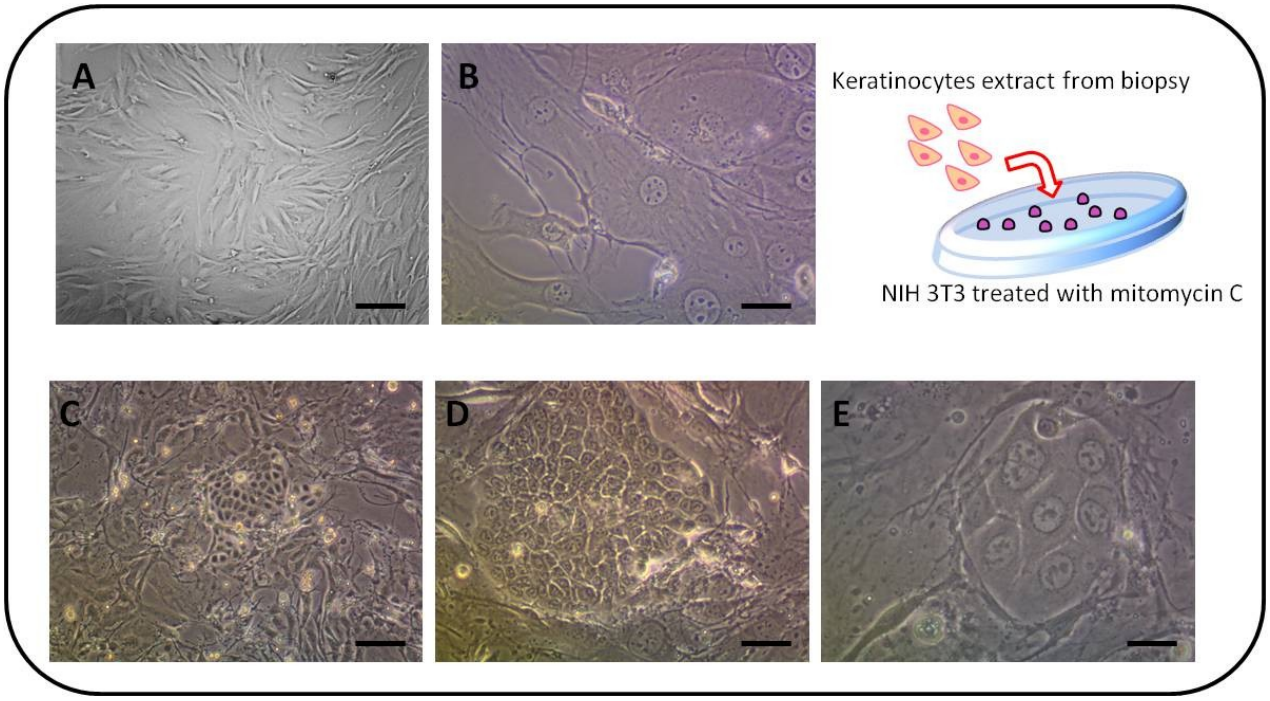

Figure 2.: procedure 1: 2D keratinocytes coltures on NIH 3t3 feeders layer. (A) NIH 3t3 on the coating collagen (scale bar 200 µm); (B) NIH 3t3 treated with mitomycin C (scale bar 100, 5 µm); (C, D,E) keratinocytes on theNIH 3t3 feeders layer (scale bar 100, 50, 5 µm)

Images (C,D,E) show the co-coltures of keratinocytes on the feeder layer of NIH 3t3 previously treated with mitomycin C. Is possible to observe that in the first four day of co- coltures the keratinocytes start to grow and invade the space between the NIH 3t3 in order to obtain the circles in which the keratinocytes assume the typical morphology called "brick stone"

The second approach relies on serum-free media, in the absence of a feeder layer. The presence of mitomycined feeder cells and/or serum can be a confounding factor in keratinocyte cultures, when used, for example, for experimental research on malignant transformation of keratinocytes, testing of potential cytotoxic agents, or

keratinocyte biology. For this reason, many investigators have tried to avoid using feeder cells and to reduce the amounts of serum and additives. In figure 3A colture of keratinocytes on petri in absence of feeder layer is shown and in particular the image 3(A,B) it is evident the typical morphology of cell, the regular shape and is more important that the cells are not large but small and regular, this is sign of undifferentiated state of keratinocytes. This second approach also offers the important advantage of modifying media selectively for culturing a particular cell type, such as melanocytes Indeed is evident in the images 3(C,D) the presence of melanocytes that are recognizable due to their starry morphology and dendrites (highlighted by the black arrow). Moreover variable concentrations of calcium in the culture medium play a vital role in the growth and differentiation of keratinocytes. In Petri the calcium concentration is 0,06mM and increasing calcium concentration is accompanied by an increasing level of keratinocyte differentiation, as evidenced by increasing numbers of formed desmosomes and by the formation of multilayers and sheets of cells [16,17]. Moreover the complexbiologic extracts such as bovine pituitary extract that is a source of putative mitogens and growth factors [18].

Maximal keratinocyte growth stimulation was observed with the combination of just EGF, insulin, and hydrocortisone. The following ingredients were added to improve the culture media and to facilitate keratinocyte sheet formation: insulin (to promote the uptake of glucose and amino acids), and transferrin (to detoxify iron); hydrocortisone (to promote the attachment of cells and cell proliferation). Further advances allowed keratinocytes to undergo up to 40 cell divisions [19]. Results with these methods are now approaching those achieved by the use of fibroblast feeder layers. Indeed by this method, keratinocytes can undergo about 50 to 60 population doublings if cultured from neonatal foreskin.

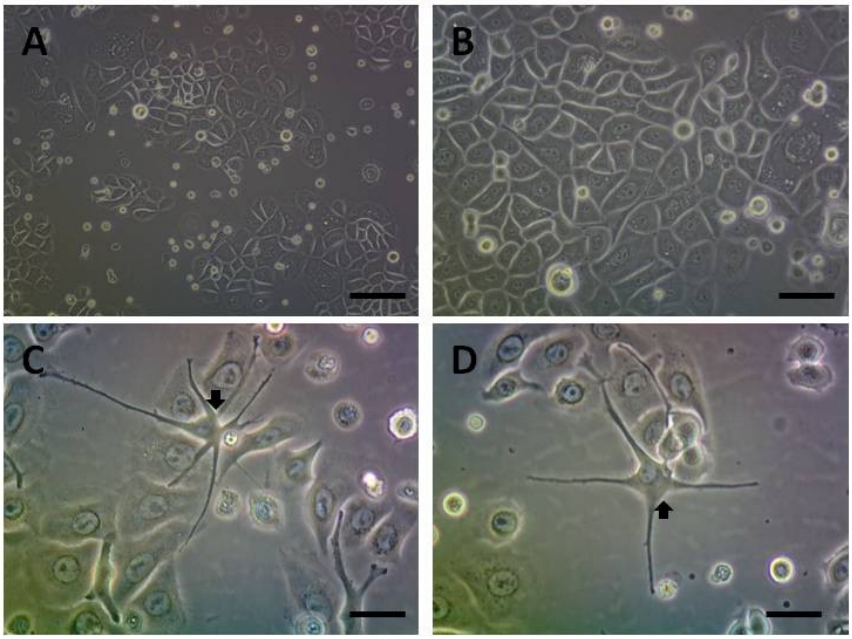

Figure 3.: 2D keratinocytes without presence of the feeders layer. (A) keratinocytes (scale bar 200 µm); (B) keratinocytes (scale bar 20 µm); (C,D) kerarinocytes around the melanocytes underlined with black arrow (scale bar 10)

This number gradually declines with donor age [20]. Translating the number of doublings to area indicates that cultured keratinocytes can be expanded to form sheets up to 10,000 times larger than the original biopsy site. Furthermore primary cells allow for the evaluation of differences in the epithelial maturation depending on the phototype of the donor, and the anatomical location of the tissue of origin. However, primary cells have a limited life span, and cannot be expanded to the large amounts that may be needed to generate multiple reconstructs needed for statistical analyses [20].

Morphologic development by histological and immunofluorescence analysis of 3D Human Skin *in vitro*: keratinocytes seeded on exogenous collagene (3D DEx) and endogenous dermis (3D DEn).

Histological and immunofluorescence analysis were conducted to observe tissue structure and marker localization of cells in organotypic culture. In figure 4, the

epidermis is grown on 3D DEx by using keratinocytes extracted from breast, cultivated in 2D systems with NIH 3t3 feeder layer (Procedure 1), and finally seeded on the 3D DEx. Hematoxylin and eosin staining in fig. A highlighted the epithelial and dermal compartments but there are not sign of stratification and cornification in the constructs. This result is confirmed by immunofluorescence analysis of Keratin 10 and 14 in fig. 4C,D that shown the absence of signals. Indeed in figure B we can see only a cellular cake on the collagen but no presence of nucleus with different shape that indicated the cell differentiation

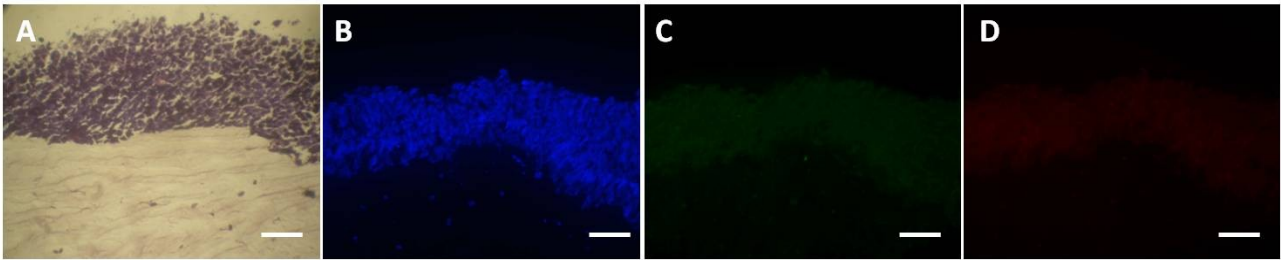

Figure 4.: histological section with thick 5 µm of human skin equivalent with exogenous collagen at 12th day. (A) hematoxilin and eosin; (B) in blu is shown nucleus staining named DAPI; (C) immunofluorecence with anti-K10; (D) immunofluorescence with anti-Keratine 14. (all the scale bar are 100µm)

The morphologic development of our human skin equivalent model is shown in figures 5 and 6. Due to the histological analysis, in particular hematoxylin and eosin and Trichromic Masson stains at the 4th, 6th and 12th day, we can observe the growth and differentiation of the epithelial layer. Indeed we observe keratinocytes grown directly on 3D DEn for 4 days (Fig 5-6 A,B,C), 6 days (fig 5-6 D,E,F), and 12 days (fig 5-6 A,B,C). Early epithelial development, highlighted by a thin epithelium, has been observed while tissue is still submerged in Epidermalization I medium (fig 5-6 A,B,C). In figure 5-6 C the high magnification highlights three layer of cells having still nuclei. The epithelium demonstrates a greater degree of tissue architecture and organization, with the presence of cuboidal basal cells. Indeed when we change the media into Epidermalizzation II it is possible to note the continuous stratum of

keratinocytes and also the beginning of vertical differentiation (fig 5-6 D,E,F). Full morphologic differentiation and stratification have been observed after cells are exposed to the air-liquid interface for 6 days. Indeed in the image 5 I, we can observe a different color of eosin on the epithelial tissue that indicates a different protein composition of tissue. Also in the image 6 I it is possible to note the red fuxin color of the epithelial tissue and in particular of corneum stratum and the completely cornification of cells that don't present the nucleus. Since in vivo epidermal cells grow on the basement membrane and are exposed to air, *in vitro* epidermal differentiation is maximized by the elevation of this skin equivalent to the air-liquid interface [21].

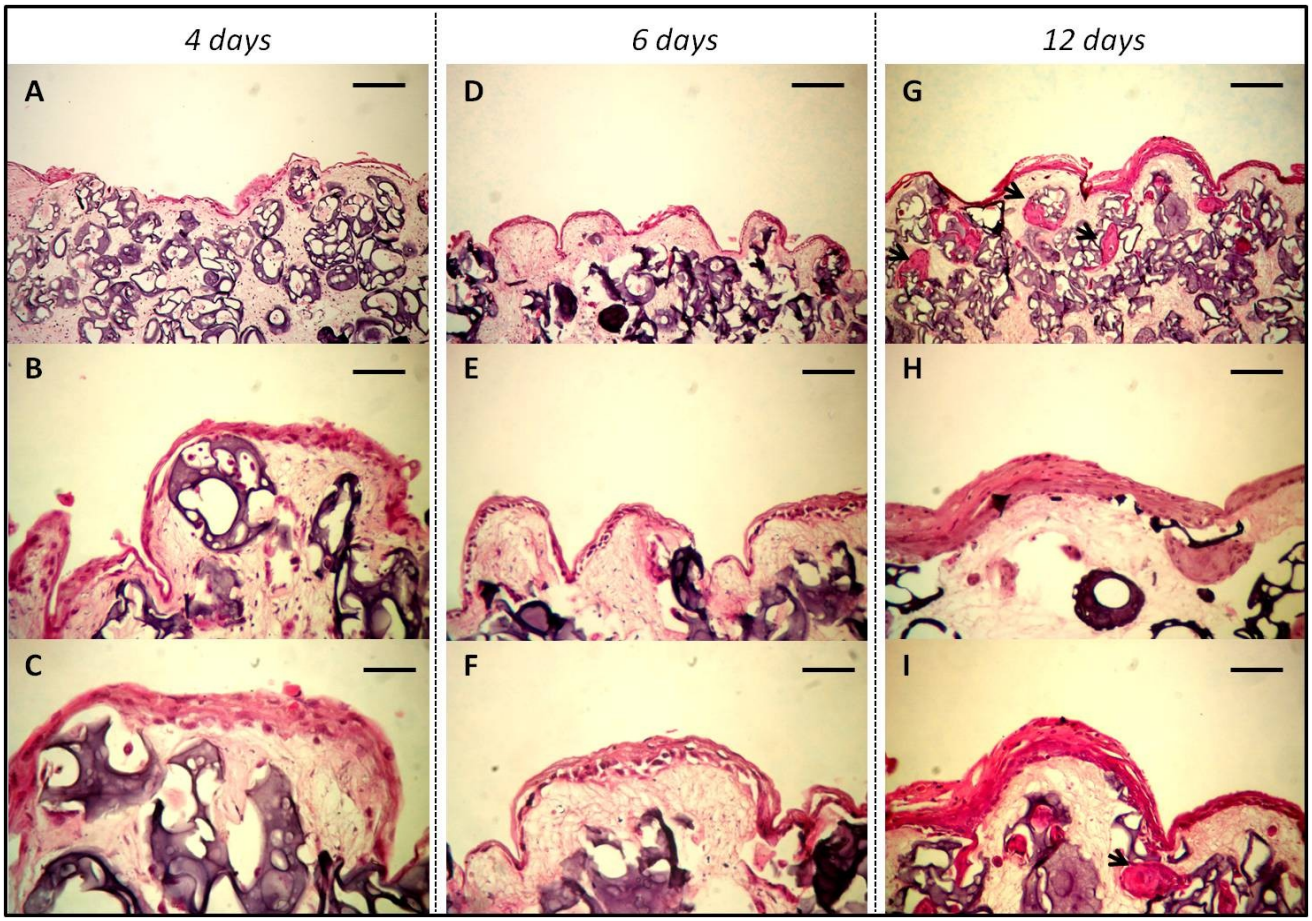

Figure 5.:Hematoxylin and eosin of histological section with thick 5 µm of skin equivalent with endogenous dermis (biohybrid) during the 4th, 6th and 12th day of cell culture in corresponding of the culture media change. Scale bar in the first line (A,B,C) is 200 µm, in second line (D,E,F)100 µm and in third line (G,H,I) is 50 µm, where the black arrow indicates the epidermal cisty-like

When keratinocytes are grown under submersion conditions (as ordinary cell culture) they are not able to synthesize some keratin polypeptides. So their differentiation results uncompleted because the culture microenvironment used, imposes on epidermal cells conditions drastically different from those existing *in vivo*. Moreover in figure 5 G,I and 6 G black arrows highlighted epithelial inclusions in the dermis of keratinocytes. Indeed Epithelial cyst like inclusions are present in dermal portion contained keratinocytes resembling a stratified squamous epithelia where keratin is present in the inner part of cysts [22].

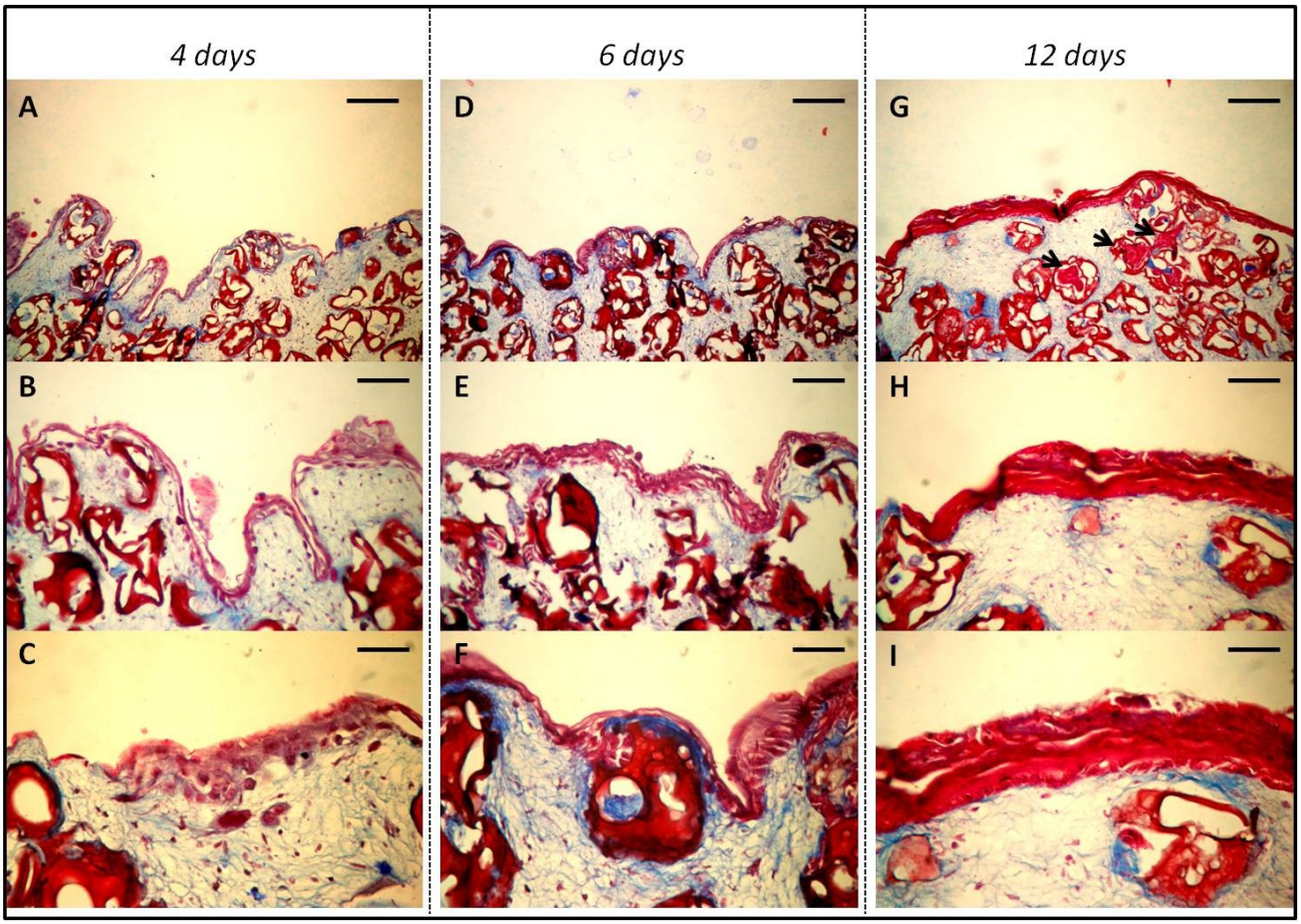

Figure 6.: Masson trichromic staining of histological section with thick 5 µm of human skin equivalent with endogenous dermis during the 4th,6th and 12th day of cell culture in corresponding of the change culture media. Scale bar in the first line (A, D, G) is 200µmand epidermal inclusion are indicated with black arrow, in second line(B, E, H) 100 µm and in third line (C, F, I) is 50 µm.

To evaluate the capacity of primary keratinocytes to generate a correct epidermal tissue on our tissue-engineered dermis we detected the epidermal markers by immunofluorescence analysis. In the figure 7 are shown morphologic evolution of the single markers of each layer that build the epithelial tissue starting from the basal layer to the spinous stratum. Indeed in the first line DAPI/K14 (A, D,G) of the figure 7 is shown that K14 is expressed in the spinous layer only in submerged culture conditions, because in air liquid interfaces condition the differentiated keratinocytes expressed k10 as highlighted in the images of the third line DAPI/K10.

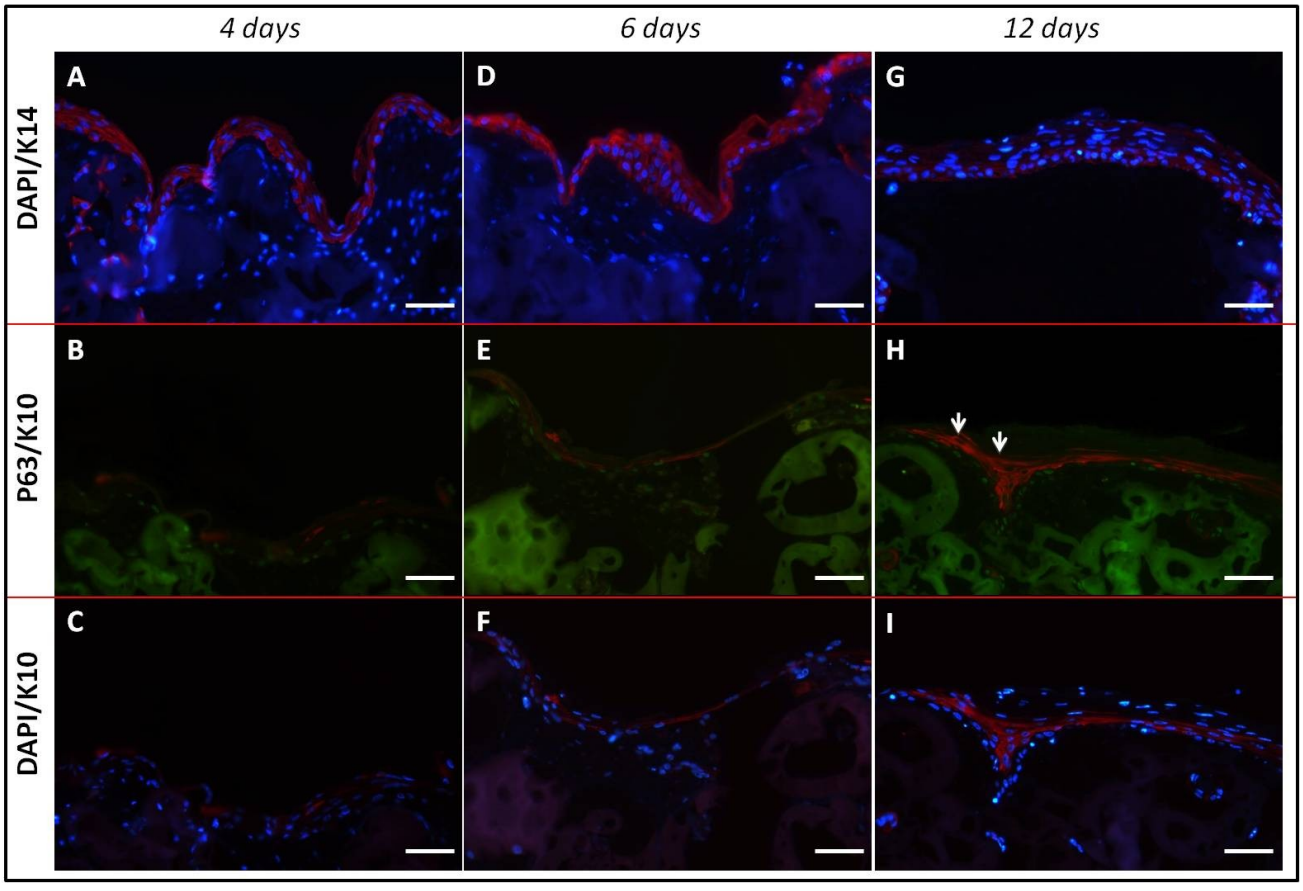

Figure 7.: immunofluorescence analysis of histological section with thick 5 µm of human skin equivalent with endogenous dermis during the 4th, 6th and 12th day of cell culture in corresponding of the culture media changes. First line shows in blu the nuclear staining with DAPI and in red Keratine 14; second line shows in green the transcriptional factor P63 localized only in basal layer and in red keratine 10, white arrows indicate the empty in the signal of keratine 10 that indicate the presence of cell differentiated; third line shows the nucleus stain with DAPI in blu and in red is shown the presence of keratine 14 (A;B,C scale bar 100µm); (D,E,F,G,H,I scale bar 50µm)

The central line P63/k10 (B, E, H) shows the correct morphological development of the tissue, indeed the layer most proximal to the dermis is the cell germinal layer as highlighted by the expression of transcriptional factor p63 in green. Moreover the cells continued to proliferate and maintained p63 expression in the basal layers after 1 week at the air liquid interface condition. Furthermore it is possible to note in the line DAPI/K10 (C, F,I) the presence of red signal of K10 only around differentiated keratinocytes of the suprabasal layer of the epidermal and the white arrow indicate the empty space occupied of keratinocytes not cuboidal [23]

In figure 8 is shown the terminal differentiation of cell in equivalent skin at 12th day in air-liquid interfaces condition by immunofluorescence analysis. Loricrin showed a staining in the granular layer in figure 8 A, while the involucrin expression in red in figure 8 C was restricted to cells of the granular and cornified layers, and it is involved in the crosslinking of cell membrane proteins in keratinocytes during terminal differentiation [22,23].

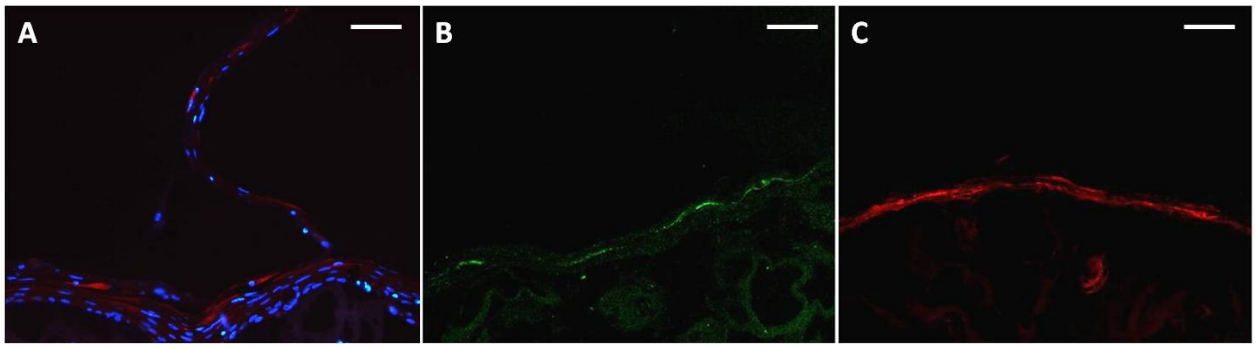

Figure 8.: immunofluorescence analysis of human skin equivalent with endogenous dermis at the 12th day in air liquid interface condition. (A) in blu is shown DAPI staining and in red loricrin in granular layer. (B) in green is shown the filaggrin in corneum layer ; (C) in red is shown the presence of involucrin in granular and part of corneum layer. (all scale bar are 100µm)

Diffuse filaggrin staining was present in the corneumn stratum in air liquid interface condition, which indicate a correct terminal differentiation of epitheliar layer. The

expression of this marker evidence the ability to respond to complex microenvironments including dermal tissue engineered stroma and basal layer.

Morphologic development by histological analysis of Gold Standard 3D Human Skin *in vitro*.

The last results obtained about 3D human skin equivalent by using the extraction and cultures in 2D of keratinocytes descried in Procedure 2 were positive on both models of dermis (3DEn and 3DEx). In particular the formulation of crosslink microbeads chosen for this experiment is 4% that, as described in chapter 1 is the best to obtain an equivalent dermis completely made with endogenous ECM, in which the micro beads will degrade leaving space for the formation of new endogenous extracellular matrix . Furthermore also the extraction and 2D colture procedure is able to preserve the keratinocytes differentiation and the proliferation of melanocytes is stimulated. Indeed in macro image showed in figure 9 brown pigmented spots could be seen on the skin equivalents containing melanocytes, after 8 days incubation beneath the medium in the CO2 incubator.

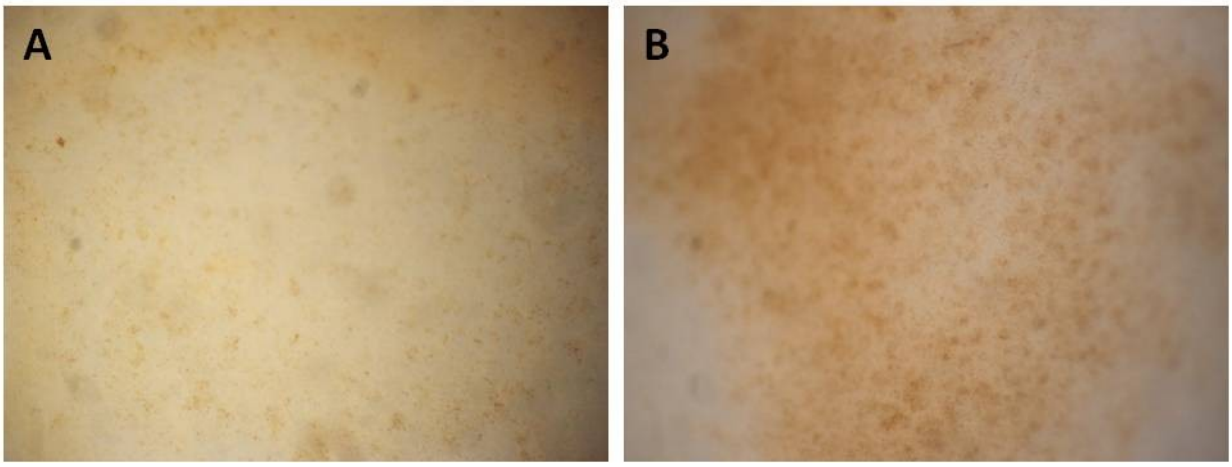

Figure 9.: brown appearance of the tissue-engineered skin containing melanocytes pigmented spots could be seen; (A) brown spot on 3D DEn; (B) brown spo on 3D DEx

This result is evidence in our 3D DEn (fig. 9A) model that in 3D DEx model (fig. 9B), but in 3D DEn model the intensity of color indicate that the melanocytes were raise onto air-liquid interface, while in the 3D DEn model the melanocytes is conceivable confined in the basal layer as in the native tissue [24]. Moreover, are in progress immunological assays to verify the presence of epithelial markers.

In figure 10 we can see histological analysis with hematoxylin and eosin stain (fig. 10 A, B, C) and Masson Trichromic stain (fig. 10 D, E, F), of human skin equivalent by using fibrillar collagen cellular such as a stroma (3D DEx). It is possible to observe in all images a large epidermal tissue, about 150 µm, and it is composed of about 5 or 7 layers of keratinocytes well differentiated. In image B and C we can distinguish a basal layer of cuboidal keratinocytes and a different intensity of eosin color that indicates the presence of melanocytes in epidermal layer.

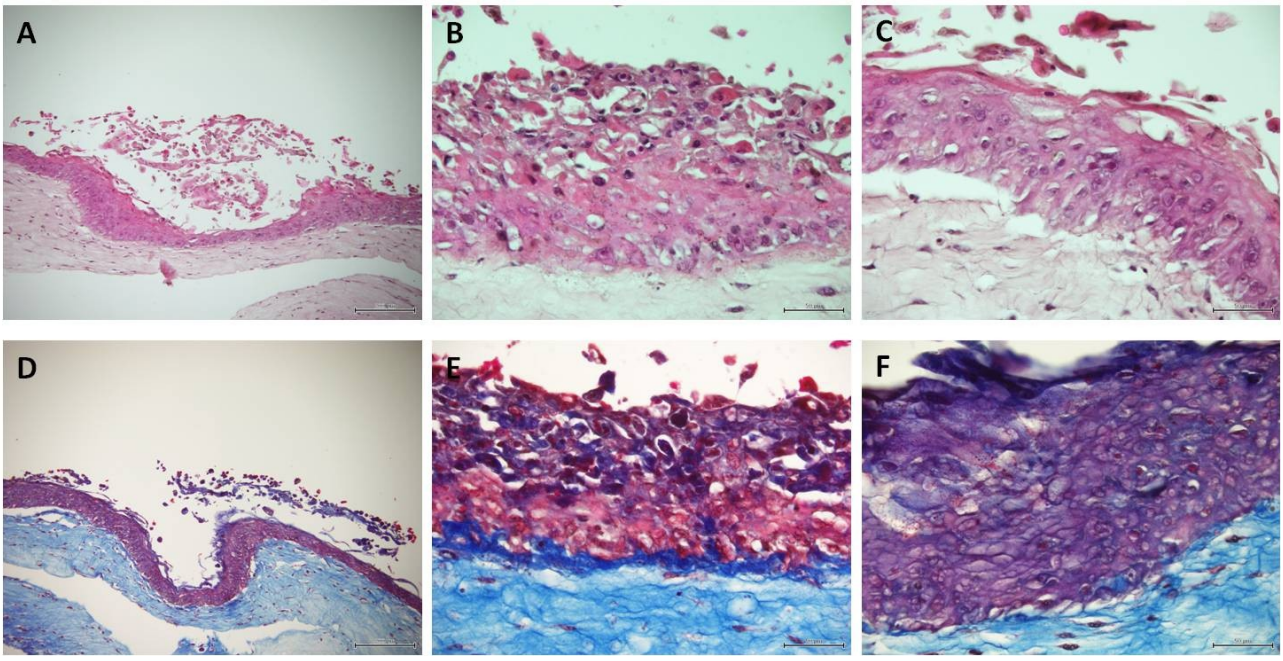

Figure 10.: histological analysis of cross section of human skin equivalent with exogenous collagen. (A, B,C) hematoxylin and eosin staining; (D,E,F) masson thricromic staining

In some parts of tissue we can observe a detach of epidermal equivalent tissue from dermis equivalent tissue and this could means un-complete morphogenesis development of basal layer. Furthermore in figure 10F we can observe the terminal corneus stratum of epithelial tissue and the absence of the cellular nuclei that indicate the keratinization of the cells.

In figure 11 is shown histological analysis with hematoxylin and eosin stain (fig. 11 A, B, C) and Masson Trichromic stain (fig. 11 D, E, F), of gold standard human skin equivalent obtained on a like dermis as endogenous ECM (3D DEn)

In detail the figure 11 A shows a large epithelial tissue, about 150 μm and in dermis it is possible to observe epithelial cyst-like inclusions as in equivalent skin described in fig 5, 6. Moreover in fig. 11 B is shown (black arrow) an introflection of basal layer of keratinocytes that has the shape and organization similar to an hair bulb, indeed the keratinocytes in periphery, or rather proximal of the dermis compartment have a cuboidal shape and in center of channel is possible to see a cell differentiation in which cells thrown out the keratin [25]. This phenomenon has been observed only in this type of dermis equivalent among those produced, probably because the surface of the 3D DEn is open and in the ECM there are no microbeads which hinder the penetration of keratinocytes and their organization in a such structure. From the biological point of view it is possible to assumed a better interaction between an extracellular matrix completely produced by fibroblasts in which there are all the components that constitute also the native tissue. Indeed, cell–cell and cell–matrix interactions either to accelerate biointegration in surgery application [1].

The reason of this progress is that the keratinocytes from the culture medium and from substrate that hosts them receive all the factors necessary for a correct morphogenesis of epithelial tissue [26] Furthermore in all images of the figure 11 we can note that the epithelial tissue covers the superficial of equivalent dermis and it is

present a different intensity of eosin color that indicates the different protein composition of epithelial tissue. Indeed in the figure 11 G is possible to distinguish 3 layer in tissue epidermal: basal layer (cuboidal cell shape), spinouse and granulose layer (elongate cell shape) corneal layer (without cells). So the mechanical integrity of ECM play a fundamental role in the cross talking between different cell lines in heterotypic tissues.

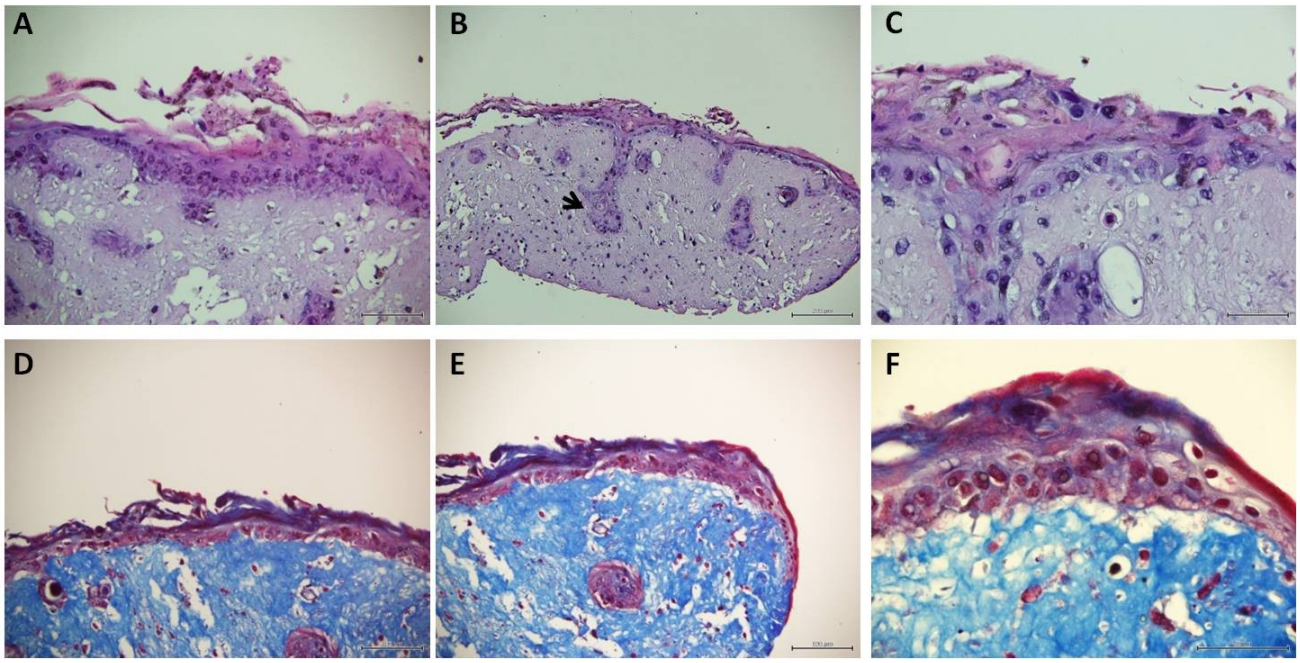

Figure 11.: histological analysis of cross section of human skin equivalent with endogenous dermis. (A, B,C) hematoxylin and eosin staining and introction of basal layer was indicated by black arrow ; (D,E,F) Masson trichromic staining

Other important result is that the mechanism of skin contraction during the coltures time is not present, because in this condition the dermis part has a stable morphological development also if the air liquid condition is not the best condition for the subsistence of the fibroblasts. Instead this phenomena occur when we combined the 3DEX with epidermal layer during colture time [21,27]. Moreover this organotypic model can be used both as screening tool and as model for the study of healthy and disease skin.

CONCLUSION

The creation of 3D human skin equivalent model proposed in this chapter won intrinsically challenges associated with the 3D nature of the organotypic culture, such as insufficient mass transfer in the interior regions of large and avascular constructs, inhomogeneous cell seeding, and difficulties in regulating distinct behavior of different cell types in the same construct [28]. Our results indicate that by setting the optimal conditions for keratinocyte extraction as well as their 2D expansion it is possible to preserve keratinocytes capability to differentiate generating a full development epidermal layer, leading to the success of the organotypic coltures. The best results we achieved in terms of 3D skin equivalent was reached by combining a dermal equivalent made up of completely endogenous ECM with keratinocytes cultured in serum-free conditions and without feeder layer during the 2D expansion. The ECM can contribute to the microenvironment specifically through its mechanical features, providing support and anchorage for cells. Interactions between cells and the ECM are extremely important for processes such as normal cell growth and differentiation. Finally, this human skin equivalent model can be used for replacing diseased or lost human skin, substitute animals for drug screening, and serve as model systems for physiological, pathological, and developmental studies

REFERENCES

1.Rostislav V. Shevchenko, Stuart L. James and S. Elizabeth James. A review of tissue-engineered skin bioconstructs available for skin reconstruction. *J. R. Soc. Interface* 2010 **7**, 229-258

2.http://www.theecologist.org/how_to_make_a_difference/campaigning_the_basics/1329786/take_action_to_end_cosmetic_testing_on_animals.html

3. Green H, Kehinde O, Thomas J. Growth of cultured human epidermal cells into multiple epithelia suitable for grafting. Proc Natl Acad Sci USA 1979;76:5665—8

4.Regnier M, Asselineau D, Lenoir MC. Human epidermis reconstructed on dermal substrates *in vitro*: an alternative to animals in skin pharmacology. Skin Pharmacol 1990;3:70— 85.

5. Ponec M. Reconstruction of human epidermis on de-epidermized dermis: expression of differentiation-specific protein markers and lipid composition. Toxicol *In Vitro* 1991;5:597— 606.

6. Gay R, Swiderek M, Nelson D, Ernesti A. The living skin equivalent as *in vitro* for ranking the toxic potential of dermal irritants. Toxic *In Vitro* 1992;6:303—15.

7. Ehrlich HP. Understanding experimental biology of skin equivalent: from laboratory to clinical use in patients

8. Lee DY, Ahn HT, Cho KH. A new skin equivalent model: use of a dermal substrate which combines de-epidermized dermis with fibroblast-populated collagen matrix. J Dermatol Sci 2000;23:132—7.

9.Lee DY, Cho KH. The effects of epidermal keratinocytes and dermal fibroblasts on the formation of cutaneous basement membrane in thre dimensional culture systems. Arch Dermatol Res 2005;296:296—302.

10.Regnier M, Prunieras M, Woodley D. Growth and differentiation of adult human epidermal cells on dermal substrates. Front Matrix Biol 1981;9:4—35

11. Cooper ML, Hansbrough JF, Spielvogel RL, Cohen R, Bartel RL, Naughton G. *In vivo* optimization of a living dermal substitute employing cultured human fibroblasts on a biodegradable polyglycolic acid or polyglactin mesh. Biomaterials 1991;12:243—8.

12. B. Pomahac T. Svensio Tissue engineering of skin. Crit Rev Oral Biol Med 9(3):333-344 (1998)

13. Rheinwald JG, Green H. Serial cultivation of strains of human epidermal keratinocytes: the formation of keratinizing colonies from single cells. Cell. 1975 Nov;6(3):331-43.

14. Liu SC, Karasek M Isolation and serial cultivation of rabbit skin epithelial cells. J Invest Dermatol. 1978 Aug;71(2):157-62.

15. Terranova VP, Aumailley M, Sultan LH, Martin GR, Kleinman HK. Regulation of cell attachment and cell number by fibronectin and laminin. J Cell Physiol. 1986 Jun;127(3):473-9.

16. Strickland JE, Hennings H, Jetten AM, Yuspa SH, Allen PT, Hellmann KB, Strickland AG Susceptibility determinants for mouse epidermal carcinogenesis.IARC Sci Publ. 1982;(39):259-68.

17. Boisseau AM, Donatien P, Surlève-Bazeille JE, Amédée J, Harmand MF, Bézian JH, Maleville J, Taieb A. Production of epidermal sheets in a serum free culture system: a further appraisal of the role of extracellular calcium. J Dermatol Sci. 1992 Mar;3(2):111-20.

18. Peehl DM, Ham RG. Growth and differentiation of human keratinocytes without a feeder layer or conditioned medium. *In Vitro*. 1980 Jun;16(6):516-25.

19. Tenchini ML, Ranzati C, Malcovati M. Culture techniques for human keratinocytes. Burns. 1992;18 Suppl 1:S11-6. Review

20.Gilchrest BA *In vitro* assessment of keratinocyte aging. J Invest Dermatol. 1983 Jul;81(1 Suppl):184s-9s.

21. Three-dimensional tissue models of normal and diseased skin. Carlson MW, Alt-Holland A, Egles C, Garlick JA.

22. Florian Groeber a,b,1, Monika Holeiter a,c,1, Martina Hampel a,b, Svenja Hinderer a,c, Katja Schenke-Layland Skin tissue engineering — *In vivo* and *in vitro* applications Advanced Drug Delivery Reviews 128 (2011) 352–366

23. Annie F. Black, Ph.D.1,* Charbel Bouez, M.S.,1,* Tissue engineering Volume 11 Number 5/6, 2005 Optimization and Characterization of an Engineered Human Skin Equivalent

24. Yuan Liu a, Fumihiko Suwa. Reconstruction of a tissue-engineered skin containing melanocytes. Cell Biology International 31 (2007) 985e990

25. Danielle Larouche, Ph.D.,1–3 Kristine Cuffley, M.Sc.,1–3 Claudie Paquet, Ph.D.,1–3 and Lucie Germain, Ph.D.1–3Tissue-Engineered Skin Preserving the Potential of Epithelial Cells to Differentiate into Hair After Grafting. Tissue engineering: Part A Volume 17, Numbers 5 and 6, 2011

26. J.Mchael Sorell, Marilyn A Baber Arnold I. Caplan. A Self-assembled Fibroblast-Endothelial Cell Co-Coulture System That Supports *in vitro* Vasculogenesis by both Human Umbilical Vein Endothelial Cells and Human Dermal Microvascular Endothelial Cells. Cell Tissue Organs 2007; 186:157-168

27. Harrison CA, Gossiel F, Layton CM, Bullock AJ, Johnson T, Blumsohn A, MacNeil S. Use of an *in vitro* model of tissue-engineered skin to investigate the mechanism of skin graft contraction. Tissue Eng. 2006 Nov;12(11):3119-33.

28. Bo Liu 1, Yang Liu 1, Andrew K. Lewis, Wei Shen Modularly assembled porous cell-laden hydrogels Biomaterials 31 (2010) 4918e4925

Chapter 5

3D DERMAL EQUIVALENT HAVING DIFFERENT SHAPES AND ITS INDUSTRIAL APPLICATION

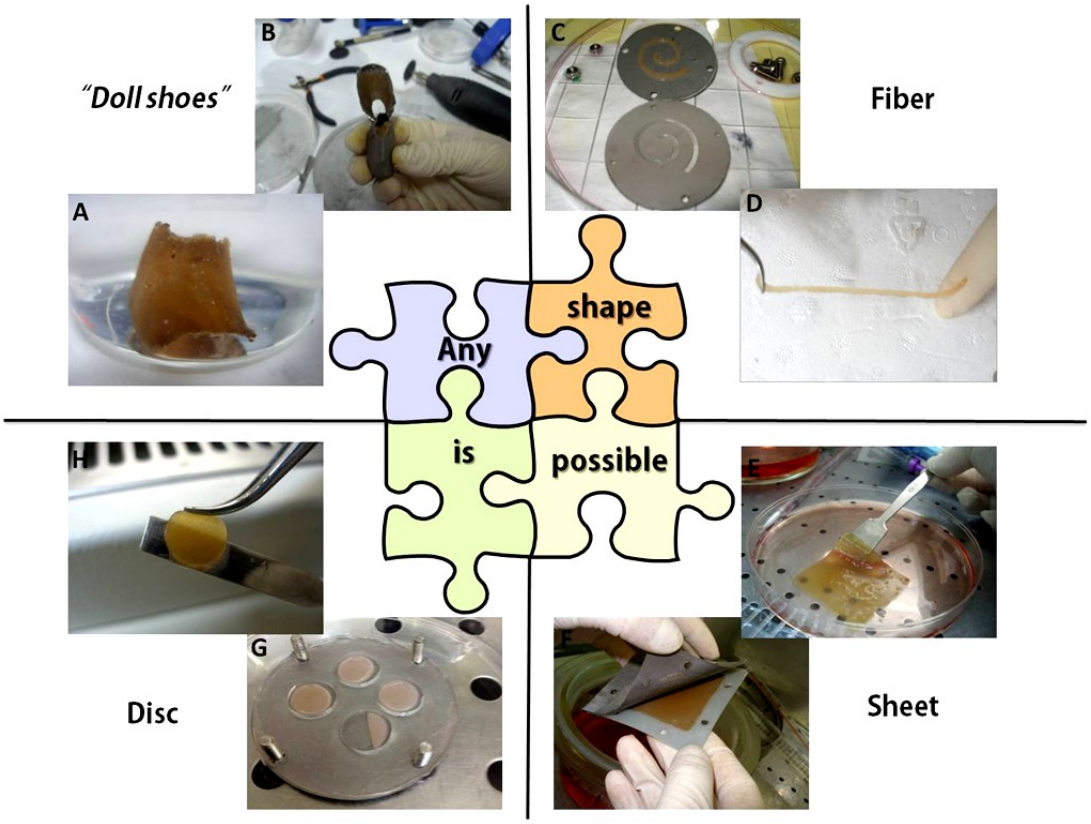

INTRODUCTION

Traditionally tissue engineering finds its mayor applications into repair or replace portions of or whole damaged tissues [1,2]. As matter of fact, tissue engineering knowledge has always been aimed at biomedical applications in which the tissue is cultured *in vitro* up to an intermediate development stage, sufficient to keep its vitality after the *in vivo* transplant, where the final development and formation of the finished tissue effectively occurs [3]. However, in the recent years there is a growing interest of researchers for an industrial application of this technology. To address this need there is the necessity to obtain *in vitro* bioengineered tissues in a finished form, i.e. tissues which may be used for a direct industrial use, without any *in vivo* passage.

Since in the last years our group has developed relevant expertise in the engineering of 3D thick tissues *in vitro*, it has been explored the possibility to use our tissue-equivalent products for applications in the tanning industry. One of the major obstacles is obtaining finished bioengineered tissues with a thickness around 1 mm suited to the successive industrial applications [4]. Indeed, such a thickness may not be obtained through currently available cellular culture techniques, essentially due to the difficulty in assuring the nutrients and maintaining the optimal chemical-physical conditions for cell proliferation through said tissue thickness [5]. This obstacle has been overcome through a bottom-up process to build up the bioengineered tissue occurring in two different stages as explained in the chapter 2. In a first stage, a product with a small thickness (around 300μm) called microtissue precursors μTP is prepared starting from a particle supports. In a second stage of the process, a plurality of said microtissue precursor (μTP) are arranged in close mutual proximity and in cell culture conditions, so as to have a process of tissue repair which determines the biological union of the μTP, thus forming the final bioengineered

tissue in the desired thickness and shape. Following this approach bioengineered tissues having shape of fiber, sheet and “doll shoes” have been produced and we demonstrate that they are able to resist the mechanical stresses of a tanning process. The possibility to obtain leather by exploiting tissue engineering methods meets also the need of consumers sympathetic to animal issues to prefer a material having the same properties and features of natural leather, whose manufacturing process does not involve the killing of animals. At last, an important goal of using bioengineered leather is also to look at ways that can make products that are superior to traditional leather.

MATERIALS AND METHODS

Fabrication of fiber shape

µTP molding injection in PTFE porous microtube

This step consists of the injection of the µTP in a micro channel that allows nutrient exchange for the cell and geometrical guidance for the tissue growth. The porosity of the micro-channel allows the exchange of nutrients and waste products of the cellular metabolism between culture medium and cells. Furthermore, the micro-channel geometry, meaning a geometric constrain for cell movement, guides cell direction and support extracellular matrix organization along micro-channel longitudinal axis. µTPs suspension was transferred into the porous PTFE microtube (Markel Corporation) or static culture in the cell culture medium, ascorbic acid was added to stimulate extracellular matrix synthesis. This microtubes present an inner diameter of 780 µm and outer diameter of 1050 µm, and they have a wall with a porous surface the dimension of the pores is about 6 µm. The system showed in fig. 1 has been used to move the cell-seeded microbeads in the microtube. This system consists of a body of syringe containing fibroblast seeded microbeads suspension; is connected to

a syringe pump.(fig. 1A). The syringe gate is connected to the microtube (fig. 1B). By switch on the motor of pump at the 5 ml/min, the cell seeded suspension moves from the chamber to the micro tube. The end of the PTFE microtube is connected of filter system (fig. 1C) with cut off 110 µm to maintain µTPs suspension inside the microtube while the medium can flow through the porous microtube wall and in second syringe pump (fig. 1D) that inspire the solution at the rate of 5ml/min.

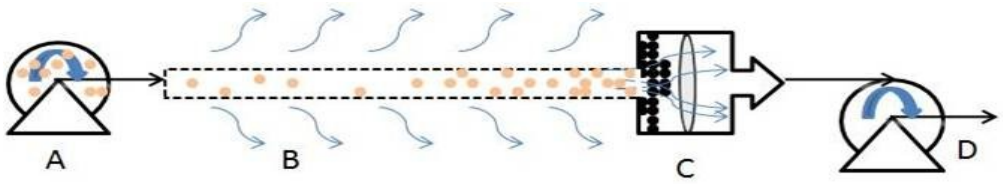

Figure 1.: µTP molding injection system

µTP "drop by drop" in an open microchannel

µTPs suspension was transferred from the spinner flask to a 50 ml Falcon centrifuge tube and, after settling, as showed in fig. 2 transferred by pipetting (fig.2A) into the maturation chamber to allow their molding in wire shape as textile fiber dermal *in vitro*. During the filling procedure, the maturation chamber (fig.2B) was accommodated on a device (fig.2 C,D) that was connected with a vacuum pump to make the process faster and to assure that any bubble was in the maturation space. Finally the assembling chamber was placed on the bottom of a spinner flask and completely surrounded by culture medium. The spinner was operated at 60 rpm and the medium was exchanged every 3 days

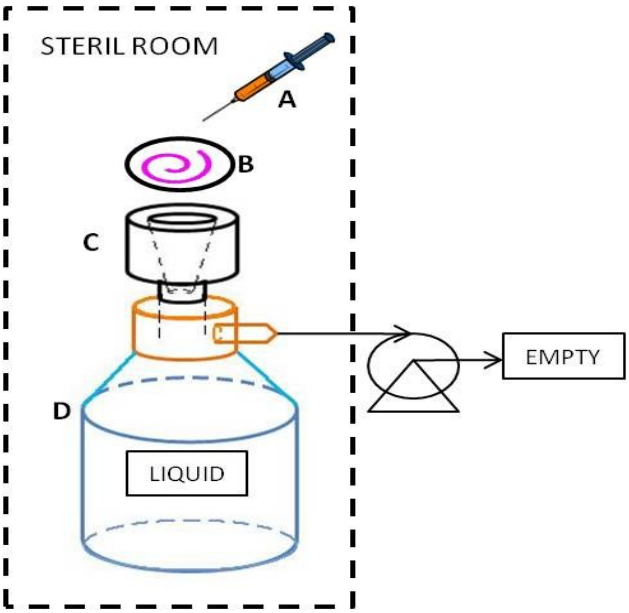

Figure 2.: µTP "drop by drop" system

Fabrication of sheet shape

The method for the production of tissue equivalent having sheet shape has been describes in the chapter 3, in this case bovine fibroblast at 3 passage have been used..

Fabrication of "doll shoes"

We obtained the shape of foot by using synthetic paste for modeling as show in fig.3A and around it, two metallic grids were envelop that followed the foot shape (fig.3B) and between the grids there was silicon slice with thickness of 1 mm. The grids were welded under and back the shoes model. After the model was dissolved in water and the silicon in trifluoroacetic acid, in this way remain only the grids empty with the hollow space (fig.3C) of 1 mm.

µTPs suspension was transferred with syringe in the hollow space of the maturation chamber to allow their molding in doll shoes shape. This system is transferred in bioreactor named spinner flask completely surrounded by culture medium. The

spinner was operated at 60 rpm and the medium was exchanged every 3 days. At the 4 weeks the chamber was open with a cut under the foot in order to obtain the upper of the shoes.

Figure 3.: maturation chamber component

Morphological analysis of 3D Engineered Tissue

All tissue have been analyzed by using method reported in the previous chapter 2 and 3 such as histology and SEM

Textile application

Vegetable tanning uses tannin that is a class of polyphenol astringent chemical The vegetable tanning was performed on the fiber and the doll shoes; the procedure used is very similar to the industrial procedures but adapted to the needs of the laboratory and to the structural characteristics of our dermis *in vitro* Indeed with our samples, we tanned a piece of leather soaked weight of 45 grams in order to have a mass ratio of mass sample tanning sustainable an analytical balance.

Moreover for mimic the mechanical force of penetration of tanning agents that involved the dermal piece we used a cylindrical vessel that turn around on the shaking platform as showed in fig 4

Vegetable tanning

Substance	Tanning agent	Greasing agent
Mimosa light	extract from mimosa	
TTP n°2	extract from tara	
Floretan SF	sintetic	
ATG	extract from quebracho	
Kroatan 494		pulishing
Suntan 170		filler
Cutamin LSD		unstrain

Table 1.: chemical component for vegetable tanning

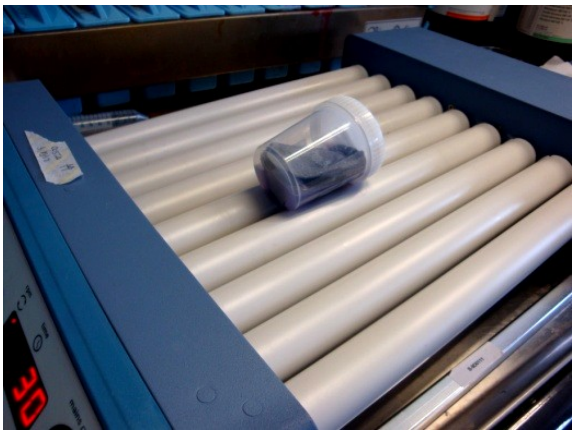

Figure 4.: shaker platform for tanned

This process consist in the following steps

- Add 100% of H_2O compared to the wet weight . After in this bath of *Pickling* increases the acidity of the hide to pH4 with addition of 0.8% formic acid solution.10% NaCl are added to prevent the hide from swelling. Time is 10 min.
- At the temperature of 25°C are added 3% Mimosa light (for a time of 15 minutes, and after 1% respectively of Cutamin LSD and Sultan 170 at the temperature of 37°C for a time of 10 minutes.
- In the second bath at the temperature of 25°C are added 150% of water compared

to the wet weight of the sample and 6% ATG,1% of Mimosa light, 4% of TTP n°2, 4%of Kroatan. Time 2 hours.

- In the end, the sample is submerged in a water solution of formic acid at the pH 4 for a time of 15 minutes and after dried and storage at 25°C. The tanning agent in this case is a salt of the ion Cr^{+++}.
- Add 100% of water compared to the wet weight. Increase the acidity of bah about 3 by using the 1.2% formic acid solution. Still the 10% NaCl are added to prevent the hide from swelling. Time of contact is 10 min

Tanned chrome

Substance	Tanning agent	Greasing agent
Cr^{+++}26/33	mineral	
Cr^{+++}sintetic	sintetic	
Global Interal G60	sintetic	
Eusapon OC		soap
Liker soft		+
Lipoderm N		filler
Licker EXN		+
Licker CAR		+

Table 2. chemical component for tanned chrome

- After pickling, when the pH is low, chromium salts (Cr^{+++}) are added at the temperature of 37°C. In detail are addiction the 2% of Sintetic Chrome for 15 min and after 4% 26/33 Chrome for 15 min and also 4%Chrome 26/33 and the 2% of Global Interal G60 that is lubricant for other 1h in mixing and after the p:iece is left 3h at rest. To fixate the chromium: the pH is slowly increased by

using a base ammonium bicarbonate and sodium hydrogen carbonate in over night**.** The process of chromium tanning is based on the cross-linkage of chromium ions with free carboxyl groups in the collagen. It makes the hide resistant to bacteria and high temperature. The chromium-tanned hide contains about 2-3 dry weight percent of Cr3. The day after the sample was wash in bath of acid formic and salt at 4 °C for several time (about 3 h) and in the end was wash in the running water and Eusapon Oc.

- The last bath consists of a lubrication to give at the sample the softness and the needed touch. Then at the temperature of 45°C add ,in 100% of water compared to the wet weight of sample, the 6% respectively of Licker EXN. Licker PU, Licker Soft, Licker Car and 1,5% of acid formic for 3 hours and in finally wash the sample in cold water and to check that pH is 3,8.

  In addition, the sample was stained with PicroSirius Red (PSR) that ah given a red carmine.

Tensile properties measurements.

From 5x5 mm dermis equivalent tanned were harvested bone dog shaped sample to perform the tensile mechanical tests using method reported in the chapter 3.

RESULTS AND DISCUSSIONS

Tissue-fiber production: µTP injection in PTFE porous microtube *vs* µTP deposited “drop by drop” in an open microchannel

The results reported herein related with the production of a bioengineered tissue yarn by using a process in which the µTPs have been induced to assemble in a fiber shape. By arranging in close mutual proximity under suitable culture conditions the µTP are able to form a 3D tissue equivalent due to their biological union. Two kinds of methods are explored to produce the fibers one is µTP injection

in PTFE porous microtube another is µTP deposited “drop by drop” in an open microchannel. Both the devices used work as geometric constrain for cell movement, guides cell direction and supports extracellular matrix organization along wire longitudinal axis; in this way it is possible to get an high density of collagen fiber aligned and arranged along the axis of propagation of the wire so that the fiber has the strength necessary to be spun. The diameter of wire could range from 300 µm to 1500 µm. The production of the fiber by µTP injection in the porous microtube does not allow the fabrication of fiber longer than 10 cm (fig.1B) due to the problems of high pressure in microtubes Teflon® (fig.1A) causing interruptions along the axis of propagation of the wire. This phenomenon occurs even if the tubes of Teflon® have high percentages of porosity on the surface leading to fluid runoff that decrease internal pressure. The main constraint of this process is that the flow inside the microtubes is not homogeneous because is composite of a solids part (µTPs) and a liquid part as the culture medium and for this reason the liquid flows around the µTPs but not carry them in the channel.

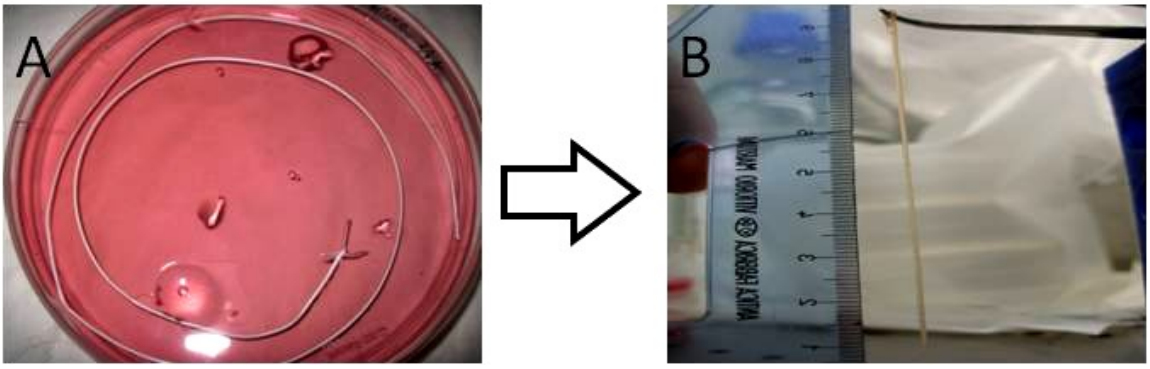

Figure 1.: µTP molding injection. (A) PTFE microchannel in the culture medium at the end of µTP filling procedure (B) dermis equivalent in fiber shape having 4 weeks of maturation culture.

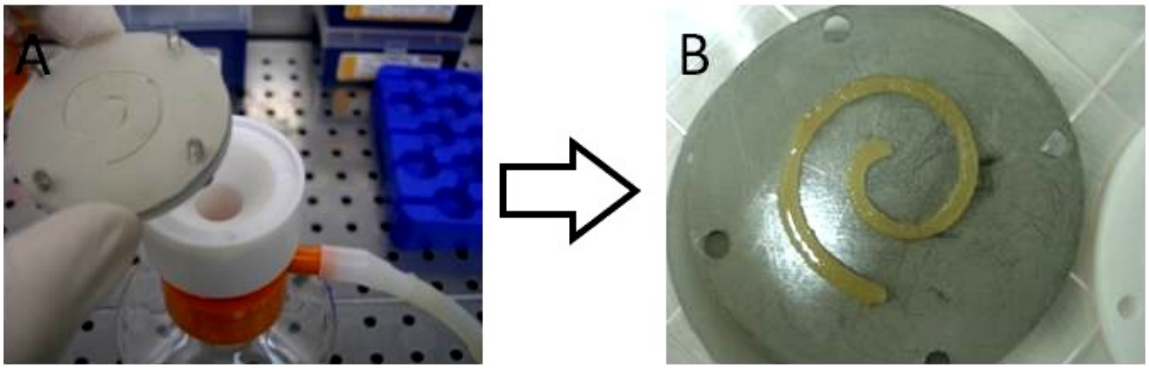

Figure 2.: µTP deposite “drop by drop”. (A) Open microchannel and system of aspiration liquid; (B) dermis equivalent in fiber shape at 4 week of maturation

The production of the tissue-fiber by depositing drop by drop the μTP in an open microchannel is very simple and by using the vacuum pump the filling procedure is faster than the injection of μTP in the porous micro tube. Futhermore, any problem due to high pressure conditions is avoided since the microchannel is open. Very important for the industrial scale-up of the process, this procedure, potentially allow to produce fiber with no limit in length in very few space

Characterization of tissue-fibers

In both methods, the fibers have the same morphological characteristics. Histological analysis with hematoxylin and eosin (fig.3A) shows that fiber is compact since the ECM stained in pink is continuous. Along the ECM thickness, microbeads are not present anymore. It is possible, only, to note the fingerprint of microbeads successively completely substituted by neo-ECM. The distribution of the cells along the thickness of the fiber appears homogeneous. Histological analysis with PSR in fig. 3B,C shows that fibrils of mature collagen in red (fig.3B) have a preferential alignment along fiber's propagation axis. Indeed, if linearly polarized light is used, bi-rifractive PSR-stained fibrils will appear dark if they are aligned parallel to the transmission axis of either of the two linearly polarizing filters revealing that only fibrils aligned along tube axis are red [6]. Flexibility and strength of the tissue depend on just these morphological characteristics. ECM analysis confirm the totally absence of microbeads (fig. 3E) and along the transversal section (fig. 3D) is possible to note that the ECM is very dense and compact. The figure 3F show the ordered orientation of the surface in which it is possible to see the collagen fibrils exposed on the surface.

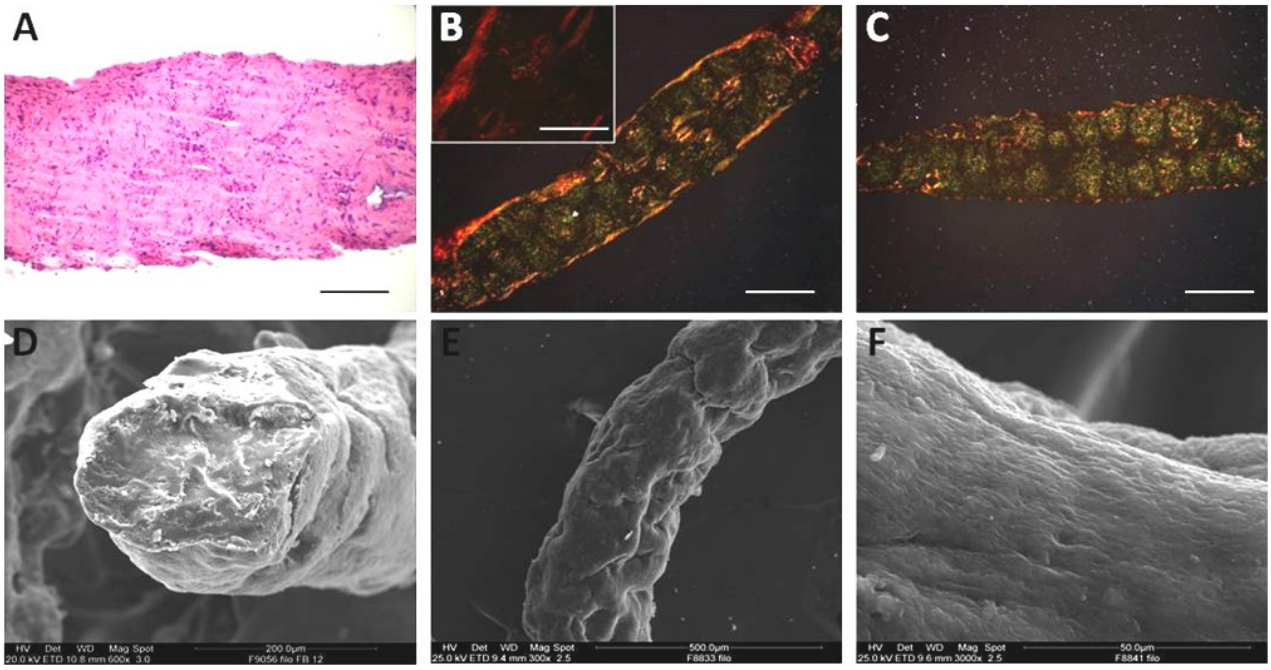

Figure 3.: analysis of dermis equivalent at fiber shape . (A) hematoxylin and eosin stain on the histological section (scale bar: 100μm); (B) picroSirius Red stain on the histological section (scale bar 200 μm),magnification (scale bar50 μm);(C) picroSirius Red stain on the histological section (scale bar 200μm); (D) SEM trasversal section;(E) SEM on the surface; SEM high magnification of the surface

Process versatility: overcoming shape limitations

In figure 4 it is possible to note how versatile our bottom-up approach is, since tissue-equivalent having different shape can be realized. The panel shows each single product (fig. A,D,E,H) and the corresponding maturation chamber designed to produce it (fig 4 B,C,F,G). Whereby the only barrier to fabricate different shapes is the fantasy and also the capability to build mold having different shape. In the fig. 4A is showed a tissue having a shape that we named “doll shoes” that has a thick of 1mm and a surface of 13 cm^2. It is possible to note that tissue has a compact structure with an intrinsic rigidity and it is able to preserve its shape without support. By following our strategy it is potentially possible to fabricate the upper of entire shoes without need a machine able to assembly and to sew. In the fig. 4D is showed the 3D structure of a fiber shape thick 1mm and longer 10 cm but as previous described, by using “drop by drop“ method, potentially there are no length restrictions. In fig 4E is showed derma equivalent with sheet shape that have a thick of 1mm and a extension surface of 25 $cm^{2.}$. This is the larger shape made by means of this technique and it is demonstrated the process adaptability to industrial application. At last, the fig.4H show the classical disc shape that we made in lab as bio-platform application that we described in chapter 2 and 3. This variety of products demonstrates that

by means of bottom up approach is possible to achieve automated geometric control of the tissues's shape for the fabrication of functional complex tissues[7]. This result indicated that by using large numbers of µ-TPs the bottom-up approach with molds is able to construct millimeter-thick complex 3D structures. µ-TPs are assembled in non-adherent silicon molds with arbitrary shapes. Metallic grid close the mold and let in nutrients.

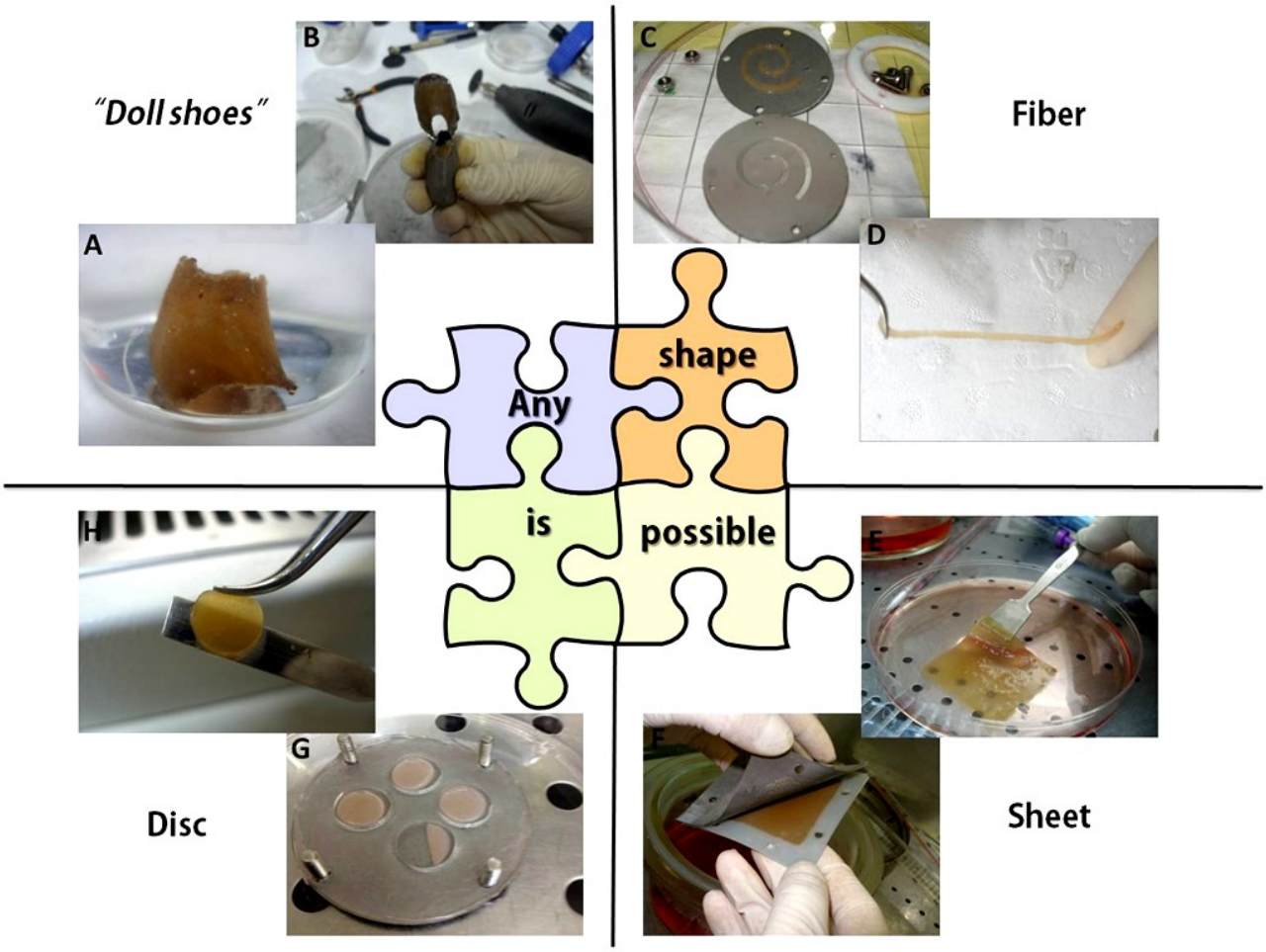

Figure 4.: different shape of dermis equivalent. (A) Dermal Equivalent in shape of doll-shoes (B) maturation chamber of the "doll shoes"; (C) open microchannel is the maturation chamber used to produce of fiber; (D) D.E. in fiber shape; (E) D.E. in sheet shape; (F) maturation chamber to produce sheet shape ;(G);maturation chamber to produce disc shape; (H) D.E disc shaped

The primary advantages of this method are rapid production of millimeter-thick 3D cell structures, homogeneous cell density, and tissue formation without necrosis in a period of less than a week because of the supply of the cell culture medium through cavities between and inside of µ-TPs [8,9].

Textile application: tanning process

In the recent years there is a growing interest of researchers for an industrial application of tissue engineering technology. To address this need there is the necessity to obtain *in vitro* bioengineered tissues in a finished form, i.e. tissues which may be used for a direct industrial use, without any *in vivo* passage. In order to explore the possibility to exploit the dermis-equivalent realized for a textile industry application, an optimized tanning process has been performed on tissues realized. In figure 5 the macroscopic images of tissue-equivalent tanned by using vegetable tannage have been shown. Vegetable tannage is a generic term to define the process of making leather by the use of tannins obtained from barks, woods or other parts of plants and trees, as distinguished from “mineral tannages”. In particular was used a natural extract from heart-wood of quebracho tree which grows in South America. Warm soluble Quebracho is rich in condensed tannins.

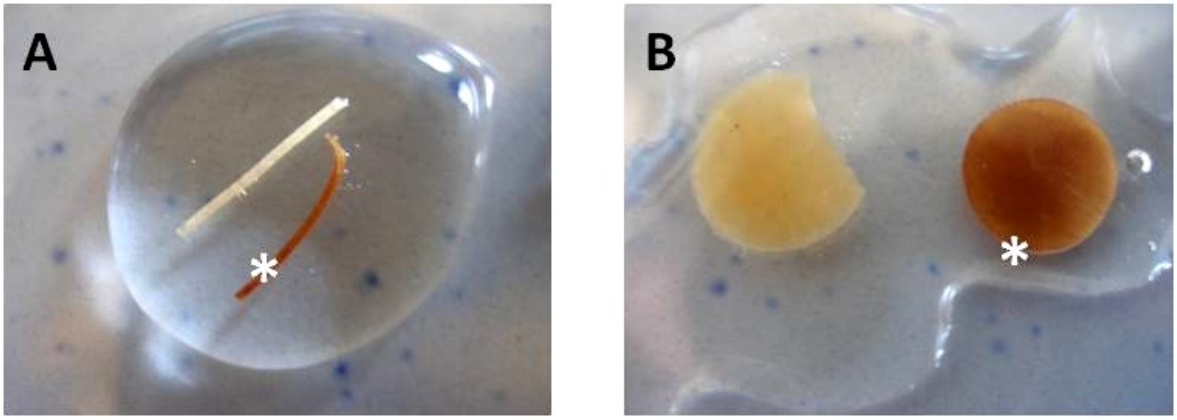

Figure 5.: Vegetable tannage of D.E and no tannage. (A) fiber with stars was vegetable tannage”; (B) disc with star was vegetable tannage

This type of bark give a typical leather color underlined in figure 5A and 5B with star. As shown in fig. 5A and 5 B after treatment the tissues are subject to an astringent effect caused just by the power of tannin agent. Other tannin that we have used is Mimosa light. This substance extract from tree have a rapid penetration followed by

high tannin fixation. The combination with other anionic tanning agents such as Suntans (Retanin SO), resins and polymers is common practice to enhance the finishing of the leather. In general, Mimosa is now the favourite natural tanning agent in the use of fast modern tanning systems in pits or drums. The light colour of our Mimosa produces light colour leather that camouflages grain defects and improves the selection of the finished leather and therefore results in higher quality of the leather. The action of these substances as can be seen also in figure 5 give the dermis equivalent a compact appearance and moreover is soft to the touch. Also the “doll shoes” has been tanned with vegetable tannage (fig. 6A), and moreover was color with a acid colorant that give a red color showed in figure 6B.

80-90% of “vera pelle” leathers in the world are tanned by chrome (also known as mineral) tanning. Chrome tanning uses a solution of chemicals, acids and salts (including chromium sulphate) to dye the hide. It's a very quick process, taking about a day to produce a piece of tanned leather. First the hide is 'pickled' by being left in the acid salt mixture, before being placed into the chromium sulphate. All hides then come out looking light blue (known as 'wet blue') as show in figure 6 C for equivalent sheet shape. After the chrome tanning the product was stained with red colorant and the result is showed in figure 6D

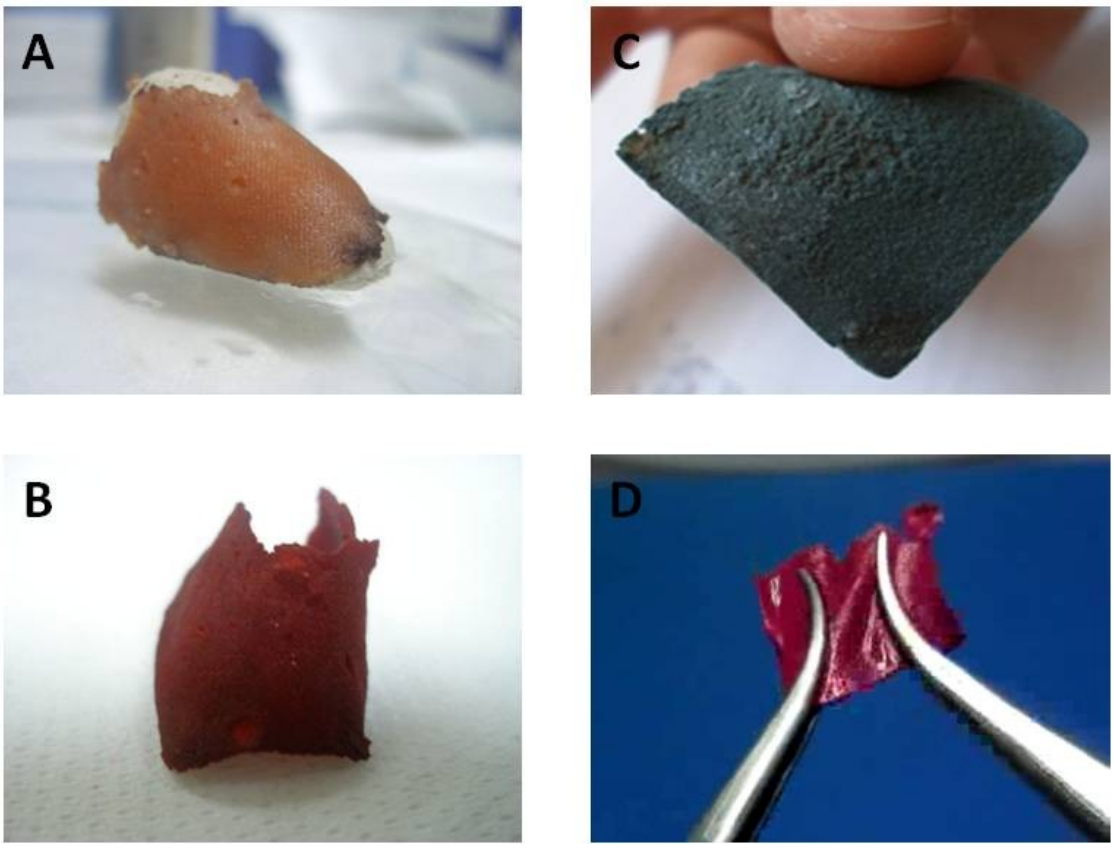

Figure 6.: tissue-equivalents products tanned and stain. (A)"doll shoes" vegetable tanned on the polymeric support (B) "doll shoe", staining with red acid. (C) tissue-sheet tanned with chrome. (D) tissue-sheet, staining with red acid.

It is quite difficult to evaluate what is the best tanning procedure, since the most important parameters for evaluation are of subjective nature. We reported Pros and Cons of each tanning procedure used in table 1.

On the basis of considerations regarding the cost and duration of the process we choose the chrome tanning 50.000 euro at 1 m^2 against 50 euro for 1m^2 raw leather. In addition, the softness, the impermeability and the resistance of the tissue after chrome tanning treatment convinced us to definitively used this tanning procedure for our products.

	Advantages	Disadvantages
Chrome tanning	Quick and easy to produce, usually only taking up to a day. Stain resistant and water can roll off the surface easily. Soft and supple to the touch. Color remains the same throughout the products life. It's cheaper to buy than vegetable tanned leather, which means it is also easier to find. It has a high degree of thermal resistance.	Chrome tanning is very bad for the environment. It's produced with little skill and very often mass produced. Chrome tanning often smells of chemicals.
Vegetable tannage	Environment friendly; meaning any leather products that have been vegetable tanned can be recycled. Due to the natural tannins used, vegetable tanned products actually improve with age and develop a patina. The colours that vegetable tanning produces are rich and warm tones that look completely natural.	The process of vegetable tanning takes a long time, can take up to 60 days. Products that have been vegetable tanned are more expensive. The colours you can produce from vegetable tanning are limited. Direct heat can cause vegetable tanned products to shrink or crack.

Table1: advantages and disadvantage of the chrome tanning and vegetable tannage

In the figure 7A is shown the dermis equivalent's thick after tanning procedure. The macroscopic appearance of tanned tissue equivalent and tanned native skin is compared in figure 7B.

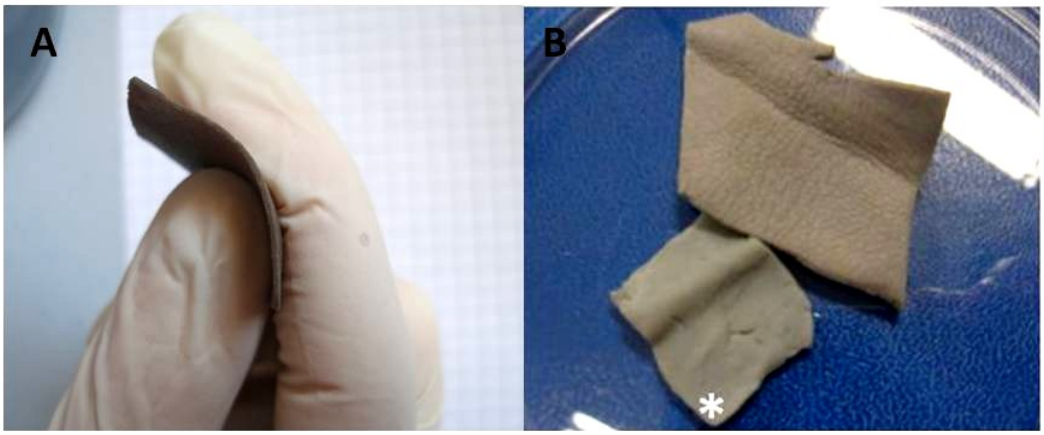

Figure 7.:D.E. at sheet shape and tanned with chrome. (A) thick of sheet; (B) surface of D.E. sheet shape is indicate with star against surface of raw skin and both were tanned with chrome

In graph 1 we showed the curve of mechanical stress of sample from dermal equivalent sheet. We have performed a constant deformation rate of 1,3 mm/min and in table 2 is shown the values of tangent elastic module (E_{tan}), maximum strain (S_{max}) and maximum stress (σ_{max}).

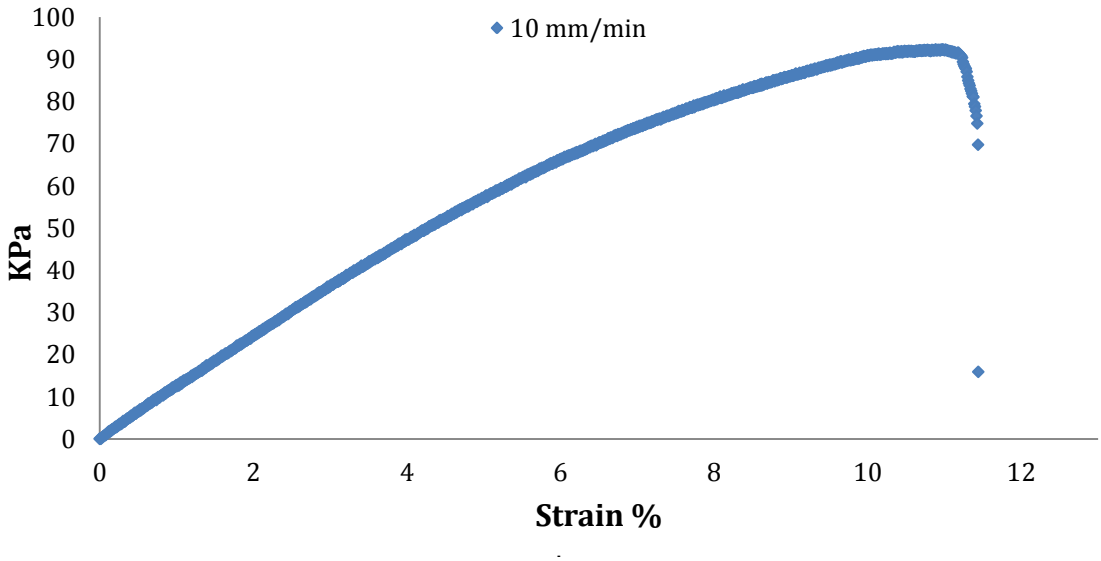

Graph 1.:mechanical stress curve of D.E.

These values are comparable with the data of the literature, about collagen and elastin, in which are reported the following values shown in Table 3. Moreover a

connective soft tissue such as our equivalent dermis, can by the point of view of the characteristics mechanical, to be schematized as a parallel of elastin and collagen, as shown in Figure 7 [10].

mm/min	E_{tan} [MPa]	σ_{max} [MPa]	S_{max} [%]
1,3	1,716	0,158	11,7

Table 2.:sumamry table of mechanical properties of D.E.

material	E_{tan} [MPa]	σ_{max} [KPa]	S_{max} [%]
collagen	1000	50-100	10
elastin	0,6	1	100

Table 3.: table of mechanical properties of collagen and elastin.

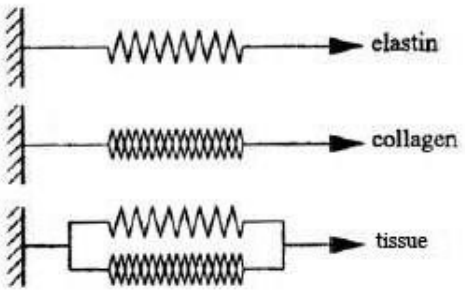

Figure 7.: schematization of the elastic behavior of elastin collagen and tissue

CONCLUSION

The results described a process able to build bioengineered tissues having different shape able to be tanned. Tissues-equivalent having the shape of disk, large sheet, fibers and “doll shoes” have been obtained thanks to versatility of the bottom-up

process developed that allow to overcome shape limitations of preformed scaffold. By morphological analysis of ECM we found that the tissues realized are very similar to native dermis and very interestingly they are able to retain the 3D structure, to be undergone a tanning process and so to be useful as possible alternative to animal skin in the textile fields. We have tested chrome tanning and vegetable tanned in order to understand which procedures, between chrome tanning and vegetable tanned, was the best on our tissue and according with economical aspect we have choice the chrome tanning. Moreover the tissue not undergoes the shrinkage by using chrome tanning that is able to give quality such as softness and a good resistance to decomposition. After chrome tanning mechanical properties demonstrates that the dermis equivalent have a Young's modulus (E_{tan}) comparable to the native tissue.

REFERENCES

1 .Vacanti, J.P. and Langer, R. Tissue engineering: the design and fabrication of living replacement devices for surgical reconstruction and transplantation. Lancet 354, SI32, 1999.

2. Yuya Morimotoa and Shoji Takeuchi Three-dimensional cell culture based on microfluidic techniques to mimic living tissues Biomaterials Science minireview 2013

3. 1 D. R. Albrecht, G. H. Underhill, T. B. Wassermann, R. L. Sah and S. N. Bhatia, Probing the role of multicellular organization in three-dimensional microenvironments, Nat. Methods, 2006, 3(5), 369–375.

4. F. Pampaloni, E. G. Reynaud and E. H. K. Stelzer, The third dimension bridges the gap between cell culture and live tissue, Nat. Rev. Mol. Cell Biol., 2007, 8(10), 839–845.

5. B. G. Chung, K.-H. Lee, A. Khademhosseini and S.-H. Lee, Microfluidic fabrication of microengineered hydrogels and their application in tissue engineering, Lab Chip, 2011, 12 (1), 45–59.

6. Lillian Rich1 and Peter Whittaker1,2 Collagen and picrosirius red staining: a polarized light assessment of fibrillar hue and spatial distribution *Braz. J. morphol. Sci.* (2005) 22(2), 97-104

7. Carmela Palmiero, Giorgia Imparato, Francesco Urciuolo, Paolo Netti Engineered dermal equivalent tissue *in vitro* by assembly of microtissue precursors Acta Biomaterialia 6 (2010) 2548–2553

8. Whitesides, G.M. and Grzybowski, B. (2002) Self-assembly at all scales. Science 295, 2418–2421

9. H. Onoe, R. Gojo, Y. Tsuda, D. Kiriya, M. Kato-Negishi and S. Takeuchi, Cell fibers: construction of centimeter-scale 3D tissues by weaving, 14th International Conference on Miniaturized Systems for Chemistry and Life Sciences, 2010, pp. 629–631.

10. Rostislav V. Shevchenko, Stuart L. James and S. Elizabeth JamesA review of tissue-engineered skin bioconstructs available for skin reconstruction. J. R. Soc. Interface 2010 7, 229-258